ALLIGATOR RIVERS ANALOGUE PROJECT

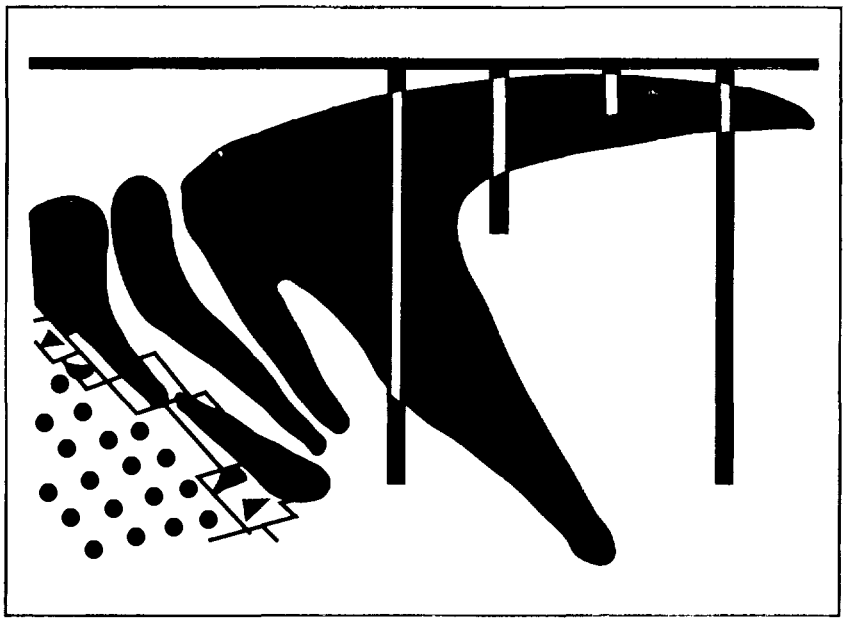

ISBN 0-642-59939-4

DOE/HMIP/RR/92/0823

SKI TR 92:20-13

FINAL REPORT
VOLUME 13

URANIUM SORPTION

1992

AN OECD/NEA INTERNATIONAL PROJECT MANAGED BY:
AUSTRALIA NUCLEAR SCIENCE AND TECHNOLOGY ORGANISATION

ALLIGATOR RIVERS ANALOGUE PROJECT

FINAL REPORT

VOLUME 13

URANIUM SORPTION

Lead Author: T.D. Waite[1,2]

Contributing Authors: T.E. Payne[1], J.A. Davis[3], and K. Sekine[4]

[1]Australian Nuclear Science and Technology Organisation,
Private Mail Bag 1, Menai, NSW 2234, Australia

[2]Present Address: Department of Water Engineering,
University of New South Wales, Sydney, NSW 2052, Australia

[3]United States Geological Survey, Water Resources Division,
MS465, 345 Middlefield Road, Menlo Park, California, 94025, USA

[4]Japan Atomic Energy Research Institute,
Tokai-mura, Ibaraki 319-11, Japan

PREFACE

The Koongarra uranium ore deposit is located in the Alligator Rivers Region of the Northern Territory of Australia. Many of the processes that have controlled the development of this natural system are relevant to the performance assessment of radioactive waste repositories. An Agreement was reached in 1987 by a number of agencies concerned with radioactive waste disposal, to set up the International Alligator Rivers Analogue Project (ARAP) to study relevant aspects of the hydrological and geochemical evolution of the site. The Project ran for five years.

The work was undertaken by ARAP through an Agreement sponsored by the OECD Nuclear Energy Agency (NEA). The Agreement was signed by the following organisations: the Australian Nuclear Science and Technology Organisation (ANSTO); the Japan Atomic Energy Research Institute (JAERI); the Power Reactor and Nuclear Fuel Development Corporation of Japan (PNC); the Swedish Nuclear Power Inspectorate (SKI); the UK Department of the Environment (UKDoE); and the US Nuclear Regulatory Commission (USNRC). ANSTO was the managing participant.

This report is one of a series of 16 describing the work of the Project; these are listed below:

No.	Title	Lead Author(s)
1	Summary of Findings	P Duerden, D A Lever, D A Sverjensky and L R Townley
2	Geologic Setting	A A Snelling
3	Geomorphology and Paleoclimatic History	K-H Wyrwoll
4	Geophysics, Petrophysics and Structure	D W Emerson
5	Hydrogeological Field Studies	S N Davis
6	Hydrogeological Modelling	L R Townley
7	Groundwater Chemistry	T E Payne
8	Chemistry and Mineralogy of Rocks and Soils	R Edis
9	Weathering and its Effects on Uranium Redistribution	T Murakami
10	Geochemical Data Bases	D G Bennett and D Read
11	Geochemical Modelling of Secondary Uranium Ore Formation	D A Sverjensky
12	Geochemical Modelling of Present-day Groundwaters	D A Sverjensky
13	Uranium Sorption	T D Waite
14	Radionuclide Transport	C Golian and D A Lever
15	Geochemistry of ^{239}Pu, ^{129}I, ^{99}Tc and ^{36}Cl	J T Fabryka-Martin
16	Scenarios	K Skagius and S Wingefors

CONTENTS

EXECUTIVE SUMMARY

Background

The oxidation of highly insoluble U(IV) to more soluble U(VI), followed by a sequence of U(VI) precipitation-dissolution reactions, appears to have contributed to the migration of uranium away from the Koongarra primary ore zones. However, adsorption-desorption (sorption) processes become increasingly important in limiting uranium mobility further downfield, where the solubility products of U(VI) minerals are no longer exceeded. In this volume, the results of an investigation into the factors influencing the sorption of U(VI) to natural substrates from the weathered zone in the vicinity of the Koongarra ore deposit are reported, and the applicability of mathematical models to describe the sorption phenomena over a range of solution conditions are assessed.

Overview

Most of the available data relating to U sorption in the natural environment are only of relevance to a particular solid substrate and groundwater composition. The distribution coefficients (K_d values) obtained from many such studies are of little use in predicting the migration of uranium through porous media of variable composition, and under solution conditions that exhibit major spatial and temporal variability. There have been some attempts over the last ten years to develop more general models of the adsorption of U(VI) to solid substrates, but most studies have only been conducted on a few simple (single mineral phase) substrates under a limited range of conditions. A variety of models has been used to describe the experimental data.

In this study, uranium sorption to well-defined mineral phases (ferrihydrite, crystalline silica, and kaolinite), and to selected natural substrates from Koongarra has been studied. The surface properties of these materials were rigorously defined, and adsorption studies conducted over a range of solution pH, ionic strength, carbonate content, adsorbent and adsorbate concentrations, and in the presence of uranium complexants and (potentially) competing adsorbates (such as phosphate and fluoride).

The wide range of chemical conditions studied in the present work has allowed the development of models of uranyl sorption which account for a greater number of environmental variables than most previous studies of U sorption, or of trace metal uptake in general.

Surface Complexation Modelling of Uranyl Sorption to Single Minerals

Results obtained in the adsorption studies to ferrihydrite were modelled using the surface complexation approach, with a diffuse double layer description of the electrical double layer. While a single site type was used in our early studies, most success has been achieved on assuming the presence of two site types - one site type corresponding to a small set of high affinity cation-binding sites, and the other type being the total reactive sites available for sorption of protons. We have found

that mononuclear uranyl surface species most appropriately describe the adsorption results.

A combination of adsorption to "strong" sites >SOH (yielding uranyl surface complexes of the form $>SOUO_2^+$) and "weak" sites TOH (yielding $>TOUO_2OH$), i.e.

$$SOH + UO_2^{2+} \leftrightarrow SOUO_2^+ + H^+$$

$$TOH + UO_2^{2+} + H_2O \leftrightarrow TOUO_2OH + 2H^+$$

appears to give the most satisfactory agreement between model and experiment with best-fit constants being derived using the non-linear optimisation program, FITEQL. Adsorption under basic conditions, where uranyl carbonate species dominate the solution speciation of U(VI), was also satisfactorily described without recourse to specific adsorption of uranyl carbonate complexes, even under elevated partial pressures of carbon dioxide typical of Koongarra groundwaters.

The effect of phosphate was studied because uranyl phosphate minerals (such as saleeite) are found in the Koongarra ore body, and phosphate is also present in Koongarra groundwaters. The addition of phosphate increased the uptake of U(VI) by ferrihydrite in the acidic pH region. The formation of ternary uranyl phosphate surface complexes appears to be the most likely reason for enhanced U(VI) uptake in the presence of phosphate. Incorporation of a ternary complex of the form $TPO_4UO_2^\circ$ in the surface complexation model of U(VI) sorption to ferrihydrite, with a formation constant determined using FITEQL, led to close agreement between model and experiment.

A surface complexation model involving only uptake on "weak" sites (to form $TOUO_2OH$) provided a good description of U(VI) sorption to quartz. This simple model adequately described the competing effect of solution complexation of U(VI) by fluoride. The results of modelling uranyl adsorption to kaolinite were less satisfactory. Good correspondence between experiment and model results was obtained at low U(VI) concentrations, using a model incorporating both ion exchange sites (-X) and specific adsorption to strong and weak sites; i.e.

$$NaX + UO_2^{2+} + H_2O \leftrightarrow UO_2OHX + H^+ + Na^+$$

$$SOH + UO_2^{2+} \leftrightarrow SOUO_2^+ + H^+$$

$$TOH + UO_2^{2+} + H_2O \leftrightarrow TOUO_2OH + 2H^+$$

but this model did not adequately describe the experimental data obtained at high U(VI) concentrations. Further insight into the factors controlling uranyl uptake on kaolinite is still required.

A range of ancillary studies has assisted in defining important sorbing surfaces and in elucidating the effects of chemical processes on uranium partitioning between the solid and solution phases. In particular, examination of U(VI) uptake on pre-formed and co-precipitated iron oxides indicated very little difference in

partitioning, and suggested that short term aging of amorphous iron oxide phases does not dramatically influence the sorbing capacity. The results of longer term aging studies (speeded up in these experiments by heating) are also reported. Ferrihydrite aging (transformation to more crystalline forms such as goethite and hematite) was found to result in a reduction in surface area with a concomitant decrease in adsorption of U(VI). Uranium which was present during the transformation process was partially incorporated into the resulting solid phase, with a consequent decrease in its availability for desorption.

Studies on Koongarra Substrates

Fine fractions (nominally < 10 μm) of selected natural substrates from Koongarra were prepared, and uranyl partitioning between solution and solid phases was examined under a variety of conditions. These studies were typically undertaken using a trace of ^{236}U, enabling exchange between ^{236}U and intrinsic ^{238}U to be studied. The accessible U(VI) present in the natural substrates was estimated from the results of these experiments, and was found to be in good agreement with the Tamm's acid oxalate (TAO) extractable uranium in these samples.

Preliminary modelling studies, in which it was assumed that all U(VI) adsorption to the natural substrates could be accounted for by uptake on amorphous (TAO extractable) iron oxides, were reasonably successful. However, more detailed analysis indicated significant difficulties with this approach. Consideration in this report is also given to an approach in which a uniform site density per unit area was assumed, but this also led to serious under-prediction of adsorption (when reasonable site densities were used).

A reasonable fit to the experimental data was obtained using a more complex model with the following features:

- a large concentration of strongly acidic, strongly binding sites, and
- an even larger concentration of weakly binding sites, with acidic properties similar to ferrihydrite.

The agreement obtained between experiment and model demonstrates that it is possible to derive a model that adequately describes the experimental data. However, the parameter values were chosen by methods little better than trial and error. We consider that considerably more insight into the nature of surface binding groups on the natural Koongarra substrate is required before undertaking more detailed modelling work.

ACKNOWLEDGEMENTS

The authors acknowledge the financial support provided by the participants in the Alligator Rivers Analogue Project and the resources provided by the Australian Nuclear Science and Technology Organisation. Particular credit must be given to Peter Duerden for his inspirational management of the project and for his ability to bring together effectively a group of individuals who were committed to carrying out high quality science focussed towards a specific need.

Specific acknowledgement is also given to J. Huang, R. Edis, R. Lowerson, D. Garton, S. Short, the electron microscopy group at ANSTO, and many other ANSTO staff who provided valuable assistance.

1 INTRODUCTION

The migration of radionuclides such as uranium, radium and thorium in water-rock systems is largely controlled by precipitation/dissolution and adsorption/desorption reactions. The relative importance of these processes will be dependent on the concentration and redox state of the radionuclide present, the tendency of radionuclide-containing minerals to precipitate, and the availability and type of sorbing surfaces. Thus, in the vicinity of the primary uranium ore body at Koongarra, where uranium concentrations are relatively high, precipitation /dissolution processes involving uranium oxide, phosphate and silicate minerals control migration of this radionuclide. Further down-field, where uranium concentrations are significantly lower, mineral solubility products are not exceeded, and sorption becomes the dominant process controlling partitioning between solid and solution phases. The processes of adsorption and desorption must therefore be accounted for in a model that will adequately describe the migration of radionuclides from deposits such as Koongarra.

Although numerous studies of the partitioning of uranium between solid and solution phases have been reported, most of the available data is only of relevance to a particular solid substrate under a specific set of solution conditions. The distribution coefficients ("K_d values") obtained from such studies are of little use in predicting the migration of uranium through porous media of variable composition, or under solution conditions that exhibit major spatial and temporal variability. There have been some attempts over the last ten years to develop more general models of the adsorption of U(VI) to solid substrates, but studies have only been conducted on a few simple (single mineral phase) substrates and little agreement exists either between the data obtained or in the optimal modelling approach (Tripathi, 1983; Hsi and Langmuir, 1985).

In this Volume, the results of studies of uranium sorption (adsorption and desorption) to both single, well-defined mineral phases, and to selected natural (Koongarra) substrates are reported. The single phases included the amorphous iron oxide ferrihydrite, crystalline silica and two naturally occurring kaolinites, KGa-1 and Nichika. The surface properties of these materials were rigorously defined, and adsorption studies were conducted over a range of solution pH, ionic strength, carbonate content, adsorbent and adsorbate concentrations, and in the presence of uranium complexants and (potentially) competing adsorbates (such as phosphate and fluoride). The results of these studies were modelled using the "surface complexation" approach, with a diffuse layer description of the electrical double layer. The impacts of mineral phase transformations (specifically the aging of amorphous ferrihydrite to more crystalline forms) on the uptake and desorption of uranium are also reported.

Prior to a detailed description of the methods and results of our studies on U(VI) sorption, we review existing models for describing trace element partitioning between solid and solution phases, and summarise the results of previous studies of uranium sorption to single and complex substrates.

2 OVERVIEW OF MODELS OF TRACE ELEMENT PARTITIONING BETWEEN SOLID AND SOLUTION PHASES

Two types of models for describing the equilibria of adsorption-desorption reactions at mineral surfaces can be distinguished (Davis and Kent, 1990): (1) empirical partitioning relationships, and (2) conceptual models for surface complexation that use the formalism of ion association reactions in solution as a representation of surface reactions. In part because of the complexity of natural systems, the empirical approach has been widely used in describing the partitioning of solutes between mineral and water phases in geochemical applications (such as transport modelling), but surface complexation models (SCM) are finding increasing acceptance in these areas. These descriptive approaches are discussed below and issues pertaining to their use in complex natural systems raised.

2.1 Empirical Adsorption Models

2.1.1 Distribution coefficients

Adsorption is often described in terms of equations or partitioning relationships that relate the activity of a solute in water to the amount of the solute adsorbed at constant temperature. The simplest of these expressions is the distribution coefficient derived from the association reaction:

$$J_{aq} \leftrightarrow J_{ads} \tag{2.1}$$

where J is an adsorbing solute, J_{aq} represents J dissolved in the aqueous phase, and J_{ads} is J adsorbed. The amount of solute adsorbed is frequently expressed as an adsorption density parameter, Γ_J, in units of adsorbed solute per unit area or weight of adsorbent. The distribution coefficient, K_d is usually defined as:

$$K_d = \Gamma_J / [J_{aq}] \tag{2.2}$$

Usually $[J_{aq}]$ represents the total concentration of all dissolved species of J, although a distribution coefficient for a specific species has been defined (Tessier et al., 1989).

The distribution coefficient for inorganic ions is highly dependent on the conditions under which it is measured, such as pH, background salt composition, concentration of dissolved carbonate, concentrations of competing adsorbates, etc. For example, Leckie and Tripathi (1985) used data on uranyl adsorption to goethite (Tripathi, 1983) to compute the K_d that would be measured in goethite suspensions as a function of pH and pCT (-log of the total concentration of carbonate species). The resulting K_d values ranged over 10 orders of magnitude, depending on pH and carbonate concentrations (Figure 2.1). Given the strong dependence of K_d values on solid and solution properties, the distribution coefficient has little value in predicting the response of solute adsorptive behaviour that may result from changes in either the aqueous or mineralogical composition of a system.

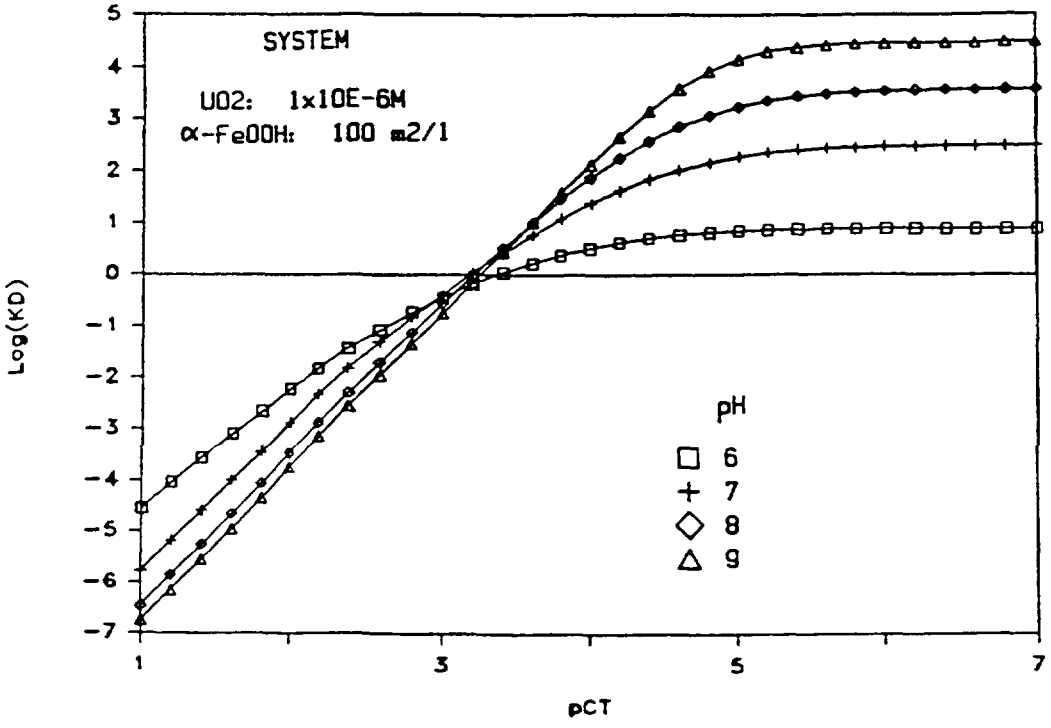

FIGURE 2.1 Log K_d versus pC_T = -log(total carbonate concentration) for goethite suspensions containing 10^{-6}M total U(VI) at 25°C.
(from Leckie and Tripathi, 1985 as reported by Kent et al., 1986).

2.1.2 Langmuir isotherm

In the early 1900's, the physical chemist Irving Langmuir (who later won a Nobel prize in chemistry for his work on surface reactions) derived an equation to describe adsorption by considering the reaction:

$$>S + J \leftrightarrow >SJ \tag{2.3}$$

where J is an adsorbing solute, >S is an adsorptive surface site and >SJ represents the species of adsorbed solute J. Assuming that all surface sites have the same affinity for solute J, a mass law equation can be written for the above equation as follows:

$$K_L = \frac{\Gamma_J}{[J_{aq}]\Gamma_S} \tag{2.4}$$

where Γ_S is the surface density of uncomplexed adsorptive sites and K_L is the conditional Langmuir equilibrium constant. Making the further assumption that the density of all adsorptive sites on the surface, S_T, is fixed and that J is the only adsorbing solute, the mass law can be combined with the mass balance for surface sites:

$$S_T = \Gamma_S + \Gamma_J \tag{2.5}$$

to yield the expression commonly known as the Langmuir isotherm:

$$\Gamma_J = S_T\left(\frac{K_L[J_{aq}]}{1 + K_L[J_{aq}]}\right) \tag{2.6}$$

The generalized shape of the Langmuir isotherm on a log-log plot is shown in Figure 2.2 where the x-axis represents $[J_{aq}]$ (shown as C). The isotherm is linear (unit log slope) at low solute concentrations (i.e. sorption proportional to dissolved concentration) and levels off (zero slope) at higher concentrations. Such an isotherm implies that sorption affinity remains constant until site saturation is approached, and is consistent with a single type of binding site (Dzombak and Morel, 1990). It should be noted that adherence of data to an adsorption isotherm provides no evidence as to the actual mechanism for the association of a solute with a mineral phase (Sposito, 1986). It has been shown that special cases of precipitation reactions may also exhibit data that conform to the Langmuir isotherm (Veith and Sposito, 1977). Like the distribution coefficient, K_L is dependent on strictly constant solution conditions and is very sensitive to changes in pH (Davis and Kent, 1990).

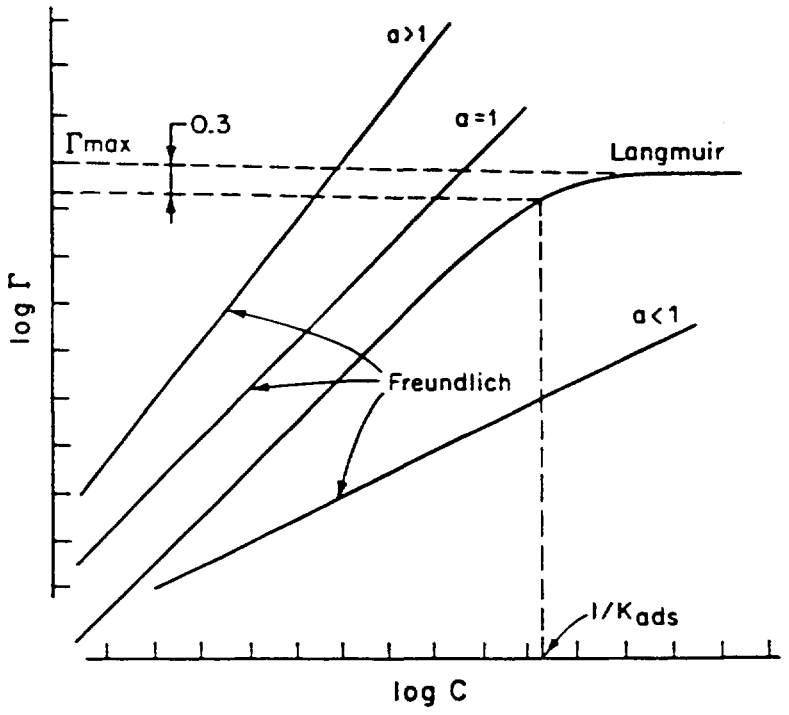

FIGURE 2.2 Characteristic shapes of Langmuir and Freundlich adsorption isotherms (from Morel, 1983).

2.1.3 Freundlich and other isotherms

For inorganic ions, it is frequently observed that a log-log plot of Γ_j versus $[J_{aq}]$ (or C in Figure 2.2) has a slope of less than 1.0, indicating that sorption is not proportional to dissolved solute concentration. Such behaviour is observed when multiple-site types are present, in which case affinity decreases as higher-affinity sites are filled and more abundant lower-affinity sites become dominant. Data yielding this behaviour may be fitted to a multiple-site Langmuir expression or a generalised exponential isotherm such as the Freundlich isotherm (Kinniburgh, 1986) (Figure 2.2):

$$\Gamma_J = A\,[J_{aq}]^a \qquad (2.7)$$

2.2 Surface Complexation Approach

An alternative to the empirical modelling approaches described above is the surface complexation model (SCM), which extends the ion-association model of aqueous solution chemistry to include chemical species on surfaces (Davis and Kent, 1990). Many workers have contributed to the development of surface complexation models, but key papers by Schindler and co-workers (Schindler and Kamber, 1968; Schindler and Gamsjager, 1972) and by Stumm et al. (1970) defined the surface complexation approach in its modern form (Dzombak and Morel, 1990). The essential elements of this approach are spelt out below:

(a) the surface is composed of specific functional groups that react with dissolved solutes to form surface complexes in a manner analogous to complexation reactions in homogeneous solution,

(b) the equilibria of surface complexation and ionization reactions can be described by mass law equations,

(c) surface charge and surface electrical potential are treated as necessary consequences of chemical reactions of surface functional groups, and

(d) the effect of surface charge on sorption is taken into account by applying a correction factor derived from electrical double layer (EDL) theory to mass law constants for surface reactions.

A number of models have been developed within this overall framework. Differences between the models are based on the interfacial structure of the EDL and the manner in which weakly-bound ions are treated (see Figure 2.3). While the models differ in their consideration of interfacial structure, all the models reduce to a set of simultaneous equations that can be solved numerically (Dzombak and Morel, 1987). These equations include:

(a) mass law equations for all surface reactions under consideration,

(b) a mole balance equation for surface sites,

(c) an equation for computation of surface charge, and

(d) a set of equations representing the constraints imposed by the model of interfacial structure.

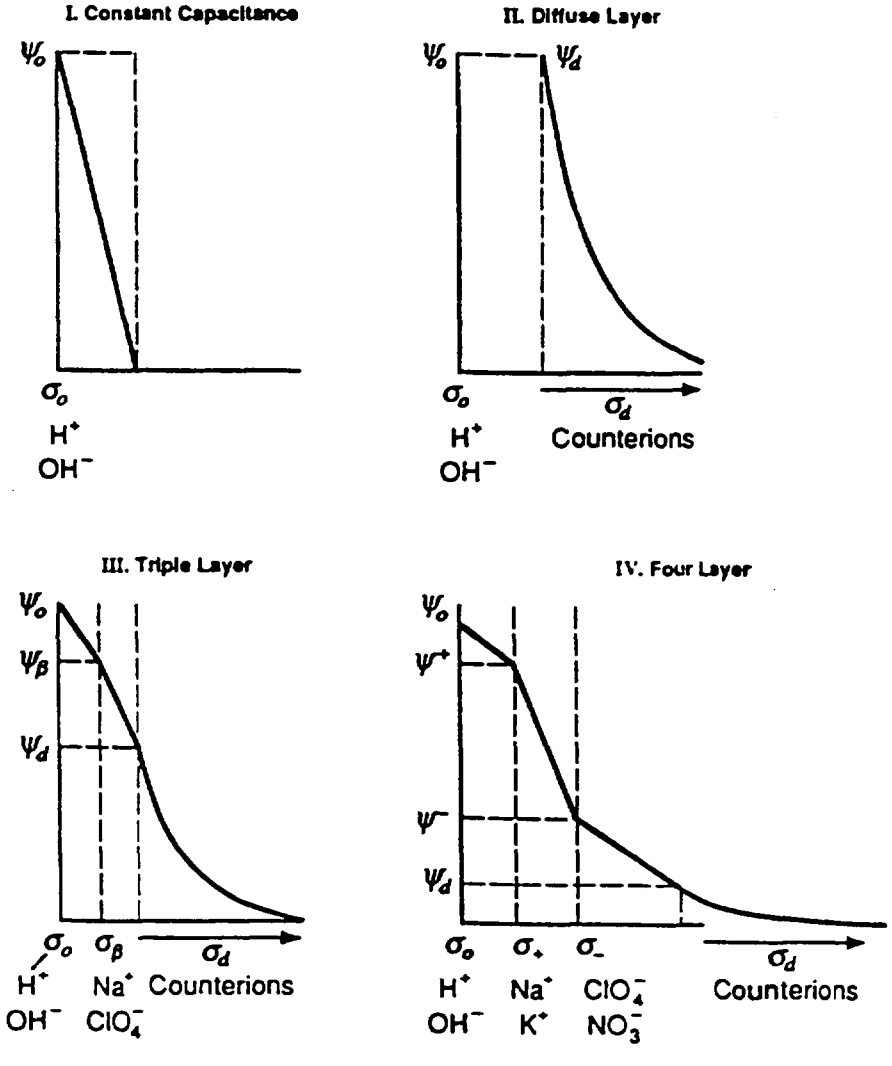

FIGURE 2.3 Idealised schematics illustrating the decay of chemical potential (Ψ) with distance from the surface for the constant capacitance, diffuse double layer, triple layer and four-layer models. Diagram assumes conditions typical of an oxide surface in a simple electrolyte (such as $NaClO_4$ or KNO_3) at a pH value different from the point of zero charge pH (pH_{pzc}). Surface charge (σ) terms at various distances from the oxide surface are also shown.

In this work, particular attention is given to the Diffuse Double Layer Model (DDLM). In this model, amphoteric surface hydroxyl groups are assumed to form ionised surface sites, i.e.

$$>SOH_2^+ \leftrightarrow >SOH + H^+ \quad (2.8)$$

$$>SOH \leftrightarrow >SO^- + H^+ \quad (2.9)$$

Surface complexation of cations such as UO_2^{2+} by hydrous oxides involves the formation of bonds with surface oxygen atoms and the release of protons from the surface. For example, the formation of a possible 1:1 surface complex between a divalent cation M^{2+} and surface oxygen atoms may be represented:

$$>SOH + M^{2+} \leftrightarrow >SOM^+ + H^+ \quad (2.10)$$

with formation constant K_M^{app}. As is the case for protons and anions, cations sorb onto oxide surfaces in response to both chemical and coulombic forces. Long-range electrostatic effects due to the surface charge on oxides can be taken into account explicitly by inclusion of a coulombic term in the mass law expressions for sorption reactions:

$$K_M^{int} = K_M^{app}\exp(\Delta ZF\Psi/RT) \quad (2.11)$$

where ΔZ is the net change in the charge number of the surface species, Ψ is the surface potential and F is Faraday's constant.

The specific sorption of cations and anions can change the net charge on oxide surfaces. For example, if a cation M^{2+} adsorbs to an oxide and forms the charged surface complex $>SOM^+$, the net surface charge density is given by:

$$\sigma = (F/AS_T)([>SOH_2^+] - [>SO^-] + [>SOM^+]) \quad (2.12)$$

where A is the surface area.

The simplest SCM approach is to ignore the electrical double layer by excluding electrostatic terms from the mass law equations for surface equilibria (Davis and Kent, 1990). When this approach is utilised in equilibrium models, surface functional groups are treated computationally in the same manner as dissolved ligands (for cation adsorption) or complexing metal ions (for anion adsorption). Such an approach is often justified because the chemical contribution to the free energy of adsorption dominates over the electrostatic contribution, and has been applied successfully in a range of instances (e.g. Davis et al., 1987; Cowan et al., 1990). The SCM approach without electrostatic correction has not been used frequently to simulate ion adsorption in systems with well-characterised mineral phases, but interest in this approach has recently been renewed because of the complexities of applying the SCM to natural materials (Davis and Kent, 1990).

2.3 Description of Partitioning in Natural Systems

In this section, we briefly consider the limitations and constraints of applying the above approaches to cation adsorption modelling in natural systems.

2.3.1 Empirical approaches

Most models currently used for the assessment of the long-term fate of radionuclides rely on distribution coefficients (K_d values - Equation 2.2). Consequently, extensive effort has been devoted to measuring K_d values in "batch" experiments, where a solid phase is suspended in a solution containing a known amount of radionuclide, and the amount of solute removed after a specified time is determined (Sibley and Myttenaere, 1986). Although some authors have used a K_d value normalised for reactive surface area (Balistrieri and Murray, 1984) or aqueous speciation (Tessier et al., 1989), in most cases very little characterisation of the solution speciation or chemical properties of the composite materials has been performed. The approach necessitates collecting K_d values over the range of conditions encountered in the system of interest. Note that reversible conditions (i.e. rapid adsorption and desorption kinetics) must be ensured, as must the linear dependence of adsorbed solute concentration on solution phase solute concentration (i.e. no site saturation). McKinley and Alexander (1992a) recommend that the term "sorption ratio" (R_d) be used rather than "distribution coefficient" (K_d) if rapid kinetics cannot be assumed.

K_d values vary over several orders of magnitude with varying solution composition even in simple mineral-water systems (Davis and Kent, 1990). The pH is a primary variable (Tessier et al., 1989), but the presence of complexing ligands (e.g., Hsi and Langmuir, 1985; Means et al., 1978) and changes in oxidation state of an adsorbing solute (Higgo and Rees, 1986) cause large changes in K_d values. K_d values are also affected by the concentration of competing ions (Davis et al., 1990; Balistrieri and Chao, 1987) and other interactions between sorption sites and solution components (Honeyman and Santchi, 1988; Kent et al., 1986).

K_d values have also been determined from in-situ measurements of solute concentrations in solid substrate and associated porewater (Santschi et al., 1988; Landstroem and Tullborg, 1989). However, caution should be exercised in interpreting partitioning information in terms of sorption processes alone, because several other processes may contribute to removal of solute from solution. These processes include molecular filtration, precipitation, mineral incorporation and ion exclusion. Application of a K_d approach is inappropriate if any of these processes are operating in addition to, or in preference to, sorption. In many cases naturally occurring radionuclides will be present in an incorporated or precipitated form rather than in an adsorbed state (e.g. Nesbitt, 1979; Guthrie and Kleeman, 1986).

McKinley and Alexander (1992a) recommend that the term *partition ratio* (P) be used (rather than K_d or R_d) for the empirical ratio of solid-phase concentration to liquid phase concentration if there is no evidence of a direct functional relationship between these concentrations, and where precipitates may be present. McKinley and Alexander (1992a) note migration calculations where P is inappropriately

substituted for K_d could lead to results which are incorrect by orders of magnitude in either a conservative or non-conservative manner.

Krishnaswami et al. (1982) developed another approach for determination of in-situ retardation coefficients, based on analysis of natural decay series radionuclide ratios in water. Although this approach has been adopted in several natural analogue studies (Laul et al., 1985; Ivanovich et al., 1988; Laul and Smith, 1988), McKinley and Alexander (1992b) consider that it is based on numerous unproven assumptions which are debatable for the gravel aquifer originally studied by Krishnaswami and co-workers, and certainly inappropriate in environments more relevant to nuclear waste disposal.

2.3.2 Surface complexation approaches

Application of a site-binding approach to model adsorption involves several steps:

i) the adsorption characteristics of the adsorbent must be determined

ii) thermodynamic data for the formation of aqueous species must be collected, evaluated and adapted to the modelling approach, and

iii) the stoichiometries and intensities for the formation of surface complexes must be determined from adsorption data (Kent et al., 1986).

Adsorbent characterisation is particularly problematic in complex natural systems. The principal objective of this characterisation is the determination of the density of adsorption sites as a function of solution composition. A variety of mineral types may be present in natural systems including (a) "simple" oxides of elements such as iron, aluminium and titanium, (b) "complex" oxides such as the aluminosilicates and manganese oxides that, in many instances, possess fixed charge, and (c) "salt type" minerals such as apatite, calcite and dolomite. Extensive information is available on the adsorbent characteristics of oxides, including the total density of surface hydroxyl sites and the extent to which the ionisation reactions proceed as a function of pH, electrolyte identity and electrolyte concentration (Kent et al., 1986).

Gas adsorption surface areas provide a reasonable measurement of chemically reactive surface area for many oxide minerals, and several methods are available for determining the number of surface sites per unit area (Kent et al., 1986; Davis and Kent, 1990). Ionisation of surface sites can be determined by performing acidimetric and alkalimetric titrations in the presence of aqueous electrolytes over a range of ionic strengths. For oxides with fixed charge, the tendency for both ion exchange and adsorption reactions to occur must be determined (Kent et al., 1986; James and Parks, 1982; Sposito, 1984). An ion exchange reaction can be considered to be a particular type of adsorption reaction where a solute ion replaces ions occupying exchange sites with no change in the surface charge (no such constraint is imposed on a general sorption reaction).

The solid phases involved in adsorption processes in natural systems are typically composite materials, consisting of mixtures of various minerals and (possibly) organic matter exhibiting a wide range of intrinsic chemical properties (Davis and Kent, 1990). Weathering reactions, diagenetic processes and interactions with bacteria give rise to the leaching of surface layers of minerals, and the deposition of extremely fine-grained, poorly crystalline minerals (Benson and Teague, 1982; Fritz and Mohr, 1984). As noted by Davis and Kent (1990), these processes may also lead to the formation of organic and Al and Fe hydroxypolymer coatings on mineral grains.

An assessment of the predominant adsorbent(s) in a mineral assemblage often facilitates the estimation of site density for modelling purposes. For example, if hydroxypolymer coatings and poorly crystalline precipitates of hydrous iron oxides are assumed to dominate the adsorptive reactions of interest, then the site density for modelling purposes can be estimated from the abundance of these mineral phases in a sample of composite material (Payne and Waite, 1991; Belzile and Tessier, 1990).

If it cannot be shown that a specific mineral component dominates the adsorptive interactions of a composite material, a more general approach is needed. Davis and Kent (1990) consider that the best approach is to multiply the measurement of reactive surface area by an average or typical value of site density for the major minerals present (Luoma and Davis, 1983). Composite materials that have large abundances of minerals with permanent structural charge (e.g. smectites) require special consideration, both in terms of the definition and measurement of reactive surface area for the solute of interest, and in the choice of surface site density.

3 REVIEW OF STUDIES OF URANIUM SORPTION

3.1 Laboratory Studies of U(VI) Partitioning Between Solution and Mineral Phases

Studies of relevance to modelling U(VI) sorption by geologic materials are reviewed here. This review includes consideration of other studies conducted within the Alligator Rivers Analogue Project that provide insight into the partitioning of U(VI) between solid and liquid phases, as well as previous studies of significance.

3.1.1 Silica and clays

Studies of U(VI) adsorption to natural substrates, such as clays, date back to the mid 1950's. However, most of these early investigations were undertaken at U(VI) concentrations far in excess of those present in natural waters (e.g., Goldstaub and Wey, 1955; Nuss and Wey, 1956). Even in relatively recent investigations (Tsunashima et al., 1981; Borovec, 1981), uranium concentrations no lower than 1 mg/L (approximately 4 μM) were considered. Under these conditions, Langmuir isotherm behaviour (indicating uniformity of sorption site affinity for U(VI)) is often observed.

The uptake of U(VI) on fine-grained kaolinite, illite and montmorillonite was investigated in some detail by Borovec (1981). This work was carried out at pH 6.0, with total U concentrations from 10^{-5} to 10^{-2} mol /L. The major findings of this work were that:

a) uptake from solutions of U(VI) species at concentrations greater than 10^{-4}M followed Langmuir isotherm behaviour whereas the Freundlich isotherm applied at lower concentrations,

b) the presence of competing divalent cations reduced U uptake,

c) the distribution coefficient rose with decreasing U(VI) concentration, becoming constant only in the region where the Freundlich isotherm was valid; and increased in the sequence kaolinite < illite < montmorillonite, and

d) equations were derived relating U adsorption capacity a_m and the cation exchange capacity (CEC), and relating a_m and the specific surface area. The average area per one UO_2^{2+} was found to be 2.73 ± 0.24 nm^2.

Although the above conclusions appear reasonable, the U concentrations used in this study were extremely high, and it is rather surprising that precipitation was not observed, particularly in the experiments with total U of 10^{-2} mol /L.

Investigations of uranyl adsorption to a range of other substrates (including amorphous silica) were described by Maya (1982). These studies were undertaken in carbonate solutions, but no evidence was found (by Raman spectroscopy) for the presence of carbonate ligands at the surface under conditions where the uranyl moiety was adsorbed.

Ames et al. (1983a) reported that U(VI) sorption to fine-grained biotite, muscovite and phlogopite is best described by Freundlich isotherms. Similar results were found for U(VI) uptake on illite, kaolinite, montmorillonite, nontronite, glauconite, clinoptilolite, opal and amorphous silica (Ames et al., 1983b). These studies by Ames et al. were only performed at single (not particularly well-defined) solution pH values, thus rendering interpretation in terms of solution speciation difficult.

Investigators at the Japanese Atomic Energy Research Institute (JAERI) have examined the adsorption of U(VI) to suspensions of smectite, kaolinite, chlorite and vermiculite as part of the Alligator Rivers Analogue Project (Ueno and Sekine, *pers. comm.*). One hundred milligrams of each mineral was equilibrated in a teflon bottle with uranium in 50 mL of water at a constant ionic strength at 20°C. After adsorption equilibrium had been reached (within one day in all cases), the pH of the solution phase was measured, and the solid and liquid phases separated by centrifugation (35,000 rpm for 20 min). A yield tracer of ^{232}U was added to each sample of solid and the amount of uranium present determined by α-spectrometry after chemical separation and electrodeposition of the uranium. Distribution coefficients obtained by this method are given in Table 3.1.

TABLE 3.1

DISTRIBUTION COEFFICIENTS FOR U(VI) SORPTION ON SELECTED CLAYS (100 mg/50 mL) AT VARIOUS pH VALUES (SEKINE AND UENO, *pers. comm.*).

Mineral	K_d(mL/g)	pH
Smectite	3.8×10^3	7.7
	2.6×10^4	7.8
	3.2×10^3	7.9
Kaolinite	4.8×10^1	4.7
	6.8×10^2	5.6
	4.1×10^3	6.2
Chlorite	8.3×10^3	6.3
	4.5×10^3	6.7
Vermiculite	7.5×10^3	7.0
	5.8×10^3	7.2

3.1.2 Iron oxides

Starik et al. (1958) studied the sorption of trace concentrations of U(VI) to Fe-oxyhydroxides. Uptake was found to be maximum at a pH of approximately 5 and declined above and below this pH value. Uranyl was desorbed by carbonate. Ames et al. (1983b) investigated U(VI) sorption to amorphous Fe-oxyhydroxide from 0.01M NaCl and 0.01M $NaHCO_3$, at temperatures of 25°C and 60°C. The initial U(VI) concentration ranged from 10^{-4}M to 5×10^{-7}M. Distribution coefficients ranged

from more than 2 x 10^6 mL g^{-1} from 0.01M NaCl to around 3 x 10^4 mL g^{-1} from 0.01M $NaHCO_3$. The uranium sorption data were found to fit a Dubinin - Radushkevich sorption isotherm (Dubinin and Radushkevich, 1947; Sokolowska and Szczypa, 1980). This isotherm has the following equation:

$$X = X_m \exp(B.\ E^2) \qquad (3.1)$$

where X is the amount of uranium sorbed, X_m is the maximum amount of uranium that can be sorbed on the solid for the experimental conditions, B is a constant with the dimensions of energy and E is equal to RT ln(1 + 1/C). R is the gas constant in kJ $K^{-1}mol^{-1}$, T is the absolute temperature (in kelvins, K) and C is the equilibrium uranium solution concentration. Sokolowska and Szczypa (1980) report that this equation implies a quasi-Gaussian distribution of sorption centers.

One of the more complete sets of data for sorption of U(VI) to an iron oxide was obtained by Tripathi (1983). In these studies, batch experiments were performed of the adsorption of uranium (VI) onto goethite as a function of pH, total uranium concentration, adsorbent/adsorbate ratio and ionic strength. The effects of complex formation between the uranyl ion and carbonate, fluoride and phosphate were also studied. The major findings by Tripathi (1983) are summarised below.

In the absence of any complexants:

(a) the adsorption data was similar to that of other hydrolyzable metal ions, with a very sharp "pH edge" separating low adsorption at low pH from high adsorption at higher pH,

(b) with increasing total uranium concentration (ΣU) the adsorption edge shifted to a higher pH,

(c) the adsorption edge was found to be independent of ΣU below 100ppb,

(d) there was a small shift of the adsorption edge to higher pH values with increasing ionic strength,

(e) at fixed ΣU the adsorption edge shifted to a higher pH with decreasing surface area (i.e. on decreasing the adsorbent/adsorbate ratio).

In the presence of carbonate:

(a) up to a pH of 7, the adsorption behaviour of U(VI) was essentially identical in carbonate-free and carbonate-bearing systems,

(b) when the $UO_2(CO_3)_2^{2-}$ and $UO_2(CO_3)_3^{4-}$ species dominate U speciation, there is a sharp decrease in the extent of uranium adsorption, with a resultant upper pH or "desorption" edge,

(c) very high U(VI) adsorption was observed under conditions where $(UO_2)_2CO_3(OH)_3^-$ was the predominant aqueous uranyl species, and

(d) on increasing goethite surface area, the upper pH edge shifted to higher pH and, as observed in the absence of carbonate, the lower pH edge moves to lower pH.

In the presence of fluoride, the formation of uranyl-fluoro complexes caused a decrease in adsorption of uranium in acidic solutions. In the presence of approximately 1 μM phosphate, a slight decrease in adsorption of uranium was observed at pH < 6.5. Otherwise, behaviour in the presence of these ligands was similar to the ligand free case.

The results of a comprehensive study of uranyl uptake on iron oxides (amorphous Fe oxyhydroxide, goethite and hematite) were reported by Hsi and Langmuir (1985). Adsorption was studied as a function of solution pH, ionic strength, electrolyte concentrations, competing cation concentrations, and carbonate complexing (with a total uranyl concentration of 10^{-5}M). Solution pH's ranged from 3 to 10 in 0.1M $NaNO_3$ solutions containing up to 0.01M $NaHCO_3$. All the iron oxides strongly adsorbed uranyl species at pH's above 5 to 6, with adsorption greatest onto amorphous ferric oxyhydroxide, and least onto well crystallized hematite. The presence of 10^{-3}M calcium or magnesium did not significantly affect uranyl adsorption. However, uranyl carbonate and hydroxy-carbonate complexing severely inhibited adsorption.

Similar results have been described by Ho and coworkers for uranyl uptake on hematite (Ho and Doern, 1985; Ho and Miller, 1986) and magnetite (Sagert et al., 1989). These workers gave considerable attention to the nature of the adsorbed uranyl species, particularly in the presence of carbonate and concluded, as did Tripathi (1983), that $(UO_2)_2CO_3(OH)_3^-$ is the active species involved in the adsorption when carbonate is present. Ho and Doern (1985) concluded that $(UO_2)_3(OH)_5^+$ was the major U(VI) species involved in the adsorption process in the absence of carbonate.

The uptake of uranyl species in the pH range 6-8 on precipitating amorphous Fe-oxyhydroxide was examined by van der Weijden et al. (1985). Very similar adsorption behaviour was observed on precipitating and pre-formed oxyhydroxides with adsorption maxima around pH 6.5.

Venkataramani and Gupta (1991) examined the sorption of 10^{-4}M U(VI) onto magnetite and other oxides (thorium and titanium) in the presence of NO_3^-, Cl^-, SO_4^{2-} and CO_3^{2-}, as a function of pH and anion concentration. The distribution of surface hydroxyl groups and the surface pH were determined from pH titration curves in the presence of varying anion concentrations. These workers concluded that a surface species resembling the dimeric aqueous hydroxouranyl species $[(UO_2)_2(OH)_2]^{2+}$ best accounted for the experimental data.

3.1.3. Natural substrates

Ames et al. (1982) reported on the partitioning of U(VI) between two synthetic groundwaters (pH 8.0 and pH 10.0) at 23°C and 60°C and basalt and associated

secondary minerals. While basalt sorption was relatively insignificant, uptake by the secondary minerals present (mainly smectites with traces of iron oxyhydroxides) was found to be important. After consideration of several sorption isotherms, the Dubinin-Radushkevich isotherm (described above) was selected as the best fit to the uranium sorption data.

The removal of the small Fe-oxide impurity on the smectites (0.676 ± 0.022 %) using a sodium dithionite-citrate-bicarbonate reagent had a profound effect on uranium sorption, with distribution coefficients decreasing by at least an order of magnitude. Ames et al. (1982) found that the U sorption data obtained after the removal of the Fe-oxides corresponded to the Freundlich isotherm, rather than the Dubunin-Radushkevich isotherm. The Freundlich equation implies an exponential distribution of sorption centres (Sokolowska and Szczypa, 1980).

The results of batch experiments of the sorption of U (and other radionuclides) to thirteen sandy and six clay sediments from Gorleben in Germany were reported by Warnecke et al. (1984). Groundwater and sediment were separated by 0.45 μm filtration and experiments were run at room temperature. The uptake of U was highly variable, with R_d values varying over a very wide range (0.5 - 5000 mL / g). The authors concluded that "many of the radionuclides had broad ranges of distribution", and the influencing parameters should be identified, particularly if the objective is to select realistic data to predict the migration of radionuclides in the geosphere. Given the results of this study (and others), it is not surprising that the sorption behaviour of radionuclides such as U has become the focus of further detailed investigations.

Results of batch studies of uranium partitioning between a synthetic groundwater and crushed rock samples from the weathered zones in the vicinity of the Koongarra and Ranger uranium deposits in northern Australia were reported by Duerden et al. (1987). The Koongarra sample was a highly weathered schist, containing 31% quartz, with kaolinite the dominant clay mineral and significant amounts of goethite and hematite. The surface area, measured using ethylene glycol monoethyl ether (EGME), was 29 m^2g^{-1}, and the total uranium content was 392 μg g^{-1}. The sample from the Ranger deposit contained 10% quartz, with smectite and kaolinite the main clay minerals. Mica, goethite, anatase and hematite were present in small amounts. The uranium content was 83 μg g^{-1}. The EGME surface area was 145 m^2g^{-1}. The higher surface area of this sample was attributed to the presence of smectites.

Separate subsamples of approximately 200 mg of crushed rock were added to 100 mL of synthetic groundwater (spiked with ^{236}U) for each experiment. The contact time was seven days, after which a sample of the aqueous phase was separated from the solid by centrifugation. A known amount of ^{232}U tracer was added and the uranium separated and electrodeposited on a planchette for α-spectrometry. Results of the sorption experiments are shown in Figure 3.1.

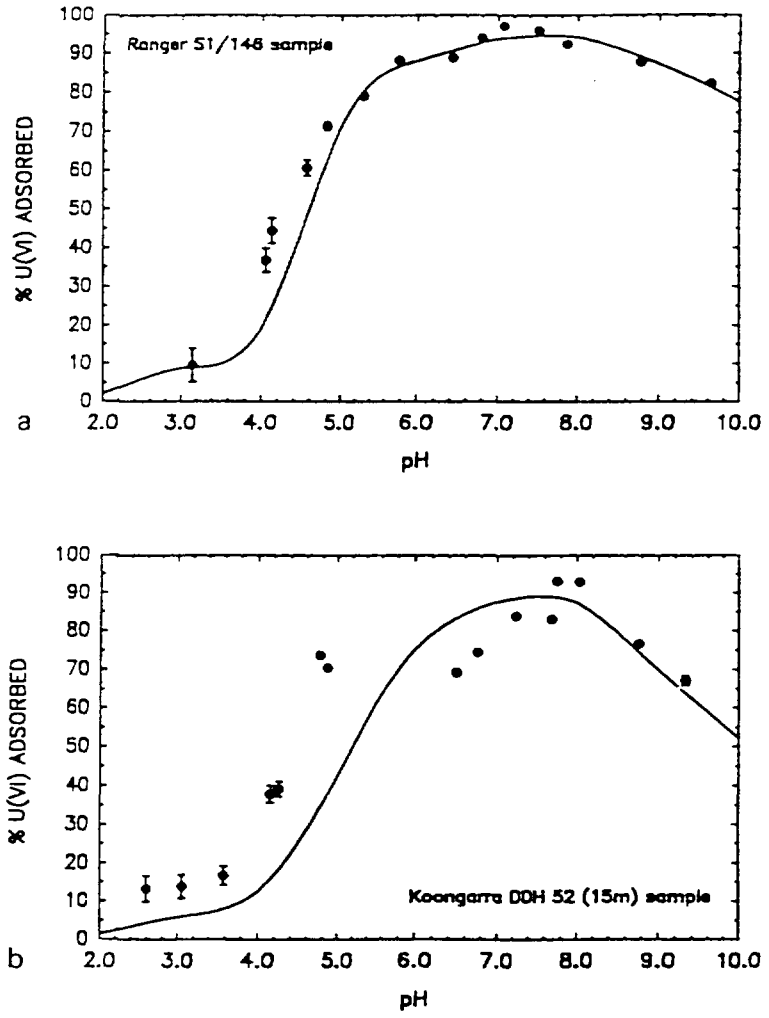

FIGURE 3.1 Uranium sorption behaviour as a function of pH on a) Ranger sample S1/146 (4 m), and b) Koongarra sample DDH5 (15 m).

The results of these experiments are qualitatively similar to those obtained by other workers for geologic substrates, with sorption being strongly dependent on pH. Maximum adsorption for both samples was between approximately pH 7 and pH 8. The greater scatter of the results for the Koongarra sample may result from sample inhomogeneity, or possibly incomplete separation of particulate material from the aqueous phase during centrifugation. Adsorption on the Ranger sample was generally greater than for the Koongarra sample, and presumably reflected the higher surface area in the Ranger case.

3.2 In-situ Studies of U Distribution at Koongarra

An extensive amount of data on ^{238}U concentrations in Koongarra cores, and for groundwaters from the same borehole at similar depths, has been obtained through the Alligator Rivers Analogue Project, and previous studies of the site. Consequently, it is possible to calculate P values (as defined in Section 2.3.1 above) for the solid phase and 'contacting' groundwaters. Uranium concentration data for groundwaters from certain depths in PH and W holes are compared with the ^{238}U content of nearby bulk rock in Table 3.2. (Details of borehole construction and water sampling are given in Sections 2.1 and 3.1 of Volume 7 of this series).

Table 3.2 shows the calculated partition coefficients (P) for the bulk rock samples and associated groundwaters. These are found to be in the range from about 1000 to 60,000 mL/g.

In addition to the concentration of ^{238}U in bulk rock, the concentration of ^{238}U in fine fractions (< 10 μm) of Koongarra weathered zone substrates has also been determined. This fraction is considered likely to dominate uranium scavenging in the system. Both total uranium concentrations and concentrations soluble in a Tamms acid oxalate (TAO) solution (an indicator of uranium bound to amorphous iron oxides) were determined for solids from specified depths. Partitioning coefficients (P) were computed using the range of uranium concentrations found at these depths (Tables 3.3 and 3.4 respectively).

In general, the P values for the fine fractions in Tables 3.3 and 3.4 (range 27,000 - 110,000 mL/g) are slightly higher than the bulk rock values presented in Table 3.2. Although there is only a relatively small amount of data, this would be consistent with the higher specific surface area of the smaller particles, leading to greater sorption on a mass basis (Megumi and Mamuro, 1977).

Comparison of Table 3.3 and 3.4 shows that the P values obtained for the TAO-extractable U content are somewhat lower than those based on total U content. This underlines the comments of McKinley and Alexander (1992a), that P values should be treated rather cautiously. In this case, the total U content clearly includes some U bound in 'inaccessible' (non-extractable) phases, and when this total U content is used to calculate a P value, the resulting value is higher than is obtained on the basis of the TAO-extraction. This second (TAO) value probably more closely represents the P value of sorbed uranium. If total U content is used, the calculated P value is certainly higher than the 'real' sorption K_d. Such an error, if inadvertently transferred to a transport code, could lead to under-predictions of radionuclide mobility.

These data are discussed in more detail (together with corresponding data for thorium isotopes) in Chapter 7 of Volume 8 of this series.

3.3 Review of Results of Modelling U(VI) Sorption

3.3.1 Application of adsorption isotherm equations

As discussed above, sorption data on a wide range of simple and complex substrates appears to be satisfactorily described by either a Freundlich or (less commonly) a Dubinin-Radushkevich expression. While such expressions are empirical, their derivation from available data does enable interpolation to other conditions (particularly the concentration of the adsorbate) and, as such, they can be considered predictive tools. In addition, the type of isotherm found to be appropriate also provides insight into the extent of site homogeneity. Thus, a Langmuir isotherm, which is linear (unit log slope) at low concentrations, and levels off (zero slope) at higher concentrations implies that sorption affinity remains constant until site saturation is approached; it is consistent with a single type of binding site.

TABLE 3.2

AVERAGED BULK ROCK ^{238}U CONTENTS COMPARED WITH ^{238}U CONCENTRATIONS IN GROUNDWATERS FROM THE SAME DEPTH

Borehole/Depth	Bulk Rock [^{238}U] (µg/g)	Groundwater [^{238}U] (µg/L)	P (mL/g)
PH14 (20-26 m)	548	30.8	1.8×10^4
PH14 (20-22 m)	670	65.2	1.0×10^4
PH49 (28-30 m)	5,865	165.6	3.5×10^4
PH49 (44-46 m)	809	199.6	4.0×10^3
PH55 (26-28 m)	26	0.5	5.8×10^4
PH55 (40-42 m)	4	1.02	3.9×10^3
PH56 (26-28 m)	32	9.69	3.3×10^3
PH56 (43-45 m)	7	7.09	9.9×10^2
PH58 (25-27 m)	4	1.82	2.2×10^3
PH58 (38-40 m)	3	0.76	3.9×10^3
PH61 (26-28 m)	8	3.44	2.3×10^3
PH61 (43-45 m)	6	3.47	1.7×10^3
PH80 (17-20 m)	69	7.8	1.1×10^4
PH88 (28-30 m)	22	2.52	8.7×10^3
PH88 (38-40 m)	8	3.14	2.5×10^3
PH94 (26-28 m)	2	0.2	1.0×10^4
PH94 (40-42 m)	3	0.38	7.9×10^3
PH96 (16-26 m)	2	0.28	7.1×10^3
W1 (13 m)	278	6.2	4.5×10^4
W1 (24 m)	250	60.4	4.1×10^3
W2 (14 m)	46	43.3	1.1×10^3
W3 (14 m)	60	5.5	1.1×10^4
W3 (24 m)	9.2	1.6	5.8×10^3
W4 (14m)	1,418	441	3.2×10^3
W4 (24 m)	3,330	367	9.0×10^3
W7 (13 m)	6.6	1	6.7×10^3

TABLE 3.3

PARTITION COEFFICIENTS (P) BASED ON TOTAL ^{238}U CONTENT OF FINE PARTICLE (< 10μm) FRACTIONS OF CORES FROM THE WEATHERED ZONE OF THE KOONGARRA ORE BODY.

Sample	Groundwater [^{238}U] (μg/L)	Solid [^{238}U] (μg/g)	P_{total} (mL/g)
W1 (13.0-13.2 m)	3.2-8.8#	356	$4.0x10^4$ - $1.1x10^5$
W2 (14.0-14.2 m)	16.1-83.3	426	$5.1x10^3$ - $2.6x10^4$
C8 (25 m)	2.27	45	$2.0x10^4$

range of U concentrations in sampled groundwaters

TABLE 3.4

PARTITION COEFFICIENTS (P) BASED ON TAO-EXTRACTABLE ^{238}U CONTENT OF FINE PARTICLE (< 10μm) FRACTIONS OF CORES FROM THE WEATHERED ZONE OF THE KOONGARRA ORE BODY.

Sample	Groundwater [^{238}U] (μg/L)	TAO extractable [^{238}U] (μg/g)	$P_{accessible}$ (mL/g)
W1 (13.0-13.2 m)	3.2-8.8	43	$4.9x10^3$ - $1.4x10^4$
W2 (14.0-14.2 m)	16.1-83.3	225	$2.7x10^3$ - $1.4x10^4$
C8 (25 m)	2.27	23.1	$1.0x10^4$

Multiple site types are implied by other isotherm equations. Thus, the Dubinin-Radushkevich equation implies a quasi-Gaussian distribution of sorption centres, while the Freundlich equation implies an exponential distribution (Sokolowska and Szczypa, 1980). As will be seen later, such site heterogeneity for oxides is usually modelled simplistically by assuming the presence of a relatively high number of lower-affinity sites and a smaller number of high-affinity sites.

3.3.2 Surface complexation approaches

During the last ten years, a number of authors have applied the surface complexation approach to modelling the partitioning of U(VI) between solid and solution phases. The basic modelling approaches have been similar, with differences in the mode of description of the electrical double layer and, more importantly, in assignment of the form of the surface complex.

Tripathi (1983) used the "Stanford Generalized Model for Adsorption" (SGMA) which contained a triple layer description of the electrical double layer (EDL), essentially as outlined by Davis et al. (1978). Some of the experimental results of Tripathi's work were discussed in Section 2.1.2.

Tripathi found that, **in the absence of complexing ligands,** only one adsorption reaction:

$$SOH + UO_2^{2+} + 3H_2O = SOH_2^{+}\text{-}UO_2(OH)_3^{-} + 2H^{+} \qquad (3.2)$$

with log K = -7.0 was required to explain the pH dependence (adsorption edge) for U(VI) onto goethite, at various adsorbate / adsorbent ratios for U(VI) < 250 ppb.

The addition of a second reaction:

$$SOH + 3UO_2^{2+} + 8H_2O = SOH\text{-}(UO_2)_3(OH)_8^{2-} + 8H^{+} \qquad (3.3)$$

with log K = -31.3 was needed to improve the model fit at U(VI) > 250 ppb.

Although polymeric uranyl species, such as $(UO_2)_3(OH)_7^{-}$ and $(UO_2)_3(OH)_5^{+}$ were the major U species in some experimental systems, adsorption of polymeric uranyl hydroxo complexes could not be used to describe the low pH adsorption edge in ligand-free solutions.

In the presence of carbonate, the above model worked well under conditions where $UO_2(CO_3)_2^{2-}$ and $UO_2(CO_3)_3^{4-}$ were the major uranyl complexes, but was less successful in modelling U uptake at smaller adsorbent / adsorbate ratios in the near-neutral pH range, where $(UO_2)_2CO_3(OH)_3^{-}$ was the predominant solution phase species. Under these conditions, the experimental data indicated almost complete removal of U(VI) from solution.

The model developed for the ligand-free system worked well in describing uranium partitioning **in the presence of fluoride,** correctly predicting the decrease in U(VI) adsorption due to the formation of UO_2F^{+} and $UO_2F_2^{\circ}$.

U(VI) uptake was not significantly affected by **the presence of phosphate,** which was inconsistent with the existence of the $UO_2(HPO_4)_2^{2-}$ complex (which had been proposed by Langmuir (1978) as being of major importance in phosphate-containing systems).

Hsi and Langmuir (1985) also used the surface complexation model with a triple layer description of the EDL to describe their experimental results on ferric oxyhydroxides. These workers assumed that the dominant solution phase species - UO_2OH^+ and $(UO_2)_3(OH)_5^+$ - were adsorbed and found good agreement between experiment and model using the following surface complexation reactions:

$$SOH + UO_2^{2+} + H_2O = SO^-\text{-}UO_2OH^+ + 2H^+ \quad (3.4)$$

$$SOH + 3UO_2^{2+} + 5H_2O = SO^-\text{-}(UO_2)_3(OH)_5^+ + 6H^+ \quad (3.5)$$

with log K values of -8.0 and -15.0 respectively. The possibility of formation of bidentate and tridentate surface complexes was also considered, with a bidentate complex of the form $(SO^-)_2\text{-}(UO_2)_3(OH)_5^+$ with log K = -20.0 (in conjunction with $SO^-\text{-}UO_2OH^+$) fitting the data equally well. In the presence of carbonate, Hsi and Langmuir (1985) found it necessary to include surface carbonate complexes, and assumed that the dominant solution phase species were adsorbed; i.e.

$$SOH + UO_2^{2+} + 2CO_3^{2-} + H^+ = SOH_2^+\text{-}UO_2(CO_3)_2^{2-} \quad (3.6)$$

$$SOH + UO_2^{2+} + 3CO_3^{2-} + H^+ = SOH_2^+\text{-}UO_2(CO_3)_3^{4-} \quad (3.7)$$

with log K values of 30.0 and 38.5 respectively. While these surface complexation reactions and the associated constants provided excellent fits to uranyl adsorption data onto goethite for total carbonate (C_T)= 10^{-2}M, the same intrinsic constants were less successful in modelling adsorption data for C_T = 10^{-3}M. To obtain the best agreement with these data, it was necessary to assume log K = 29.5 for $SOH_2^+\text{-}UO_2(CO_3)_2^{2-}$ and log K = 42.5 for $SOH_2^+\text{-}UO_2(CO_3)_3^{4-}$.

Payne and Waite (1991) attempted to use a similar reaction set in modelling U(VI) uptake on a weathered schist, based on the assumption that the amorphous iron oxide component dominated U uptake. In order to fit the experimental data, considerable adjustment of the adsorption constants (by trial and error) was required. At the carbonate concentrations used in these studies (2 mM), the $UO_2CO_3^\circ$ species was assumed to be important in the pH 4.8-6.4 range, and improved fits were obtained to the adsorption data when a uranyl monocarbonate complex was included in the suite of possible surface complexes. Good fits over a wide pH range were then obtained, for uranyl adsorption data to two different weathered zone substrates. A major conclusion from the study was that even after major simplifications regarding the nature of the surface, considerable fitting of adjustable parameters was required to model the data. This study highlighted some of the problems in modelling sorption data on natural substrates.

Gupta and Venkataramani (1988) examined the sorption of uranyl ions on a range of oxides including magnetite as a function of pH. These authors visualised the sorption process as the linking of uranyl ions with two adjacent free surface hydroxyl groups without deprotonation and formation of dimer-like structures on the surface, i.e.

$$2SOH + UO_2^{2+} = (SOH)_2UO_2^{2+} \quad (3.8)$$

Only for pH > pH_{pzc} was the deprotonation of the surface hydroxyl groups considered to occur, i.e.

$$2SOH + UO_2^{2+} = (SO)_2UO_2^{o} + 2H^{+} \quad (3.9)$$

Venkataramani and Gupta (1991) reported extensive additional studies of U(VI) sorption to the same oxides in the presence of nitrate, chloride, sulfate and carbonate ions as a function of pH and anion concentration and concluded that their "surface hydrolysis" model adequately accounted for the observed results.

3.4 Summary

In conclusion, a review of previous studies indicates a multiplicity of modelling approaches. In addition, experimental design has often lacked adequate rigour in definition and / or control of experimental conditions, such as presence / absence of CO_2, pH control, presence of ligands, etc. In some studies, high uranium concentrations which considerably exceed those normally found in natural (or even polluted) water samples, and possibly exceed solubility limits, have been used. With some exceptions (such as Tripathi, 1983) there has not been a significant attempt to examine U sorption over a wide range of conditions, with experimental variables such as pH, ionic strength, total U, and pCO_2 varied in a systematic manner to probe the characteristics of U uptake. These limitations seriously limit the worth of a considerable portion of the previous experimental and computational work in the sorption field.

4 EXPERIMENTAL METHODS

4.1 Preparation and Properties of Single Substrates

Methods of preparation and/or purification of ferrihydrite, kaolinite and quartz are detailed below, as is basic characterisation information. Adsorption studies were also undertaken on aged ferrihydrite and in systems in which uranium was co-precipitated with the ferrihydrite. Details of these studies are given in Section 7 and Section 4.3.3 respectively.

4.1.1 Ferrihydrite

The ferrihydrite was formed by raising the pH of a Fe^{3+}/HNO_3 solution to 6.0, and then aged for 65 hours in a continuously stirred, pH - controlled vessel at 25°C. The resulting slurry contained a reddish-brown precipitate of ferrihydrite (also referred to as 'amorphous iron oxyhydroxide' or 'hydrous ferric oxide'), which is usually assigned a chemical formula $Fe_2O_3.H_2O$, although sometimes the formulae $Fe_5HO_8.xH_2O$, or $Fe(OH)_3$ may be used. In recent years it has been commonly assigned a surface area of 600 m^2 / g of $Fe_2O_3.H_2O$ (Dzombak and Morel, 1990). Experiments were typically carried out with total Fe concentrations of 10^{-3} M, this is referred to in the text as '10^{-3} M ferrihydrite'.

4.1.2 Quartz

Commercially available quartz particles of narrow size range (8-15 micron in diameter) were exhaustively cleaned by repeated acid and base washings. The particles were thoroughly rinsed prior to use in sorption studies.

4.1.3 Kaolinite

Two kaolinites, the Clay Minerals Society standard, KGa-1 (from Georgia, USA), and a Japanese standard, Nichika #15-27-2 (from California, USA) were chosen for the study of uranium sorption. KGa-1 has been described in detail by Van Olphen and Fripiat (1979). As indicated in Table 4.1, the bulk chemical composition of the two clays is similar, except that the Nichika kaolinite contains significantly more iron than the KGa-1 standard.

A measure of "excess" iron (extractable by the CDB reagent - Yanase et al., 1991) confirmed the greater abundance of iron in the Nichika sample (Table 4.2). The Nichika kaolinite also has a significantly higher cation exchange capacity (CEC) and BET surface area than the KGa-1 kaolinite (Table 4.2). The CEC was determined by saturation of the sample with Ba, followed by replacement of the Ba with Mg. The amount of Mg lost from solution gives a measure of the cation exchange capacity (Page et al., 1982).

TABLE 4.1

CHEMICAL COMPOSITION OF NICHIKA #15-27-2 AND KGA-1 KAOLINITES

Component	Nichika #15-27-2[2]	KGa-1[1]
SiO_2	45.53%	44.2%
Al_2O_3	35.71	39.7
Fe_2O_3	1.52	0.13
FeO	0.09	0.08
MgO	0.08	0.03
CaO	0.04	n.d.[3]
MnO	-	0
Na_2O	0.03	0.01
K_2O	0.28	0.05
TiO_2	1.4	1.39
H_2O	13.47	12.6
H_2O^-	0.71	1.18
F	-	0.01
P_2O_5	-	0.03
Total	99.86	99.4

[1] Source: Georgia, USA

[2] Source: Dixie Rubber Pit, CA, USA
SiO_2:Al_2O_3 = 210:100
Kaolinite 92.95%
Impurities 7.05%

[3] n.d. = not detectable

TABLE 4.2

CATION EXCHANGE CAPACITY (CEC), SURFACE AREA AND EXCESS IRON CONTENT OF KAOLINITE SAMPLES

Parameter	Nichika #15-27-2	KGa-1
CEC (meq/100 mg)	3.9	1.9 (2.0)[1]
Surface area (m^2/g)	26.38	8.68 (10.05)
Excess iron (mg/g)	0.99	0.13

[1] Figure in parenthesis is from Van Olphen and Fripiat, 1979

4.2 Preparation and Properties of Naturally Occurring Koongarra Substrates

4.2.1 Preparation

Cores were obtained from a number of locations (W1, W2, M2 and W7) in the Koongarra weathered zone using a cable-tool rig, which produces intact samples (rather than the pulverised samples obtained with a percussion rig). Samples from the 14.0-14.2 m depth of W2, and from the 13.0-13.2 m depth of W1, were given particular attention in the sorption studies reported here. The W1 core is a highly weathered schist from above the upstream edge of the orebody - a region considered to be the former upward extension of the primary ore. W2 is near the leading edge of the dispersion fan in the sub-economic ore zone, approximately 50 metres down-gradient from the primary ore zone.

For the batch sorption studies, large particles (> approx. 10 μm) were excluded because most of the surface area (and the bulk of the U(VI) affinity) is associated with small particles (Megumi and Mamuro, 1977; Megumi et al., 1982). Furthermore, small particles can be more reproducibly sampled, as a much larger number are present in a given mass (hence minimizing statistical fluctuations).

The following treatment and subsampling procedure (modified from Gee and Bauder, 1986) was applied to the W1 and W2 samples. Firstly, the (non-dried) sample was crumbled by hand then gently shaken in mQ water to break it up further. The material was then passed through a mesh of approximately 1.5 mm diameter, removing the larger size fraction ("wet sieved"). The < 1500 μm fraction thus obtained was then vigorously shaken, and allowed to settle in a tall measuring cylinder. After 40 minutes settling, the upper 500 mL of the suspension was sampled. Application of Stoke's law suggested that this fraction contained particles of less than 10 μm effective (nominal) diameter.

The resulting slurry contained a homogeneous suspension of fine particles which could be reproducibly sub-sampled by vigorous agitation, followed by removal of an aliquot of known volume. The fine particle stock slurries contained between 20 mg and 200 mg of particles per mL, and repeat samplings showed that the sample removal technique was reproducible to within 3% (considered more than adequate for sorption experiments).

The mass distributions of particles in the original samples were computed after allowing for the partial recovery of the <10 μm fraction (although efficient in removal of the large particles, the sedimentation technique does not fully recover the fines). The fine fraction comprised approximately 31% of the total mass of the W1 sample, but only about 8% of the total mass of W2 (Table 4.3).

The size distributions in the two slurries were measured with a Malvern autosizer. This suggested that the particle sizes were slightly greater than estimated on the basis of applying Stoke's law to the separation procedure, with the fine slurry of W2 containing generally smaller particles than W1 (Figure 4.1). The results may be ascribed to a number of factors including particle geometry, density, aggregation and the lower mass loadings used in the auto-sizer sample.

TABLE 4.3

PERCENTAGE OF MASS OF CORE MATERIALS FROM W1 (13.0-13.2 M) AND W2 (14.0-14.2 M) IN VARIOUS SIZE CLASSES

Core	% by mass in size class		
	> 1500 μm	10-1500 μm	< 15 μm
W1 (13.0-13.2 m)	27	42	31.5
W2 (14.0-14.2 m)	56	36	7.7

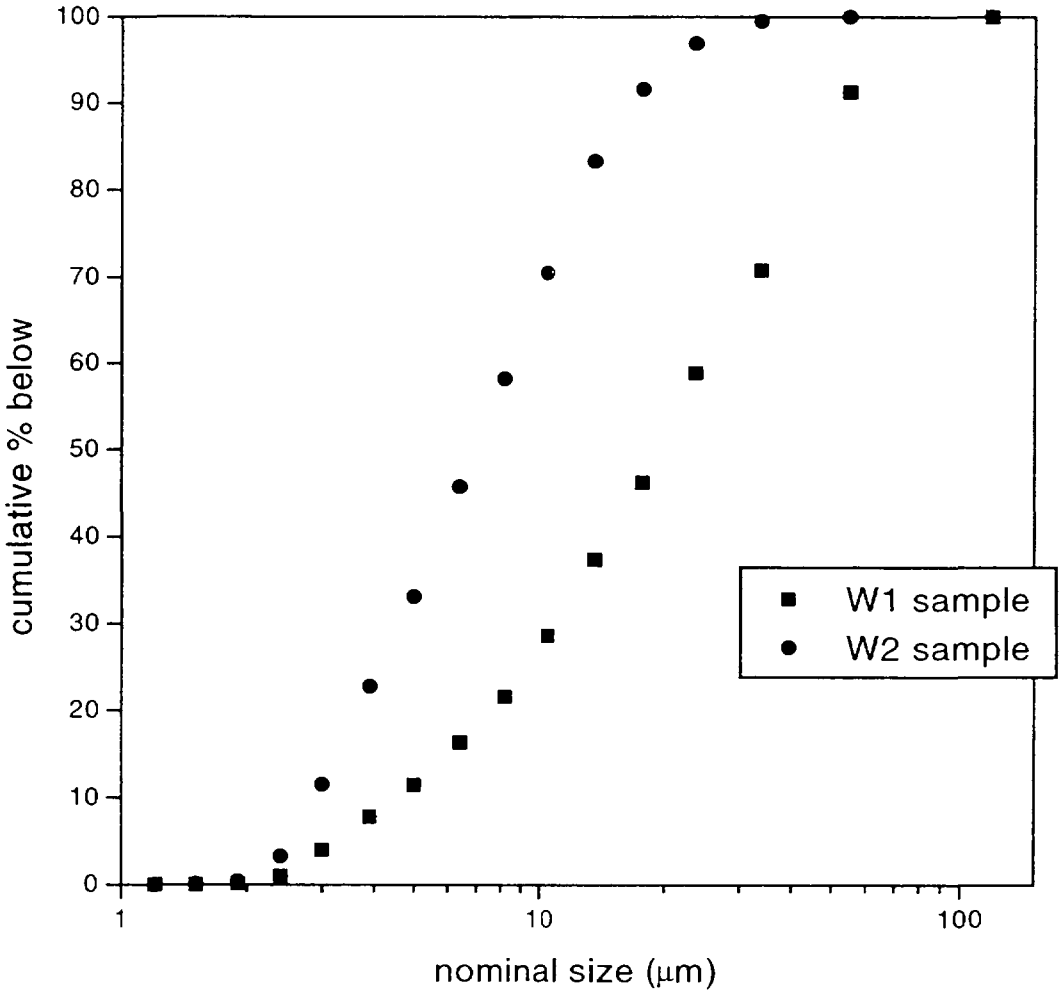

FIGURE 4.1 Size distribution of solids from bores W1 and W2

4.2.2 Properties

Both W1 and W2 are predominantly kaolinite, however the W1 sample has greater amounts of hematite as evidenced by its brick-red colour. In contrast, the W2 sample is yellow / brown.

Detailed scanning electron microscopy of the W1 and W2 fine fractions was undertaken with energy dispersive spectra (EDS) obtained for chosen particles and agglomerates. All EDS spectra exhibited peaks of Si and Al. Where only Si and Al were present, the particles were assumed to be kaolinite. Where K was observed in the EDS, it was attributed to the presence of mica. A peak of Mg was assumed to indicate chlorite, or more probably altered chlorite (this may include vermiculite or smectite). Characteristics of individual points in W1 and W2 examined by EDS are reported in Table 4.4, and a summary of characteristics given in Table 4.5.

TABLE 4.4

COMPOSITION OF INDIVIDUAL POINTS ON W1 AND W2 SAMPLES (SEM/EDS)

Sample	Mineral phases	Size	Elements present[1]
W1	Kaolinite	30 μm	Si, Al > Fe
(13.0-13.2 m)	Fe-dominated	Coating on 30 μm kaolinite	Fe > Si, Al, P
	Kaolinite/mica	10 μm	Si, Al > K
	Fe-dominated	1 μm	Fe > Si, Al
	Kaolinite	15 μm	Si, Al >
	Kaolinite	80 μm	Si, Al >
	Kaolinite (Fe)	2 μm	Si, Al > Fe
W2	Kaolinite/mica	3 μm	Si, Al > Fe, K
(14.0-14.2 m)	Chlorite, probably altered (Fe)	6 μm	Si, Al, Fe, Mg >
	Kaolinite/altered chlorite (Fe)	5 μm	Si, Al, > Fe, Mg
	Kaolinite/altered chlorite (Fe)	5 μm	Si, Al > Fe, Mg
	Kaolinite	11 μm	Si, Al >
	Fe-dominated	2 μm	Fe > Si, Al

[1] In order of EDS peak size
">" separates major and minor components
Brackets indicate only a trace component

The main features of the samples can be generalised as follows:

(a) the mineralogy of W1 and W2 is very uniform being dominated by kaolinite in both cases,

(b) W1 contains large flakes of over 50 μm in size. These particles presumably settle slowly due to their shape hence are included in the nominal < 10 μm fraction obtained by sedimentation,

(c) as indicated in Table 4.3, a relatively large proportion of W1 is found in the nominal < 10 μm fraction. This may result from the greater depth of weathering at W1,

(d) mica is a minor component of both samples,

(e) altered chlorite is found in W2 but is almost absent from W1. This may be attributed to the greater depth of weathering (leading to alteration of chlorite) near to the fault,

(f) iron, as well as being found as coatings on clay particles also constitutes numerous separate fine particles of around 1 μm in size (i.e. generally finer than the clays examined),

TABLE 4.5

SUMMARY OF SEM/EDS RESULTS FOR CORES FROM W1 AND W2

Parameter	W1 (13.0-13.2 m)	W2 (14.0-14.2 m)
Size	Flakes to 60 μm	Largest flakes about 10 μm
Bulk EDS - order of peak size	Si, Al > K, Fe > Mg	Si, Al > Fe, Mg > K
Other elements in EDS	P (in Fe dominated coatings)	-
Minerals present	1. Kaolinite	1. Kaolinite
	2. Mica	2. Altered chlorite
	3. Fe-minerals	3. Fe minerals
		4. Mica
Colour	Red	Brown/yellow

(g) these fine iron dominated particles appear to be aggregates of smaller iron-rich particles. Particles of iron above 1 μm in size also appear to be aggregates, and

(h) the minor components of P, Ti and Mn are only observed in particles rich in Fe, indicating a possible association of these elements.

The BET surface area of the fine fraction of the W2 material (52.3 m^2/g) was significantly higher (per unit mass) than that of the W1 material (24.6 m^2/g). This result is consistent with the observation of larger particles in W1. Details are summarised in Table 4.6.

TABLE 4.6

BET SURFACE AREA RESULTS FOR BULK AND FINE FRACTIONS OF W1 (13.0-13.2 M) AND W2 (14.0-14.2 M) CORE MATERIALS

Core	Mass in fines (%)	S.A.[1] of fines (m^2/g)	Bulk S.A. (m^2/g)	% total S.A. in fines (%)
W1 (13 m)	31.5	24.6	17.2	45.1
W2 (14 m)	7.7	52.3	8.4	47.8

[1] S.A. = surface area

A more detailed characterisation of the fine fractions used in the sorption studies was undertaken using selective extraction methods. These methods involve treating the sample with a sequence of chemical reagents, with the objective of partitioning the contained elements amongst a series of phases (e.g., adsorbed metals, carbonate minerals, iron oxides, etc). Although in some cases considerable information about the extracted phases has been obtained, it should be remembered that these phases are operationally defined by the extractants used to remove them. The problems with selective extraction techniques are well documented (Gruebel et al. 1988), but it is generally agreed that the resulting information is of greater use in environmental studies than merely determining total metal concentration (Tessier et al. 1979, and others).

Sequential extraction techniques were successfully applied to samples from the Alligator Rivers region (Yanase et al., 1991), and have been extensively used within the ARAP project. For the samples used in the sorption studies, a TAO-extraction (aimed at removing amorphous coating minerals of iron and other oxides), and a CDB extraction (crystalline iron minerals such as goethite and hematite), were used to provide details of the distribution of U and other elements in the samples, and to estimate the surface area associated with extracted phases. A detailed discussion of the application and results of these techniques is given in Volume 8 of this series. Sequential extraction data for the W1 and W2 samples are presented in Tables 4.7 and 4.8.

TABLE 4.7

EFFECT OF TAMM'S ACID OXALATE (TAO) AND DITHIONITE-CITRATE-BICARBONATE (CDB) EXTRACTION ON BET SURFACE AREAS OF THE FINE FRACTIONS OF THE W1 AND W2 CORE MATERIALS

Treatment	Surface area (m^2/g)		% Surface area remaining after extraction	
	W1 (13 m)	W2 (14 m)	W1 (13 m)	W2 (14 m)
None	19	53.3		
TAO	16.4	48.2	86.3	90.4
CDB	13.3	29.5	70	55.3

The TAO extraction removed 14% and 10% of the surface area of W1 and W2 respectively, whereas the CDB treatment resulted in a greater loss of surface area from the two samples (Table 4.7).

The distribution of the elemental composition amongst the phases removed by a more extensive sequence of extractions is given in Table 4.8, and the percentage distribution is presented in Table 4.9. In these cases, the TAO extraction was preceded by an extraction with Morgan's reagent (to remove adsorbed U and carbonate minerals), and the CDB extraction was followed by a strong acid extraction (clay and some refractory minerals), with a subsequent digestion of residual phases (Yanase et al., 1991).

As shown in Table 4.9, relatively large amounts of the uranium in the substrates were removed by Morgans reagent (8% from W1 and 43% from W2). This reagent (1M sodium acetate, pH 5.0) appears to remove adsorbed uranium, since there is only minor dissolution of other mineral phases. This would be expected since NaOAc, particularly at these concentrations, should outcompete U(VI) for available surface sites and complex U in the solution phase.

Tamms acid oxalate, which dissolves amorphous phases of Fe, Al and Si and some secondary U(VI) minerals, removed 3.5% of the total uranium from W1 and approximately 10% from W2. Crystalline iron oxides are dissolved by the CDB reagent (Edis et al., Volume 8 of this series) and 37% of the uranium in W1 and 15% in W2 was solubilised by this reagent. This indicates uranium is associated with crystalline iron mineral phases, either by structural incorporation or occlusion.

Only 1% of the iron in both the W1 and W2 samples was removed by TAO, but 44% of the total iron present in W1 was solubilised by CDB. This compared with only 6% of iron removed from W2 by CDB extraction. For this substrate, the more severe HCl treatment was required to solubilise the bulk of the iron present.

TABLE 4.8

ELEMENTAL CONCENTRATIONS OF SEQUENTIALLY-EXTRACTED PHASES FROM THE W1 AND W2 FINE FRACTIONS

W1 (13 m)	Elemental distribution (μg extracted/g of solid)							
Extractant	Fe	Al	Mn	Mg	Ca	Ti	K	U
Morgans	119	176	0.3	521	79	0.7	218	30
TAO	875	576	0.5	56	5	4.9	247	12.6
DCB	35,100	1,080	2.8	33	68	45.1	595	131
HCl	35,300	6,370	4.3	278	11	155	1,420	177
Fusion	9,140	166,000	28.3	4,295	7	2,760	9,820	5.2
Σ(mg/g)	80.6	173.8	0.04	5.2	0.2	3	12.3	0.36

W2 (14 m)	Elemental distribution (μg extracted/g of solid)							
Extractant	Fe	Al	Mn	Mg	Ca	Ti	K	U
Morgans	520	605	7.1	3,930	195	3	370	182
TAO	1,170	1,210	147	246	8	5.7	36	43
DCB	6,770	888	30	128	112	2.9	537	65
HCl	79,200	35,000	126	9,670	12	54	280	130
Fusion	20,800	90,300	35	3,480	31	841	7,840	6.4
Σ(mg/g)	108.4	128.1	0.3	17.5	0.4	0.9	9.1	0.43

The data in Table 4.9 show that unusually low $^{234}U/^{238}U$ ratios are measured in the readily extracted phases (Morgan's and TAO extractions) of the W1 and W2 samples. These low ratios are similar to the ratios found in the contacting groundwaters at these two locations (Volume 7 of this series). This observation suggests that in the natural environment adsorption / desorption equilibrium is reached between the groundwater and the accessible phases of the solid.

TABLE 4.9

ELEMENTAL DISTRIBUTION AND URANIUM ACTIVITY RATIOS OF PHASES EXTRACTED FROM W1 (13 M) AND W2 (14 M) FINE FRACTIONS USING VARIOUS REAGENTS

W1 (13 m)	Elemental distribution (% of total)								$^{234}U/^{238}U$
Extractant	Fe	Al	Mn	Mg	Ca	Ti	K	U	
Morgans	0.15	0.1	0.83	10	46.5	0.02	1.8	8.4	0.82
TAO	1.1	0.33	1.4	1.1	2.9	0.16	2	3.5	0.85
DCB	43.6	0.62	7.8	0.64	40	1.5	4.8	37	0.93
HCl	43.8	3.7	11.9	5.4	6.5	5.2	11.5	50	1.02
Fusion	11.3	95.3	78.6	82.9	4.1	93.1	79.8	1.5	1.71
Single TAO	1.7	0.49	1.7	8.7	4	0.2	2.7	9.5	

W2 (14 m)	Elemental distribution (% of total)								$^{234}U/^{238}U$
Extractant	Fe	Al	Mn	Mg	Ca	Ti	K	U	
Morgans	0.48	0.47	2.1	22.5	54.5	0.33	4.1	43	0.61
TAO	1.1	0.94	42.6	1.4	2.2	0.63	0.39	10	0.64
DCB	6.2	0.69	8.7	0.73	31.3	0.32	5.9	15	0.9
HCl	73	27.4	36.5	55.4	3.4	5.9	3.1	31	1.2
Fusion	19.1	70.5	10.1	19.9	8.6	92.8	86.5	1.5	1.83
Single TAO	1.4	1.3	42.6	21.4	8.1	1.2	0.67	50.5	

4.3 Procedures Used in Sorption Investigations

4.3.1 pH edges

In the case of ferrihydrite, aliquots of the pre-aged slurry were transferred directly to open 25 mL polypropylene centrifuge tubes, and sufficient $NaNO_3$ was added to bring the suspensions to the correct ionic strength (typically 0.1 M $NaNO_3$ except in the ionic strength dependency studies). The volume of the aliquots was such that the suspension in each tube was 10^{-3}M in iron. For studies at pH > 7.0, $NaHCO_3$ was added, sufficient to achieve equilibrium with the CO_2 in air at the experimental pH. The pH of the slurry was adjusted to the experimental value, and the tube was shaken for 24 hours in a water bath at 25°C. The required amount of uranium was then added (10^{-6}M except in studies of dependency on total uranium concentration), with immediate readjustment of the pH.

After 48 hours (this duration was chosen after preliminary kinetic studies, discussed below), the solid and liquid phases were separated by centrifugation at 10,000 rpm (>6500 g). The pH stability of the system was checked by measuring the pH after

24 hours and again at the time of sampling. The amount of uranium remaining in solution was typically determined using kinetic phosphorescence analysis (KPA, discussed below) except in cases where very low concentrations of uranium (below the KPA detection limit) were used. In these experiments, the artificial isotope ^{236}U was added and the uptake quantified using α-spectrometry after the addition of a known quantity of ^{232}U (another artificial isotope) as a yield tracer.

For the kaolinite studies, 100 mg of kaolinite was weighed into 30 mL teflon centrifuge tubes, 2.5 mL of 1M $NaNO_3$ was added, and the pH of the solution adjusted to the experimental value using dilute nitric acid or sodium hydroxide solutions. $NaHCO_3$ was again added in appropriate amounts for studies at pH > 7.0. The suspension was then made up to 25 mL and the tube shaken for 24 hours in a water bath at 25°C. Uranium was then added and the adsorption study conducted in an identical fashion to that described for ferrihydrite.

Similar procedures were followed for the studies of uranyl uptake on quartz. A quartz concentration of 100 g/L was typically used, with the quartz substrate suspended in KNO_3 (rather then $NaNO_3$) to avoid NaF precipitation in studies of the effect of fluoride complexation of U(VI). Solute uranium concentrations were determined routinely by kinetic phosphorescence analysis.

In the case of the natural substrates, the stock slurry of fine particles was vigorously agitated to fully suspend the solid and, in the case of W2, aliquots containing 100 mg of particles were transferred to 25 mL polypropylene centrifuge tubes. Each tube had a 2mm hole in the lid to permit air equilibration without loss of sample during agitation. To compensate for the lower ^{238}U content of the W1 core (than found in W2), 500 mg of W1 (rather than the 100 mg for W2) was added to the 25 mL tubes. These experimental procedures ensured that accurate information on ^{238}U desorption could be obtained.

Sodium nitrate and $NaHCO_3$ (if required) were added and the system allowed to equilibrate for 24 hours in a shaking water bath at 25°C. At this stage, ^{236}U (84 dpm or 10^{-7}M) was added and the pH readjusted. After 48 hours of equilibration, the solid and liquid phases were separated by centrifugation. A known amount of ^{232}U tracer was added to the clear supernate and the activities of ^{238}U, ^{236}U and ^{234}U were measured by α-spectrometry.

pH edges were obtained over a wide range of solution/suspension conditions for the single and natural substrates. The range of conditions over which sorption studies were undertaken is summarised in Table 4.10. While most studies were undertaken under atmospheric conditions, some investigations were performed in a glove box at an elevated partial pressure of carbon dioxide. A special gas mixture of 2% CO_2 and 98% N_2 was obtained for these experiments. The gas composition used in the glovebox was a 50:50 mixture of this gas with ordinary air. The gas composition in the glove box was thus approximately 1% CO_2:10% O_2:89% N_2. The presence of oxygen derived from the air ensured the stability of the solid phases against reductive dissolution, and provided a convenient means to monitor the mixing ratio of the air and special gas. This was done by measuring the oxygen

concentration in the glovebox and maintaining the measured value at close to 10%, i.e. half the value in normal air.

TABLE 4.10

RANGE OF CONDITIONS UNDER WHICH pH EDGES HAVE BEEN OBTAINED FOR URANYL ADSORPTION TO VARIOUS SUBSTRATES

Condition	Ferri-hydrite	Nichika kaolinite	KGa-1 kaolinite	Quartz	W1 core	W2 core
Ionic strength	0.004 0.02 0.1 1	0.004 0.1 1	0.1	0.005[1] 0.01 0.1	0.1	0.022 0.1 0.2 2.2
[U(VI)], M	10^{-8} 10^{-6} 10^{-5} 10^{-4}	10^{-6} 5.10^{-7} to $2.7.10^{-4}$[2]	10^{-6}	10^{-6}	see text	see text
Solid to liquid ratio	10^{-3}M, 2.10^{-2}M (as Fe)	1 g/L 4 g/L 16 g/L	4 g/L	100 g/L	20 g/L	4 g/L
CO_2, %	0.03 1	0.03	0.03	0.03	0.03 1	0.03 1
Phosphate, µM	0 2.5, 10, 30[3], 100	0	0	0 2	0	0
Fluoride, mM	0	0	0	0 0.1 0.5	0	0
DCB leach	No	Yes	Yes	No	No	Yes

[1] KNO_3 rather than $NaNO_3$ used to avoid NaF precipitation

[2] Uranium adsorption determined at pH 6.5 only

[3] Effect of phosphate at these concentrations examined only at pH 4.0

It is important when interpreting (and modelling) the experimental results to take into consideration that the amount of U adsorbed was determined from the measurement of *dissolved* uranium concentrations. The percentage of U adsorbed was calculated by subtracting the measured U concentration in solution (which is generally assigned an error of ±4%) from the total U initially added to the experiment. The principal advantages of the experimental technique are that it is simple, reproducible, provides suitable samples for direct U analysis (i.e. liquid phases of low acid strength), and allows the position of the centre of the pH edge to be precisely determined. However, small uptakes of U (corresponding to 15% or less of the total added) cannot be precisely measured by this technique. Consequently, experimental scatter tends to be greatest at low (and high) pH values where U sorption is minimal. To reduce complexity in the figures contained in this Volume, error bars have been omitted, but it is essential to note this feature of the data when considering the experimental results.

4.3.2 Kinetics of U(VI) uptake

As indicated above, preliminary studies of the kinetics of uranium uptake on ferrihydrite and Nichika kaolinite were undertaken in order to choose the appropriate time delay between uranium addition and measurement of partitioning between solid and solution phases. These experiments were carried out using a similar procedure to to that described above, but with only two pH values chosen for each solid, and larger volumes were used to permit repeated sub-sampling from each experimental slurry. Thus, pH's of 4.5 and 5.0 were chosen for ferrihydrite, while pH's of 5.0 and 6.5 were used for kaolinite. Aliquots (10 mL) were removed from the suspension at frequent intervals over 14 days in the case of ferrihydrite. The kinetics of U(VI) adsorption to kaolinite were examined over a much shorter time period (33 hours).

Based on the results of these kinetic investigations, an equilibration period of two days was selected for subsequent uranium sorption experiments. Complete results are presented and discussed below.

4.3.3 Co-precipitation of U(VI) with ferrihydrite

In the sorption studies on ferrihydrite described above, the interaction of U(VI) with a previously formed (and briefly aged) amorphous oxide was investigated. However, in the Koongarra system, the possibility exists of co-precipitation of uranium with iron oxides. In such a case, the partitioning of U(VI) between solid and solution phases may differ from that observed with pre-formed oxide. Laboratory studies of U(VI) co-precipitation over a range of pH were conducted in an attempt to simulate this potential natural process.

In the usual experiments, ferrihydrite was formed by raising the pH of an acidic solution of $Fe(NO_3)_3$ to 6.0. After formation of the precipitate, samples of the ferrihydrite were transferred to a number of 25mL centrifuge tubes. After 24 hours, U was added and the pH was adjusted to the experimental value. The resulting system contained total uranium and iron of 10^{-6}M and 10^{-3}M respectively, in a background electrolyte of 0.1M $NaNO_3$.

For the co-precipitation experiments, a stock solution containing U(VI), ferric ions and $NaNO_3$, in dilute HNO_3 was prepared (the pH of this solution was 2.6). A sample of this solution was removed, and transferred to an open polypropylene centrifuge tube. The pH of the remaining solution was raised to 3.0. This process was repeated, each time transferring a sample then raising the pH, until samples had been collected across the pH range from 2.6 to 6.5. This procedure was carried out as quickly as practicable (within 1 hour), so that the contact time for all the samples was similar to one another, and to that used previously in the adsorption experiments. The samples were then allowed to equilibrate for 2 days in individual tubes at the various pH values. The final pH was then determined and a sample of the supernate separated and analysed using the Kinetic Phosphorescence Analyser (KPA).

The total amounts of uranium and iron in these experiments were the same as those previously used. Therefore, the main difference in the procedure was that the uranium was present and capable of being incorporated within the ferrihydrite (or adsorbed on its surface) during its formation, rather than contacting pre-formed ferrihydrite. However, it should be pointed out that in the co-precipitation experiments, the ferrihydrite is formed at each experimental pH, rather than a single batch being formed at a pH of 6.0.

4.4 Methods of Quantification of Sorbed Uranium

4.4.1 Kinetic phosphorescence analysis

The uranium content of the supernate was determined in many instances using a kinetic phosphorescence analyser (Chemchek Instruments, model KPA-10). In the KPA, a laser pulse is used to electronically excite uranyl-containing ions. The excited phosphor then returns to the ground state with the emission of a photon following first order kinetics. The KPA measures the time-dependent decay of light intensity, and by extrapolation to time zero (i.e. the end of the laser excitation pulse) calculates the initial intensity, which is proportional to the uranium concentration. For good precision, several hundred laser pulses are used in each measurement and the results averaged.

A detection limit of about 0.2 ppb can be achieved, with lower limits possible when interfering substances such as chloride are absent from the system. Comparison with results obtained by α-spectrometry and ICP-MS analysis indicated that the KPA results were accurate to within ±3%, with reduced accuracy when interferences are present (Volume 7 of this series). Most sorption experiments were carried out in 0.1 M $NaNO_3$, which is an excellent medium for KPA measurements.

4.4.2 Alpha spectrometry

Alpha spectrometry was used in these studies for the determination of uranium in instances where ^{236}U was added to the adsorption experiments to access concentration ranges below the detection limit of the KPA. Particular use was also made of α-spectrometry in studies with natural substrates, as it was possible to monitor both the uptake of ^{236}U and the desorption of a portion of the natural ^{238}U

from the samples. The various U isotopes can be simultaneously measured using α-spectrometry.

For these analyses, a known amount of ^{232}U was added to the supernate immediately after separation of the aqueous and solid phases. Following standard radiochemical separation procedures (Volume 7 of this series), the uranium isotopes were counted in an ORTEC ALPHA-KING α-spectrometer, and the amounts of dissolved ^{236}U (and ^{238}U if required) were determined from their count rates relative to ^{232}U.

The uranium spectrum of the solution phase on completion of one experiment using a Koongarra core is shown in Figure 4.2. The ^{238}U peak results from the leaching of natural uranium into the aqueous phase, whereas the ^{236}U peak indicates the amount of the ^{236}U spike remaining in solution after adsorption. The amounts of ^{238}U and ^{236}U in the solution phase were calculated from their count rate relative to the ^{232}U peak after correction for the minor background count rates.

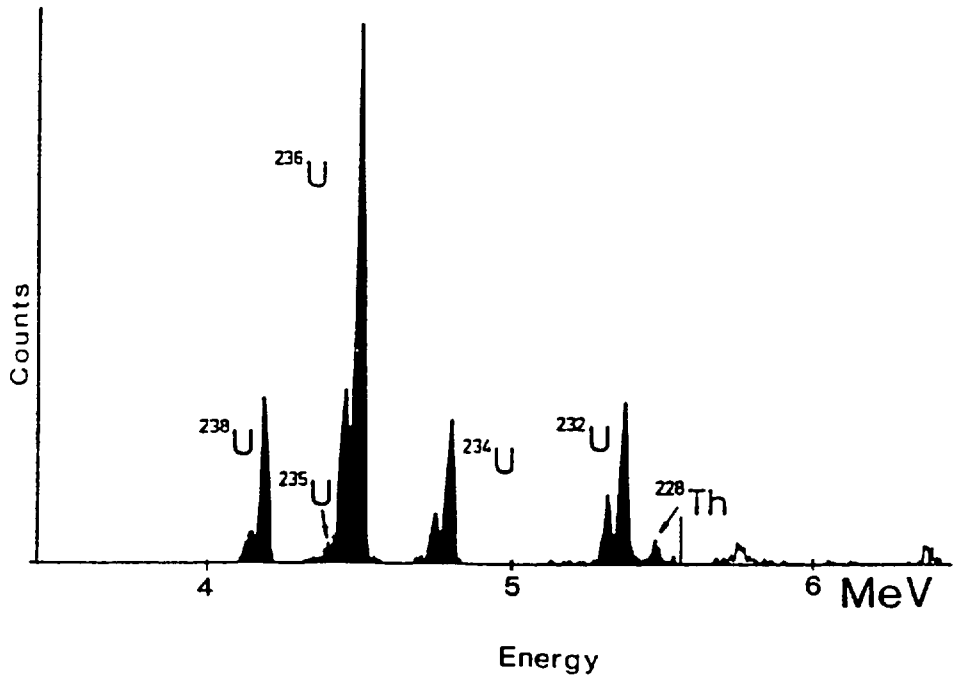

FIGURE 4.2 Alpha spectrum of uranium in solution on completion of an adsorption/desorption experiment using a Koongarra solid.

5 RESULTS OF STUDIES ON SINGLE SUBSTRATES

In this chapter, results of investigations of uranium sorption on ferrihydrite, kaolinite (Nichika and KGa-1) and quartz are reported.

5.1 Uranium (VI) Adsorption to Ferrihydrite

5.1.1 Kinetics of adsorption

The concentration of uranium measured in solution decreased rapidly within the first few hours, indicating a rapid initial uptake of uranium on ferrihydrite (Figure 5.1). Subsequently, a slower uptake of uranium which continued for at least two weeks was observed.

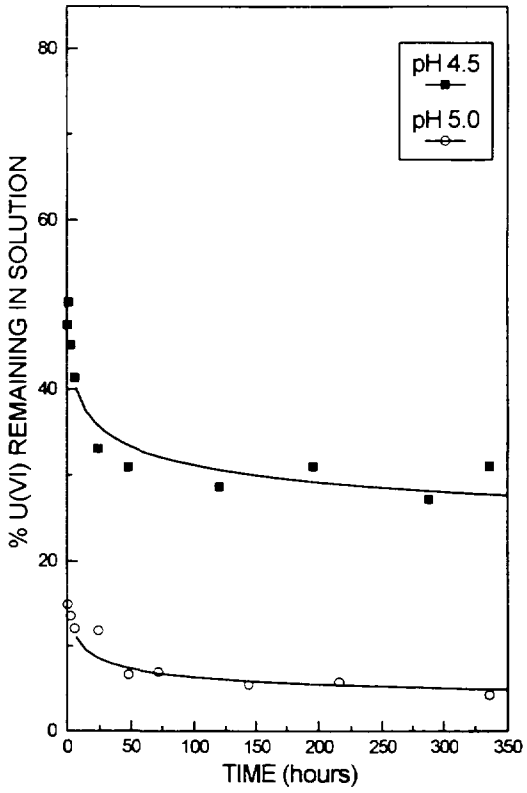

FIGURE 5.1 Kinetics of U(VI) uptake on 10^{-3}M ferrihydrite at pH 4.5 and 5.0. (25°C, total U(VI) = 10^{-7}M, 0.1M $NaNO_3$, ferrihydrite aged for 3 days prior to U addition, equilibrium with air)

A two-step process consisting of a short period of rapid initial uptake followed by a slower process (or processes) is typical of the sorption of inorganic ions to mineral surfaces (Davis and Kent, 1990). The rapid step is usually assumed to be a diffusion-controlled adsorption reaction, that takes minutes to reach equilibrium when mass transport in the bulk solution is not limiting. The slow step has been attributed to various processes, such as surface precipitation or solid solution

formation, micropore diffusion, formation of aggregates or structural rearrangement of surface species (Davis and Kent, 1990). Such processes can take weeks to months to attain equilibrium. The relative importance of the second step has been reported to increase with increasing ionic strength and with an increasing ratio of adsorbate/surface site concentrations (Dzombak and Morel, 1990).

5.1.2 Studies on pre-formed ferrihydrite

The results of studies of U(VI) partitioning to ferrihydrite over the pH range of 3-10 and at equilibrium with the atmosphere (pCO_2=$10^{-3.5}$atm) are shown in Figure 5.2. The data exhibit the sharp rise in percent U(VI) adsorbed between pH's of 4-5 and sharp fall between pH's of 8-9 observed by other workers (Hsi and Langmuir, 1985).

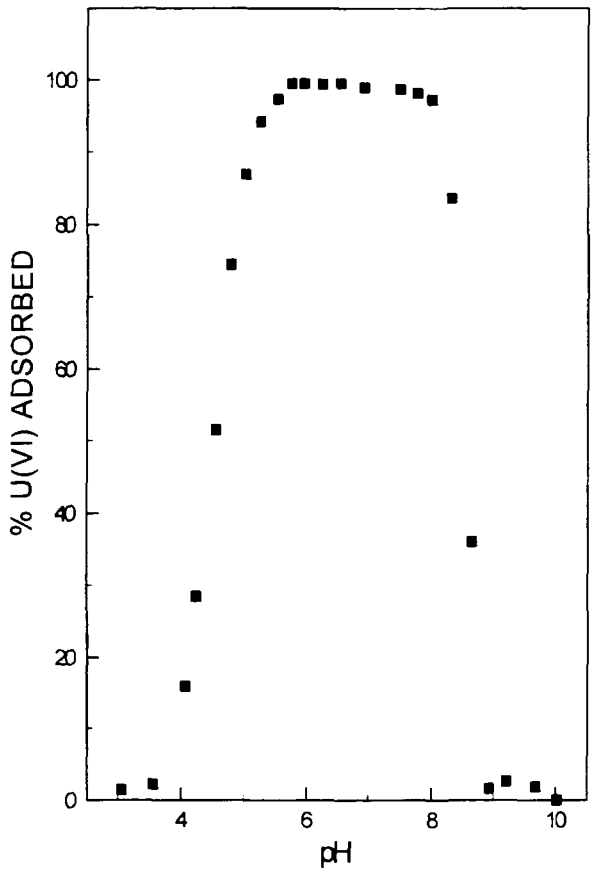

FIGURE 5.2 pH dependence of adsorption of 10^{-6}M U(VI) to 10^{-3}M ferrihydrite. Experiments were carried out in 0.1 M $NaNO_3$ in equilibrium with air.

While there is some scatter in the adsorption data obtained at various ionic strengths (Figure 5.3), a consistent shift in the position of the low pH edge with change in ionic strength is not evident.

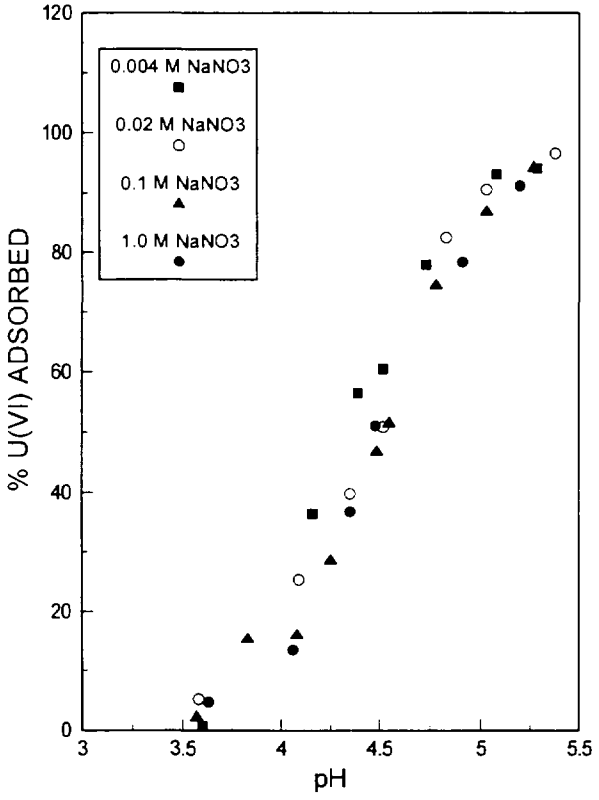

FIGURE 5.3 Effect of ionic strength on uptake of 10^{-6}M U(VI) by 10^{-3}M ferrihydrite.

In order to encompass conditions experienced in the field and (more importantly) to provide a set of experimental data suitable for the deduction of a unique mathematical description of U(VI) sorption to ferrihydrite, studies were undertaken over a range of U(VI) concentrations. The adsorption curves for the uptake of U(VI) on 10^{-3}M ferrihydrite for total uranium concentrations of 10^{-8}M, 10^{-6}M, 10^{-5}M and 10^{-4}M over a pH range of 3-7 are shown in Figure 5.4. The pH edge moves to a lower pH region with a decrease in the total uranium concentration in the system. Plotting the data obtained at pH 4.50(±0.05) in isotherm form (log[UO_2^{2+}] versus log [adsorbed uranium]) results in a Freundlich isotherm (Figure 5.5) with slope of approximately 0.7. This indicates that sorption is not proportional to dissolved uranium concentration (as occurs in the case of a Langmuir isotherm) and suggests the presence of more than one binding site type (Dzombak and Morel, 1990). This issue is discussed in more detail in Section 6 below.

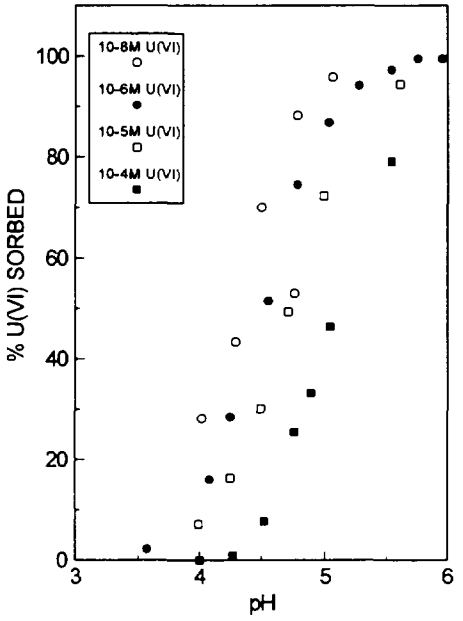

FIGURE 5.4 U(VI) sorption to 10^{-3}M ferrihydrite for total uranium concentrations of 10^{-8}M, 10^{-6}M, 10^{-5}M and 10^{-4}M over a pH range of 3-6. Experiments carried out in 0.1 M $NaNO_3$ in equilibrium with air.

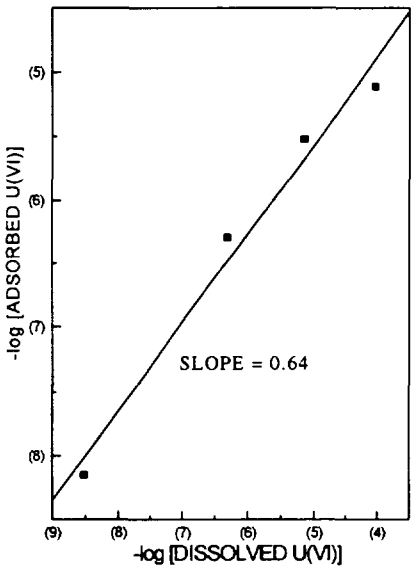

FIGURE 5.5 Adsorption isotherm for uranyl adsorption to ferrihydrite at pH 4.50(±0.05).

As shown by the results in Figure 5.6, the position of the upper pH edge is also significantly affected by total U(VI) concentration.

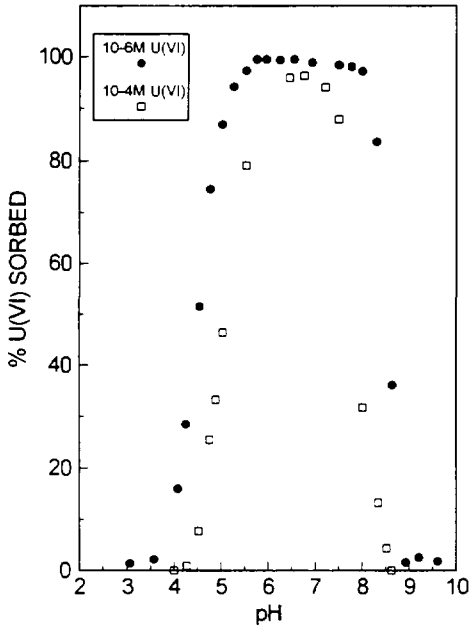

FIGURE 5.6 U(VI) sorption to 10^{-3}M ferrihydrite for total uranium concentrations of 10^{-6}M and 10^{-4}M over a pH range of 3-10.

It should be recognised that in all 'sorption' experiments, it is difficult to distinguish experimentally between surface adsorption and precipitation phenomena. Therefore, in interpreting the results, the possibility of precipitation reactions should be considered, particularly in experiments with higher uranium concentrations. At 10^{-4}M, the concentration of uranium approaches that of iron, the sorbing phase, in the system. These factors are being addressed further in modelling aspects of this study (Section 7).

Given the importance of carbonate complexation to U(VI) speciation, and the elevated partial pressures of carbon dioxide found in sub-surface waters in the Koongarra region (and elsewhere), investigation of the impact of CO_2 partial pressure on U(VI) partitioning between solution and solid phases was considered to be a high priority. Results of studies under atmospheric conditions (pCO_2 = $10^{-3.5}$ atm) are reported above.

As described earlier, studies at higher pCO_2 were undertaken in a glove box with a gas composition of approximately 1% CO_2 / 10% O_2 / 89% N_2. The extent of adsorption of U(VI) to ferrihydrite at ambient and elevated CO_2 partial pressures is shown in Figure 5.7. The sorption edges at low pH (where carbonate complexation of U(VI) is not significant) are almost identical, while the edges at high pH (where carbonate complexes dominate U(VI) speciation) are significantly different. Not

surprisingly, at the higher pH values, more uranium remains in solution at the elevated CO_2 partial pressure compared to that observed under ambient conditions (i.e. the pH edge is shifted to lower pH values).

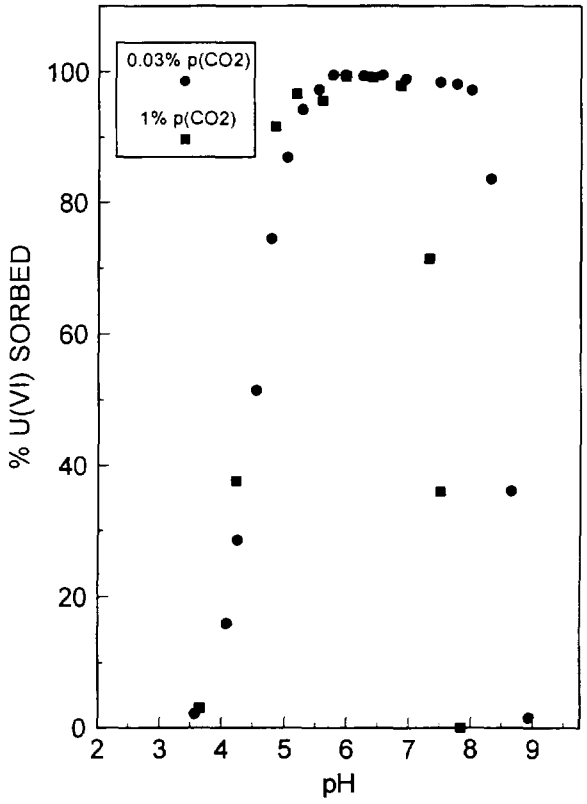

FIGURE 5.7 Comparison of extent of adsorption of 10^{-6}M U(VI) to ferrihydrite at ambient (0.03%) and elevated (1%) CO_2 partial pressures.

The effect of another potential uranyl ligand, phosphate, on the adsorption of U(VI) to ferrihydrite was also investigated. Solution-phase binding of U(VI) by phosphate has been proposed to be important by some workers (Langmuir, 1978). If this is the case, the presence of phosphate might be expected to inhibit U(VI) uptake. However, significantly enhanced adsorption of U(VI) to ferrihydrite was observed in the low pH region for $[PO_4^{3-}]_{TOT} = 10^{-4}$M, with the pH edge occurring at approximately one pH unit lower than in the phosphate-free case (Figure 5.8). While this observation demands additional investigation, it may be hypothesized that formation of a $SOH\text{-}PO_4\text{-}UO_2$ ternary surface complex accounts for these observations. Lauerer et al. (1992) have recently reported that pre-adsorption of phosphate on titanium dioxide results in a similar increase in uptake of UO_2^{2+}.

Experimental results showed that phosphate is strongly adsorbed by ferrihydrite in the acidic pH region (Figure 5.9). If ternary complex formation were not occurring, the adsorption of phosphate should decrease the uptake of U(VI), because of competition for available surface sites. The results therefore strengthen the case for some association between U(VI) and phosphate uptake.

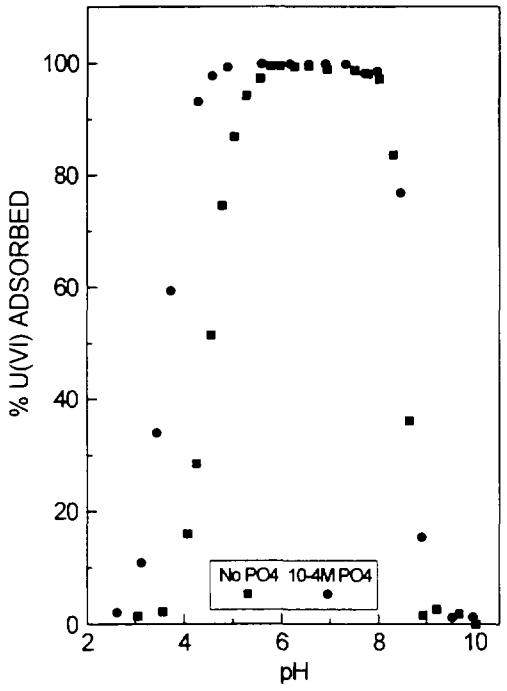

FIGURE 5.8 pH dependence of 10^{-6}M U(VI) adsorption to ferrihydrite in the absence and presence of 10^{-4}M phosphate (0.1 M $NaNO_3$, open to air).

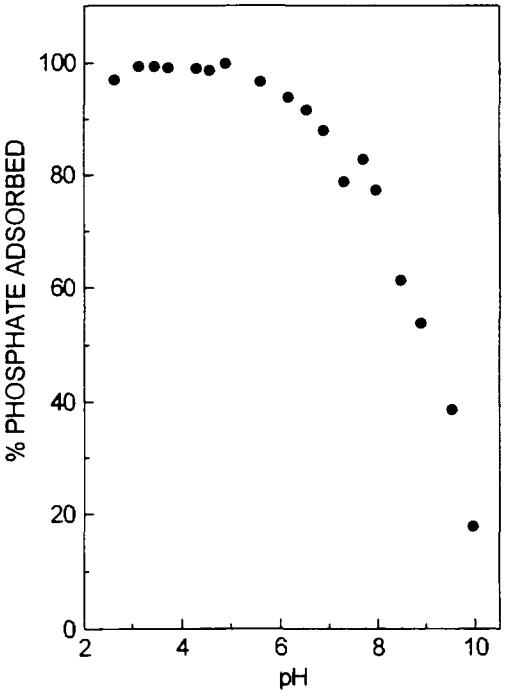

FIGURE 5.9 pH dependence of adsorption of 10^{-4}M phosphate to ferrihydrite in the presence of 10^{-6} M uranium(VI) (from same study shown in Figure 5.8 above).

As shown in Figure 5.10, a reasonably linear dependence exists between % U(VI) adsorbed and total added phosphate concentration (at pH 4).

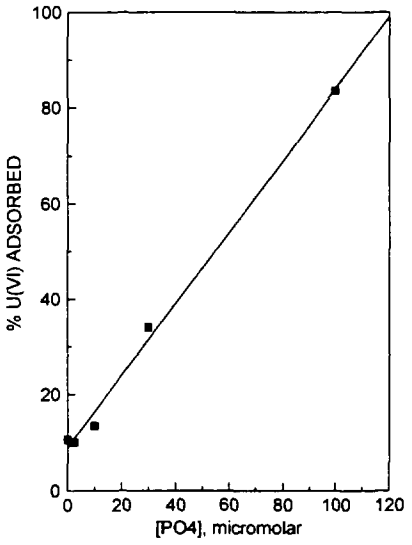

FIGURE 5.10 Dependency of the proportion of U(VI) adsorbed on total added phosphate concentration at pH 4.0.

Uranium sorption to ferrihydrite was studied across the pH range from 2.5 to 10 using a higher concentration of ferrihydrite than previously used (total Fe of 2 x 10^{-2}M rather than 10^{-3}M). As might be expected, the increase in concentration of one of the reactants (surface site concentration), increased the extent of sorption over both the low and high pH edges (Figure 5.11)

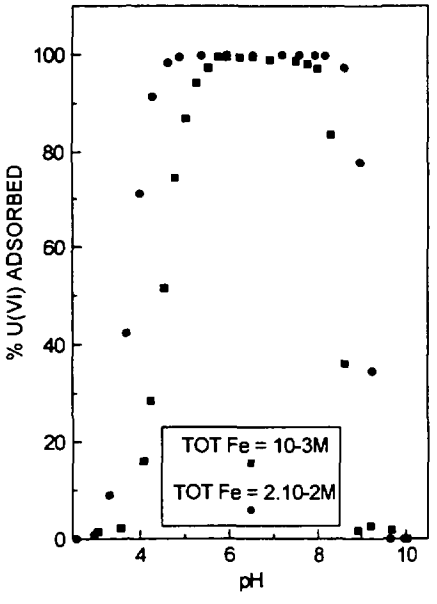

FIGURE 5.11 Uranium sorption to ferrihydrite across the pH range from 2.5 to 10 at 10^{-3}M and 2 x 10^{-2}M ferrihydrite (total U = 10^{-6} mol/L).

5.1.3 Studies on co-precipitated ferrihydrite

As shown in Figure 5.12, the pH-dependences of U(VI) uptake on pre-formed and co-precipitated ferrihydrites are fairly similar. A very small shift in the pH-edge towards lower pH values (approximately 0.1 to 0.2 pH units) could be assigned to the edge obtained under co-precipitation conditions. However, this is only slightly greater than the uncertainty in the final equilibrium pH value which is approximately 0.05 units. The similarities in the data might be considered surprising given the different experimental protocols employed.

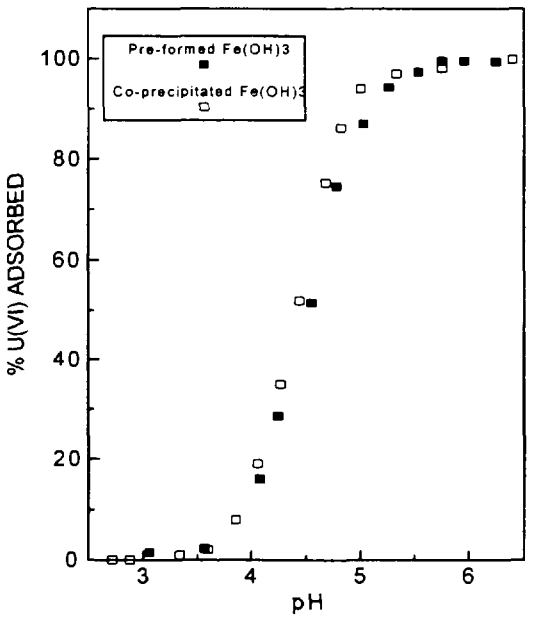

FIGURE 5.12 Comparison of adsorption of U to pre-formed and co-precipitated ferrihydrite (total U = 10^{-6} mol/L, total Fe = 10^{-3} mol/L, 0.1 M $NaNO_3$)

The slight shift in pH edge may be attributed to kinetic aspects of uranium incorporation in the two systems. In the experiments with pre-formed ferrihydrite, the kinetic studies (discussed above) indicated that the system is not fully at equilibrium after the two days contact time. Therefore, in time, one might expect increasing uptake of uranium as it diffuses further into the ferrihydrite particles. In the case of the co-precipitate, diffusion would be improbable since the uranium would presumably be incorporated homogeneously within the ferrihydrite at the time of formation. Therefore, one might expect the co-precipitation data to be similar to that obtained in an adsorption experiment with extended contact time. This explanation tends to confirm the data obtained in previous kinetic adsorption experiments, where slight increases in uranium uptake were still occurring after several days contact time.

Whilst a reasonable hypothesis for a shift in the pH edge has been put forward, the main feature of this data is that any such shift is very small, despite substantial differences in the experimental procedure.

5.2 Uranium (VI) Adsorption to Quartz

U(VI) adsorption to quartz also exhibited a sharp pH edge between 4 and 5. In addition, the ionic strength of the medium had no measurable effect on the extent of U(VI) adsorption (Figure 5.13) over the experimental pH range (<7).

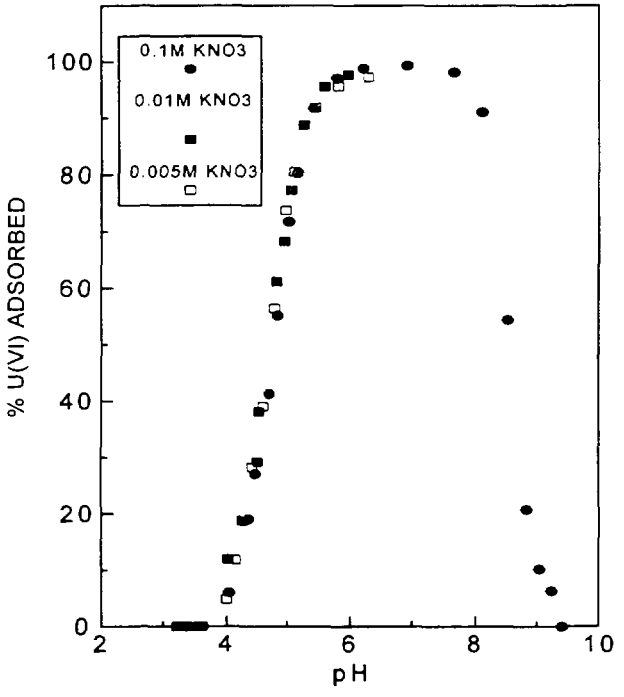

FIGURE 5.13 U(VI) adsorption to quartz (100 g / L) over pH 3-10, and (at pH < 7) for various ionic strengths (TOT U(VI) = 10^{-6}M; T = 25°C).

The addition of fluoride, a powerful, non-sorbing U(VI) complexant, significantly inhibited uranyl adsorption to quartz. The results in Figure 5.14 show that the low pH edge was progressively shifted to higher pH values as the concentration of fluoride was increased from 0 to 0.5 mM.

Addition of 2 µM phosphate had little effect on U(VI) adsorption to quartz (Figure 5.15). This result suggests that little complexation of U(VI) by phosphate is occurring in solution and also suggests that ternary complex formation on this substrate is negligible. When comparing the data with the results for ferrihydrite, it should be noted that the phosphate concentrations used for the quartz experiments were lower than most of the corresponding experiments with ferrihydrite.

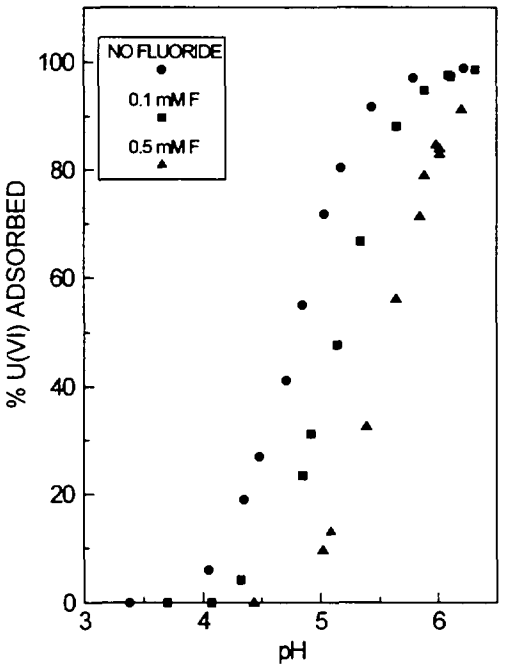

FIGURE 5.14 Effect of fluoride addition on 10^{-6}M U(VI) uptake on 100 g/L quartz suspended in 0.1M KNO_3.

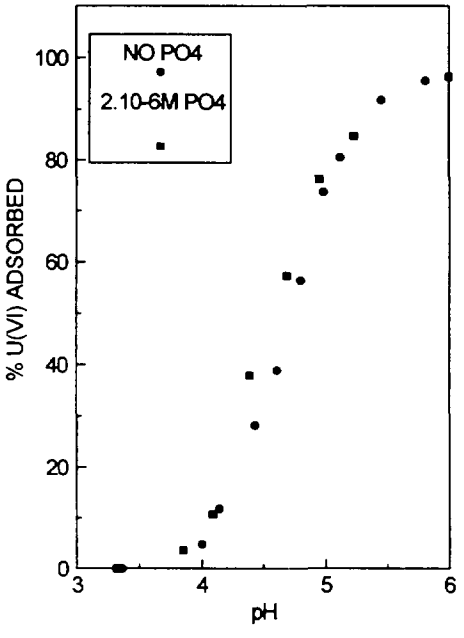

FIGURE 5.15 Effect of addition of 2 μM phosphate on uptake of 10^{-6}M U(VI) on 100 g/L quartz in 0.1 M KNO_3.

5.3 Uranium (VI) Sorption to Kaolinites

5.3.1 Kinetics of U(VI) uptake on Nichika kaolinite

As found for ferrihydrite, U(VI) uptake on kaolinite follows a two stage process with an initial rapid step followed by slower uptake (Figure 5.16).

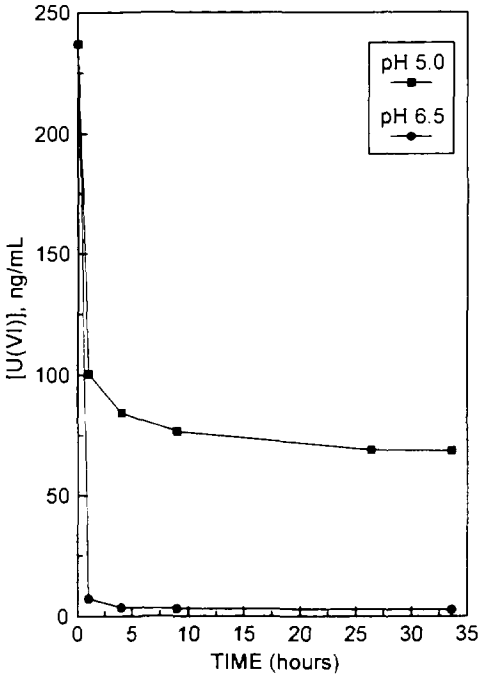

FIGURE 5.16 Kinetics of U(VI) uptake on Nichika kaolinite at pH 5.0 and 6.5 (T = 25°C; TOT U(VI) = 10^{-6}M; 0.1M $NaNO_3$).

5.3.2 Equilibrium studies on Nichika and KGa-1 kaolinites

The pH dependence of U(VI) adsorption to Nichika kaolinite (Figure 5.17) is qualitatively similar to that for U(VI) adsorption to ferrihydrite. Comparison of the Nichika and KGa-1 kaolinites (Figure 5.18) indicates that the pH edge for the KGa-1 kaolinite occurs at slightly higher pH than for the Nichika sample. This difference may be associated with the higher iron content of the Nichika kaolinite.

U(VI) adsorption to Nichika kaolinite for total uranium concentrations of 10^{-8}, 10^{-6} and 10^{-4} M (Figure 5.19) exhibits a shift in the pH edge to higher pH with increasing total U(VI), as observed for ferrihydrite. As discussed previously, this indicates a non-proportionality between sorption density and sorbate concentration, and is caused by either a multiplicity of site types or saturation of available sites. More detailed data are available at pH 6.5, and the resulting adsorption isotherm is shown in Figure 5.20. Log Γ is observed to increase linearly with log $[U]_{TOT}$ with a slope < 1, as expected for a surface possessing multiple sites of differing concentration and affinity. Such a curve is adequately described by the empirical Freundlich isotherm:

$$\Gamma = AC^a \qquad (5.1)$$

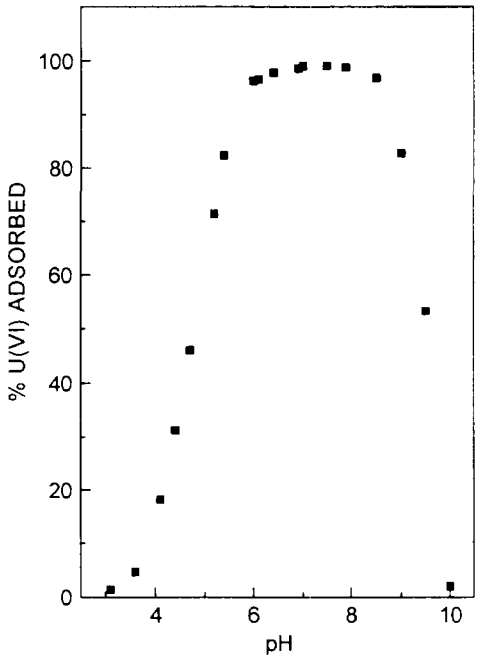

FIGURE 5.17 pH dependence of U(VI) adsorption to 4 g/L Nichika kaolinite (TOT U(VI) = 10^{-6}M; T = 25°C; 0.1 M $NaNO_3$; 1 day pH equilibration, at equilibrium with air).

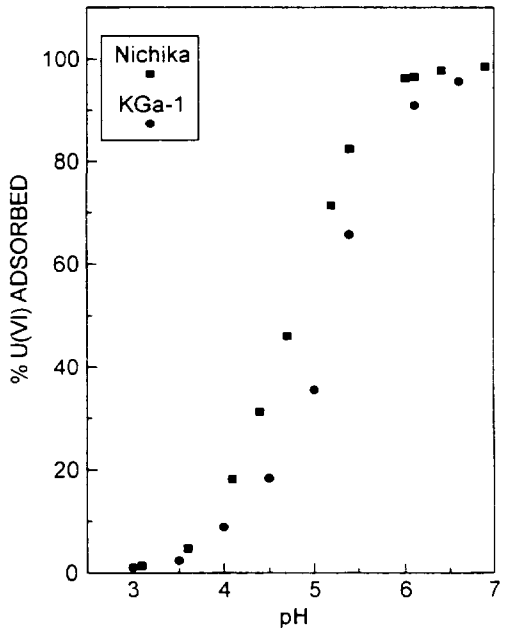

FIGURE 5.18 Comparison of U(VI) adsorption to Nichika and KGa-1 kaolinites (4 g kaolinites/L, 0.1 M $NaNO_3$; T = 25°C; TOT U(VI) = 10^{-6}M).

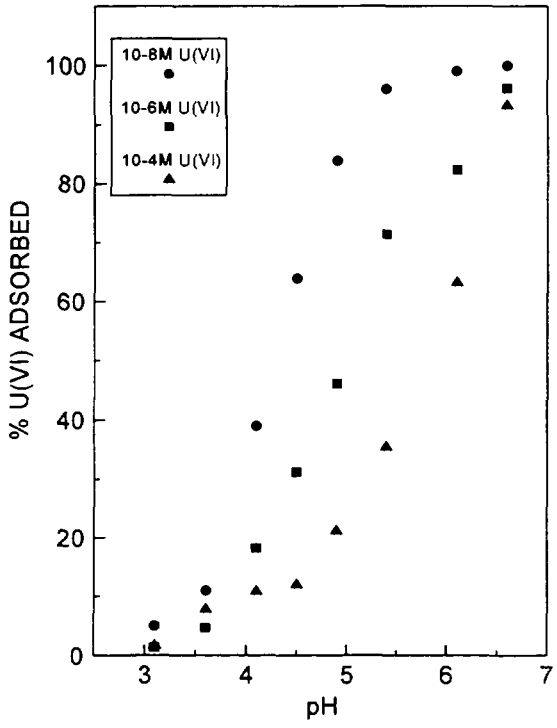

FIGURE 5.19 U(VI) adsorption to 100 mg/25 mL Nichika kaolinite for total uranium concentrations of 10^{-8}M, 10^{-6}M and 10^{-4}M in 0.1 M $NaNO_3$.

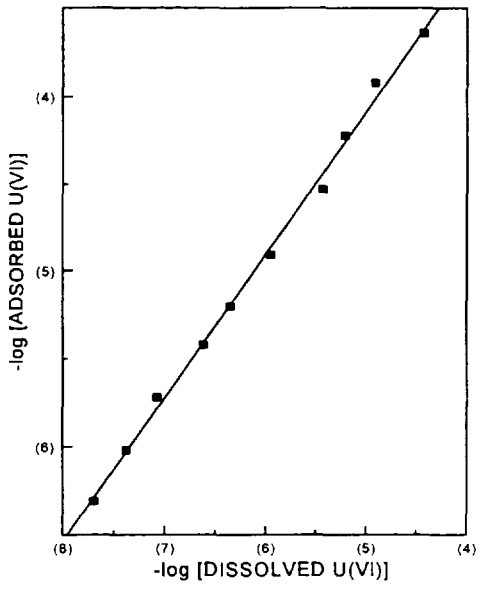

FIGURE 5.20 Effect of total U(VI) concentration on amount of U(VI) adsorbed to 4 g/L Nichika kaolinite at 25°C and pH 6.5.

The ionic strength dependence of U(VI) adsorption to KGa-1 kaolinite (Figure 5.21) suggests a small apparent increase in affinity for U(VI) at low ionic strength (0.004M $NaNO_3$). This may indicate a contribution of ion exchange processes to uranyl adsorption by this clay material (Cowan et al., 1991). However, as previously discussed (Section 4.3.1), caution should be exercised in interpreting data obtained under conditions of low sorption. The relative errors are greater in these cases, as the amount of U in solution is experimentally measured, with the percentage of U(VI) sorbed being determined by difference.

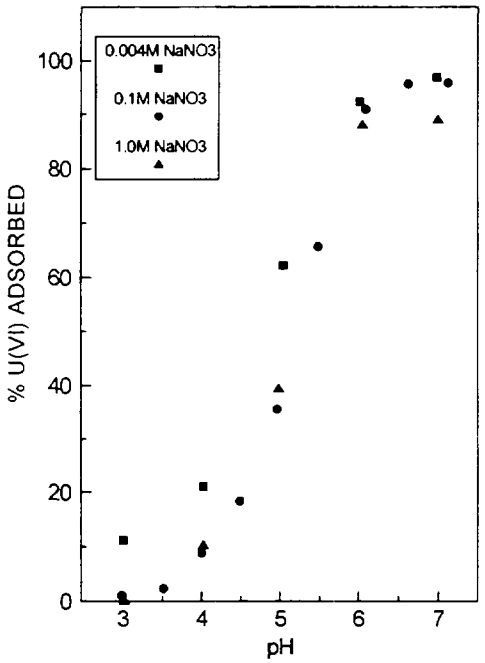

FIGURE 5.21 Effect of ionic strength on adsorption of U(VI) to KGa-1 kaolinite (TOT U(VI) = 10^{-6}M; T = 25°C).

The effect on the U sorption edges of varying the kaolinite / liquid ratio across a range from 25 mg / 25 mL to 400 mg / 25 mL is shown in Figure 5.22. As with ferrihydrite (Figure 5.9), an increase in the loading of kaolinite caused a shift in pH edge to more acidic pH (increased adsorption). While not surprising, this trend in sorption data is sometimes absent. The data obtained at the loading of 25 mg / 25 mL suggest that saturation of surface sites occurs at the lower kaolinite loadings.

As shown in Figure 5.23, CDB treatment of KGa-1 kaolinite (removing iron-oxides) had little effect on the partitioning of U(VI) between solid and solution phases. This result indicates that association of U(VI) with accessible iron oxide phases is minor. The result also confirms that CDB treatment does not markedly alter the characteristics of the kaolinite surface responsible for U(VI) uptake.

However, CDB treatment of the Nichika kaolinite did modify the U(VI) uptake characteristics, with a higher proportion of uranium adsorbed at a given pH (particularly at pH values < 5) than in the untreated system (Figure 5.24). A similar increase in sorption affinity following CDB treatment was attributed to removal of iron oxides blocking exchange sites (Cowan et al., 1991). Elliott et al. (1986) found

that removal of iron oxides from soils (using the CDB reagent) increased heavy metal adsorption, and attributed this either to a reduction in the pH_{pzc} as a result of removal of the high pH_{pzc} iron oxides, or to exposure of additional exchange sites through removal of bound cationic species, and elimination of hydroxy-polymeric Fe and Al compounds physically obstructing such sites. The Nichika kaolinite certainly contains significantly more iron oxide than the KGa-1 and a blocking of exchange sites would not seem out of the question. However, such a conclusion implies that the exchange sites (most likely AlOH groupings) possess a greater affinity for U(VI) than the Fe-oxide surface sites.

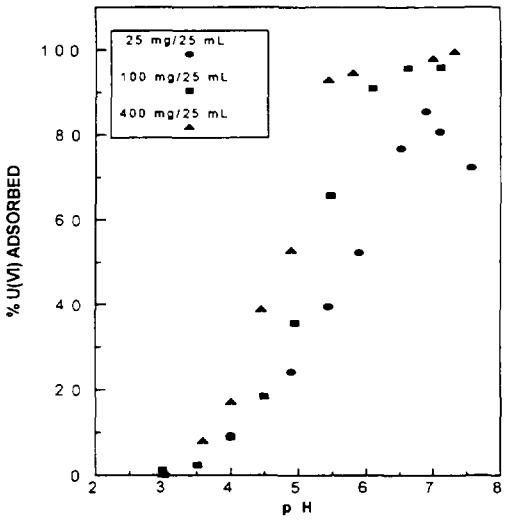

FIGURE 5.22 Effect of solid/liquid ratio on adsorption of 10^{-6}M U(VI) to KGa-1 kaolinite as a function of pH. Results are shown for solids loadings of 25 mg, 100mg and 400 mg of KGa-1 in 25 mL of solution.

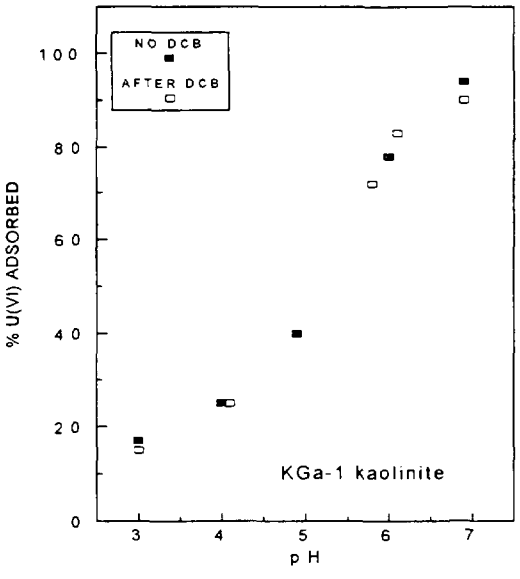

FIGURE 5.23 U(VI) sorption on KGa-1 kaolinite - effect of treatment with CDB reagent to dissolve amorphous and crystalline iron oxides (0.1 M $NaNO_3$, TOT U(VI) = 10^{-6} M).

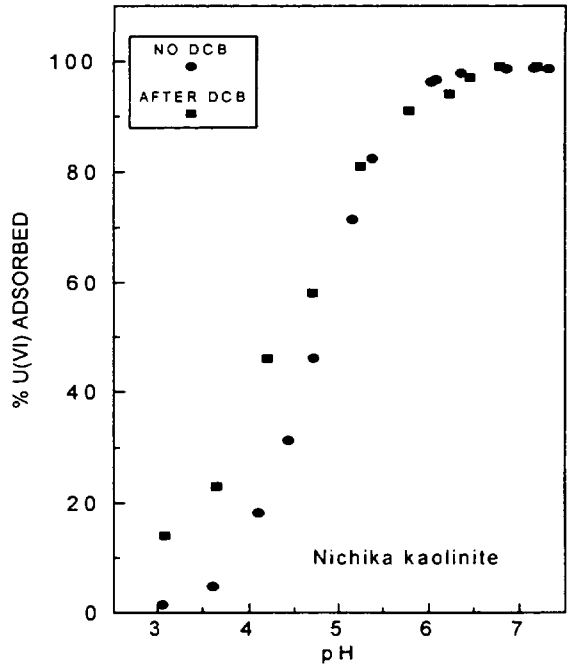

FIGURE 5.24 Effect of CDB treatment on U(VI) sorption by Nichika kaolinite.

6 MODELLING URANYL SORPTION TO SINGLE SUBSTRATES

6.1 Introduction

In this Section, we present the results of modelling U(VI) uptake on ferrihydrite, quartz and kaolinite. A preliminary modelling study of uranyl sorption to natural substrates is presented in Section 8.

6.2 Results of Surface Complexation Modelling to Ferrihydrite

6.2.1 Derivation of surface complexation constants

Dzombak and Morel (1990) compiled an extensive set of data for adsorption of anions and cations to ferrihydrite (otherwise known as hydrous ferric oxide, HFO), and investigated the applicability of selected surface complexation models. Freundlich behaviour is often observed for cation adsorption to HFO, and can be satisfactorily described using a "generalized two-layer" model, in which two types of binding sites are assumed to be present:

(1) a small set of high-affinity sites, and

(2) a large population of relatively low-affinity sites.

Dzombak and Morel (1990) reported that surface complexation reactions for cation sorption to HFO are typically of the form:

$$SOH + M^{2+} = SOM^{+} + H^{+} \quad (6.1)$$

$$TOH + M^{2+} = TOM^{+} + H^{+} \quad (6.2)$$

where SOH and TOH represent high-affinity (type 1) and low-affinity (type 2) binding sites, and M^{2+} is a divalent cation. Based on the results of a number of cation sorption studies, Dzombak and Morel (1990) selected the density of high-affinity reactive sites available for cation sorption on HFO to be 5 mmol / mol Fe (the arithmetic mean of the 1-10 mmol / mol range reported). Type 2 sites are the total sites available for sorption of protons, cations and anions, with site densities (from sorption maxima) generally in the range 0.1 - 0.3 mol/mol Fe. Dzombak and Morel (1990) use a value of 0.2 mol/mol Fe. Using the surface area for ferrihydrite of 600 m^2/g (Davis and Leckie, 1978b), a total site concentration of 0.205 mol/mol Fe is equivalent to a site density of 2.31 sites/nm^2.

The effect of electrostatic charge at the oxide surface on the apparent strength of binding of protons, anions and cations in the "generalized two-layer" model is calculated from the Gouy-Chapman theory of the electrical double layer, with one layer of surface charges and a diffuse layer of counter charges in solution. This "diffuse layer" (or two-layer) model was originally proposed by Stumm and co-workers (Stumm et al., 1970; Huang and Stumm, 1973). It was selected by Dzombak and Morel (1990) as the basis for the generalized two-layer model,

because it can be used to fit titration and ion sorption data over a range of solution conditions. In this respect, it is not inferior to the more complicated models of the interfacial region. Additionally, the single-surface-layer representation incorporated in the diffuse layer model is consistent with the disordered "porous" layer believed to exist at the surface of ferrihydrite.

The values of formation constants of the U(VI)-HFO surface complexes were optimised using the nonlinear least squares program FITEQL (Westall, 1982), which adjusts the unknown surface complex formation constants in a chemical equilibrium model to yield the best fits of the model to experimental data. In this approach, the mass balance equation residuals $Y_R I_{(m)} = TOT_R(m)_{calc} - TOT_R(m)_{expt}$ are computed for all "R" components and for each equilibrium condition (data point) *m*. The sum of squares of these residuals weighted to reflect uncertainties in the data constitutes the "objective function" to be minimised; i.e.

$$\text{weighted sum of squares (SOS)} = \Sigma[Y_R(m)/S_R(m)]^2 \qquad (6.3)$$

where $S_R(m)$ is the error calculated for $Y_R(m)$ from the experimental error estimates. In FITEQL, point-by-point absolute error estimates are determined by the formulae:

$$S_T(m) = S_T[\text{abs}] + S_T[\text{rel}] \times T(m) \qquad (6.4)$$

$$S_X(m) = S_X[\text{abs}] + S_X[\text{rel}] \times X(m) \qquad (6.5)$$

where *S*[rel] and *S*[abs] are input estimates for the relative and minimum absolute experimental error in the particular measurement (total, *T* or activity, *X*). In the output from FITEQL, the main indicator of the goodness of fit is the overall variance, V_Y, which is the weighted sum of squares of residuals divided by the degrees of freedom; i.e.

$$V_Y = \frac{SOS}{DF} = \frac{\Sigma[Y_R(m)/S_R(m)]^2}{n_p n_R - n_u} \qquad (6.6)$$

where n_p is the number of data points, n_R the number of R components, and n_u the number of adjustable parameters. The goodness of fit of the proposed model to the data is indicated by the proximity of V_Y to 1.

The formulation of the chemical model for systems involving surface complexation reactions has been described by Westall (1982), Morel (1983), and others. Changes in the FITEQL program required to incorporate the diffuse layer model are described by Dzombak and Morel (1990).

Initial modelling studies of our experimental data, in which input uranyl activities were first derived from the total U(VI) concentrations in solution, resulted in seriously biased fits, apparently as a result of inappropriate weighting of some data points. Following the recommendation of Westall (*pers. comm.)*, we adopted a procedure enabling the direct fitting of the experimental data from the sorption studies. In this approach, UO_2^{2+} was retained as a conventional FITEQL Group I component (only T known). In addition, a Group II "dummy component" (U^{sol}, T and

X known) was used to describe a dummy set of solution phase U(VI) species. For this component, T_U^{sol} equals the experimental values (U(VI) in solution) while X_U^{sol} = 1. The tableau appropriate to this approach is shown in Table 6.1.

FITEQL was applied to the low pH edge U(VI) sorption data, assuming the formation of positively charged $SOUO_2^+$ and $TOUO_2^+$ surface species, with the loss of one proton. The concentrations of strong and weak sites were 5 x 10^{-6}M and 2 x 10^{-4}M respectively (taken from Dzombak and Morel (1990)), with corresponding best fit log formation constants of 3.92 and 1.98 (Table 6.2). This model was far from satisfactory, as shown by the overall variance of the fit (SOS/DF = 24.2), and also by comparing model predictions with experimental data at various total U(VI) concentrations (Figure 6.1). Uranium (VI) sorption at 10^{-4}M and 10^{-5}M U(VI) was seriously over-predicted, particularly at low sorption densities, whereas the data for 10^{-8}M were generally under-predicted. This suggested the following changes:

(a) introduction of a surface species exhibiting a stronger pH dependence than that of $SOUO_2^+$ and $TOUO_2^+$ (for which the stoichiometric coefficient of the proton is unity), and

(b) decrease the concentration of strong sites to produce differentiation between the model results at low total uranium concentrations.

The first change was implemented by considering formation of the strong and weak hydroxylated uranyl surface complexes, $SOUO_2OH$ and $TOUO_2OH$, which exhibit a squared dependency on pH, i.e.

$$SOH + UO_2^{2+} + H_2O = SOUO_2OH + 2H^+ \qquad (6.7)$$

Using these complexes, optimal fits were then obtained using FITEQL for various concentrations of the strong site, [SOH]. As can be seen from Figure 6.2, the lowest variance in fit was obtained for a strong site concentration of only 7 x 10^{-7}M. Comparison between the model results (with the parameters in Table 6.2) and the experimental data at the various U(VI) concentrations (Figure 6.3) indicated very good agreement in most instances, with the largest differences between model and experiment apparent for the 10^{-5}M U(VI) data. Not surprisingly, the inclusion of both $SOUO_2OH$ and $SOUO_2^+$ (and their weak site analogues) in the model reduced the overall variance (Table 6.2).

Consideration was also given to formation of the bidentate complex $(SO)_2UO_2$ according to the reaction:

$$2SOH + UO_2^{2+} \leftrightarrow (SO)_2UO_2 + 2H^+ \qquad (6.8)$$

but poor fits were obtained.

TABLE 6.1

TABLEAU SHOWING IMPORTANT SOLUTION PHASE U(VI) SPECIES AND U(VI) SURFACE COMPLEXES FOR SURFACE WITH TWO SITE TYPES (SOH AND TOH), ASSUMING ACIDIC CONDITIONS WHERE CARBONATE COMPLEXATION OF U(VI) IS NOT IMPORTANT. SERIAL INPUT DATA IS SUPPLIED FOR $T_{U(VI)}$, T_U^{soln} AND LOG X_{H^+}. VALUES FOR T_{SOH} AND T_{TOH} ARE KNOWN AND FIXED AS ARE $T_P=\sigma(AS/F)$ ($T_P=0$), AND X_U^{soln} (LOG $X_U^{soln}=0$)

	Components					
Species	SOH	TOH	P^1	UO_2^{2+}	U_{sol}	H^+
H^+	0	0	0	0	0	1
OH^-	0	0	0	0	0	-1
UO_2^{2+}	0	0	0	1	1	0
$UO_2(OH)^+$	0	0	0	1	1	-1
$UO_2(OH)_2^0$	0	0	0	1	1	-2
$UO_2(OH)_3^-$	0	0	0	1	1	-3
$UO_2(OH)_4^{2-}$	0	0	0	1	1	-4
$(UO_2)_2(OH)^{3+}$	0	0	0	2	2	-1
$(UO_2)_2(OH)_2^{2+}$	0	0	0	2	2	-2
$(UO_2)_3(OH)_4^{2+}$	0	0	0	3	3	-4
$(UO_2)_3(OH)_5^+$	0	0	0	3	3	-5
$(UO_2)_3(OH)_7^-$	0	0	0	3	3	-7
$(UO_2)_4(OH)_7^+$	0	0	0	4	4	-7
SO^-	1	0	-1	0	0	-1
SOH	1	0	0	0	0	0
SOH^{2+}	1	0	1	0	0	1
$SOUO^{2+}$	1	0	1	1	0	-1
$SOUO_2OH^0$	1	0	0	1	0	-2
TO^-	0	1	-1	0	0	-1
TOH	0	1	0	0	0	0
TOH^{2+}	0	1	1	0	0	1
$TOUO^{2+}$	0	1	1	1	0	-1
$TOUO_2OH^0$	0	1	0	1	0	-2
Totals	T_{SOH}	T_{TOH}	T_P	$T_{U(VI)}$	T_U^{soln}	T_H

[1] $P = \exp(-F\Psi/RT)$

TABLE 6.2

BEST FIT FORMATION CONSTANTS OBTAINED USING FITEQL FOR SURFACE COMPLEXATION MODELS OF U(VI) ADSORPTION TO FERRIHYDRITE IN WHICH DIFFERENT SURFACE COMPLEX TYPES AND STRONG SITE CONCENTRATIONS WERE ASSUMED.
A weak site concentration of 2 X 10^{-4}M was assumed in all cases.
The goodness of fit is indicated by the overall variance, V_y, equal to the weighted Sum Of Squares of residuals divided by the Degrees Of Freedom (SOS/DF)

[SOH]	log K (±1σ)				V_Y
(M)	$SOUO_2^+$	$TOUO_2^+$	$SOUO_2OH$	$TOUO_2OH$	(SOS/DF)
5 x 10^{-6}	3.92 (0.03)	1.98 (0.01)	n.a.	n.a.	24.2
7 X 10^{-7}	5.05 (0.04)	2.05 (0.01)	n.a.	n.a.	16.4
7 X 10^{-7}	n.a.[1]	n.a.	-1.60 (0.04)	-5.21 (0.02)	6.2
7 X 10^{-7}	4.98 (0.09)	1.20 (0.17)	-2.14 (0.02)	-5.33 (0.06)	4.2

[1] n.a. = not applicable

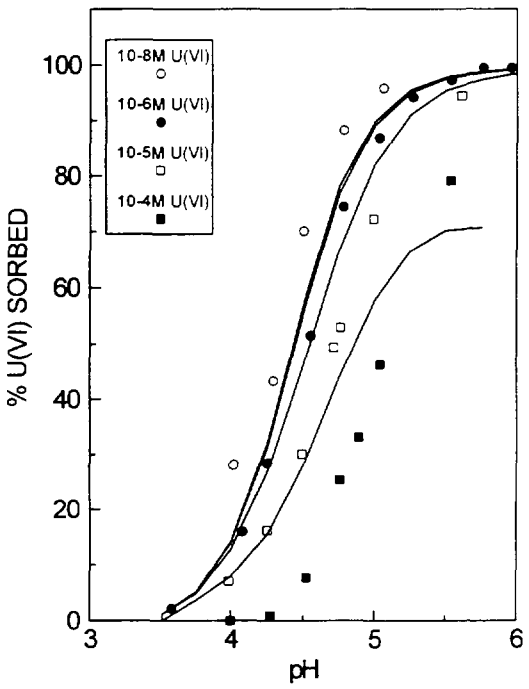

FIGURE 6.1 Results of surface complexation modelling of U(VI) sorption to 10^{-3}M ferrihydrite assuming the formation of $SOUO_2^+$ and $TOUO_2^+$ at strong and weak adsorbing sites (SOH and TOH) at concentrations 5 x 10^{-6} M and 2 x 10^{-4} M, with log(formation constants) for surface complexes of 3.92 and 1.98 respectively. (Experimental sorption data as presented in Figure 5.4).

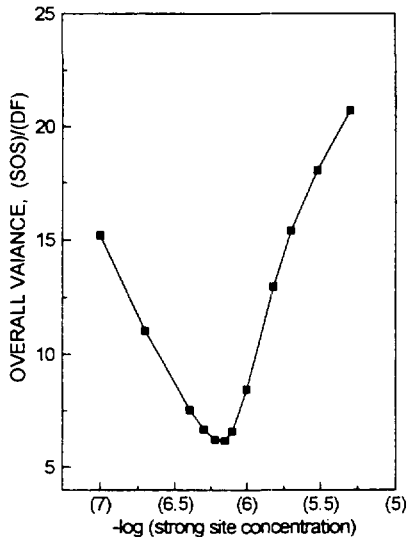

FIGURE 6.2 Variation in overall variance of fit (i.e. sum of squares of residuals divided by degrees of freedom) for a surface complexation model of experimental data, as a function of the concentration of strong surface sites.

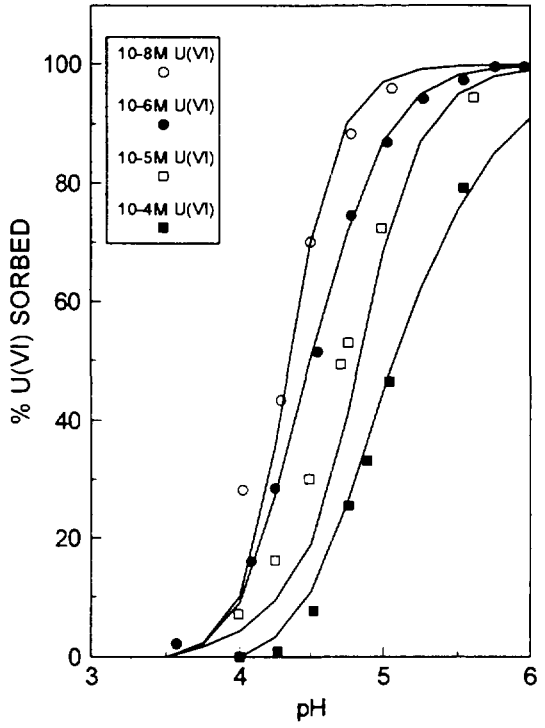

FIGURE 6.3 Results of surface complexation modelling assuming the formation of $SOUO_2OH$ and $TOUO_2OH$ at strong and weak adsorbing sites (SOH and TOH) of concentrations 7 x 10^{-7}M and 2 x 10^{-4}M respectively with log(formation constants) at these sites of -1.60 and -5.21 respectively.

6.2.2 Effect of carbonate complexation

The FITEQL modelling described above was undertaken at pH < 6, where carbonate complexation of U(VI) is minor, and has an insignificant impact on uranium partitioning between the solid and solution phases. In this section, we examine the applicability of the derived surface complex formation constants to experiments at higher pH or elevated pCO_2, where carbonate complexes of dissolved U(VI) are important.

The derived model was compared with the high pH sorption data for experiments undertaken at atmospheric partial pressure of CO_2 (0.03% CO_2 or $pCO_2 = 10^{-3.5}$atm), with 10^{-4}M and 10^{-6}M total U (Figure 6.4). Some under-prediction is evident for 10^{-6}M U(VI), but the agreement between model and experiment is quite good.

Comparison of model results (using the same constants) with experimental data for a system containing 1% CO_2 (Figure 6.5) again revealed slight under-prediction in adsorbed U(VI) in the vicinity of the high pH edge, but exhibited general agreement. There may be some association between uranyl carbonate species and the oxide surface, or formation of ternary uranyl carbonate surface complexes (as proposed by Hsi and Langmuir (1985), Payne and Waite (1991) and Kohler et al. (1992)). These effects appear to be relatively minor in U(VI) uptake by ferrihydrite.

6.2.3 Effect of ferrihydrite concentration

Comparison of experimental data with model results using the optimal set of surface complex constants derived above, but for a system containing 2 x 10^{-2}M Fe (rather than 10^{-3}M Fe as used in the studies reported above) is shown in Figure 6.6. Good agreement is obtained, with possibly slight under-prediction of adsorption at low pH. The model predictions at low pH values can be increased by adding additional surface species (Figure 6.6), but this is not warranted given the uncertainty in the experimental data when only a small proportion of U is adsorbed.

6.2.4 Effect of phosphate addition

As indicated previously, the addition of phosphate increased the uptake of uranium, particularly at low pH values. Simplistically, it might be assumed that phosphate will reduce uranyl uptake, because of complexation of U in the solution phase, or competition for surface sites. Phosphate adsorption on oxides and clays is well documented, and detailed studies of the uptake of phosphate on a range of solid substrates have been undertaken by many workers. Dzombak and Morel (1990) analysed the data of Ryden et al. (1977), and derived surface complexation constants for a diffuse double layer model with a single surface site type. The most appropriate surface complexation reactions are given below:

$$TOH^\circ + PO_4^{3-} + 3H^+ = TH_2PO_4^\circ + H_2O \quad (6.9)$$

$$TOH^\circ + PO_4^{3-} + 2H^+ = THPO_4^- + H_2O \quad (6.10)$$

$$TOH^\circ + PO_4^{3-} + H^+ = TPO_4^{2-} + H_2O \quad (6.11)$$

with best estimate log (formation constants) of 31.29, 25.39 and 17.72 respectively obtained by Dzombak and Morel (1990) using FITEQL.

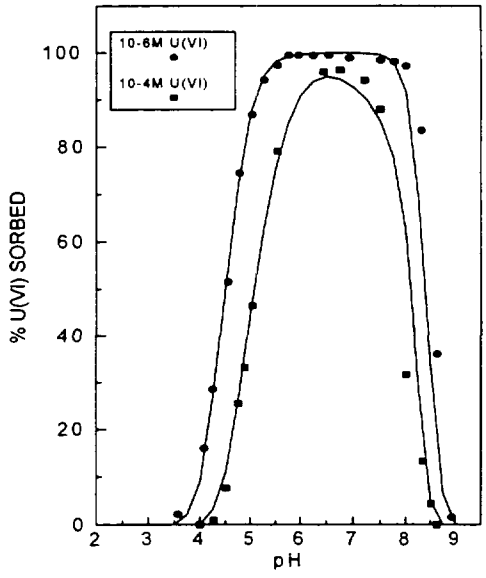

FIGURE 6.4 Results of surface complexation modelling of adsorption of 10^{-4}M and 10^{-6}M U(VI) to 10^{-3}M ferrihydrite over the pH range of approximately 3-10. The model assumes formation of $SOUO_2OH$ and $TOUO_2OH$ at strong and weak adsorbing sites (SOH and TOH), with respective site concentrations of 7 x 10^{-7}M and 2 x 10^{-4}M and log(formation constants) of -1.60 and -5.21.

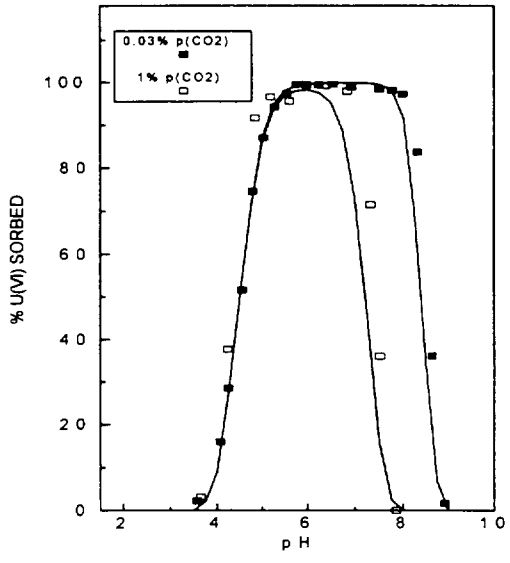

FIGURE 6.5 Results of surface complexation modelling of adsorption of 10^{-6}M U(VI) to 10^{-3}M ferrihydrite over the pH range of approximately 3-10 at two partial pressures of CO_2.The formation of $SOUO_2OH$ and $TOUO_2OH$ at strong and weak adsorbing sites (SOH and TOH) of concentrations 7 x 10^{-7}M and 2 x 10^{-4}M respectively, was assumed with log(formation constants) at these sites of -1.60 and -5.21 respectively.

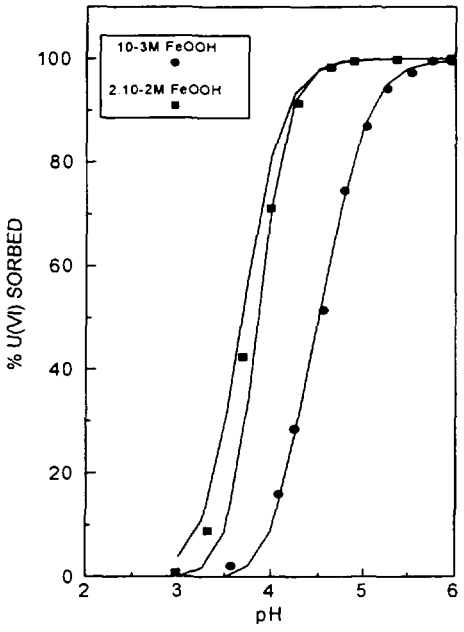

FIGURE 6.6 Results of surface complexation modelling of adsorption of 10^{-6}M U(VI) to 10^{-3}M and 2 x 10^{-2}M ferrihydrite. The two curves (to the right of the figure) were derived assuming formation of $SOUO_2OH$ and $TOUO_2OH$ at strong and weak adsorbing sites (SOH and TOH) of concentrations 7 x 10^{-7}M and 2 x 10^{-4}M respectively for 10^{-3}M ferrihydrite, and 1.4 x 10^{-5}M and 4 x 10^{-3}M respectively for 2 x 10^{-2}M ferrihydrite. Log(formation constants) for surface complexes at the strong and weak sites of -1.60 and -5.21 respectively were used. The other line represents a model in which $SOUO_2OH$ and $SOUO_2^+$ (and their weak site counterparts) were assumed to form with formation constants as indicated in Table 6.2.

Speciation calculations incorporating these equations indicated that phosphate is strongly adsorbed, with a pH dependence similar to that shown in Figure 5.9. As indicated previously, the formation of ternary uranyl phosphate surface complexes appears to be the most likely reason for the enhanced U(VI) uptake in the presence of phosphate. Given the form of the phosphate surface complexes described above, a ternary complex of the following stoichiometry may be envisaged:

$$TOH + PO_4^{3-} + UO_2^{2+} + H^+ = TPO_4UO_2^{\circ} + H_2O \qquad (6.12)$$

FITEQL optimisation of the fit to the low pH edge obtained in the presence of phosphate, with Equation 6.12 added to the suite of surface reactions, resulted in a best-fit log (formation constant) of 28.3 for the ternary complex. The results of these calculations (Figure 6.7) were in close agreement with experiment. Note that, since the predominant phosphate species in the vicinity of the low pH edge is H_3PO_4, the pH dependence of U(VI) uptake under these conditions is best represented by rewriting Equation 6.12 in the form:

$$TOH^{\circ} + H_3PO_4 + UO_2^{2+} = TPO_4UO_2^{0} + 2H^+ + H_2O \qquad (6.13)$$

This representation confirms the squared dependency of U(VI) uptake on pH that is observed experimentally.

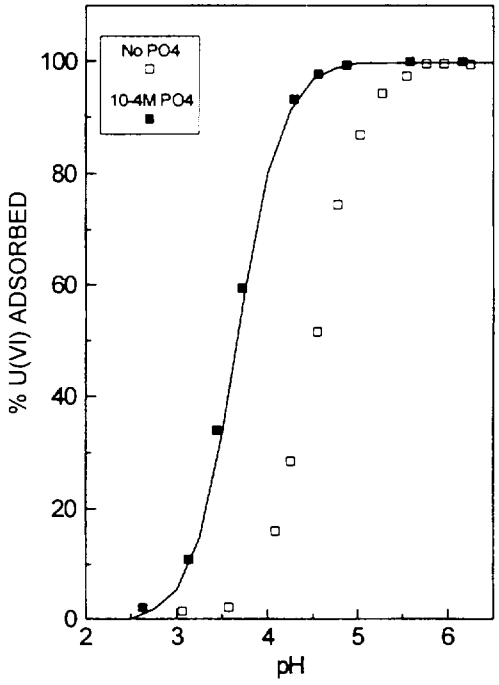

FIGURE 6.7 Surface complexation model incorporating both the previously defined $SOUO_2OH^0$ and $TOUO_2OH^0$ surface complexes (with respective log formation constants of -1.60 and -5.21) and the ternary $TPO_4UO_2^0$ surface complex with log formation constant of 28.3. $[SOH]_T = 7 \times 10^{-7}M$, $[TOH]_T = 2 \times 10^{-4}M$, $[U(VI)]_T = 10^{-6}M$, $[PO_4]_T = 10^{-4}M$ and $[Fe]_T = 10^{-3}M$.

6.3 Results of Surface Complexation Modelling to Quartz

6.3.1 pH and ionic strength dependency

Since data for adsorption of U(VI) to quartz are not available for multiple U(VI) concentrations, analysis in terms of a single site type only can be undertaken. Assignment of the concentration of these sites is obviously critical in developing a suitable model for U(VI) uptake on quartz. As noted by Davis and Kent (1990), the site density used by Dzombak and Morel (1990) of 2.31 sites/nm^2 for ferrihydrite closely approximates the site densities of a variety of minerals, and is used here for quartz. The surface area for the quartz substrate used is 0.32 m^2/g giving a site concentration for 100 g/L quartz of $1.229 \times 10^{-4}M$.

Using this site concentration with the sorption data for pH <6, and assuming formation of $TOUO_2OH$ surface complexes only, resulted in a log(formation constant) of -5.42 (±0.02). The overall variance of this fit (SOS/DF) was 3.13. As

can be seen from Figure 6.8, this single site type model describes the low pH edge data very well, although significant under-prediction of U uptake in the high pH region is evident.

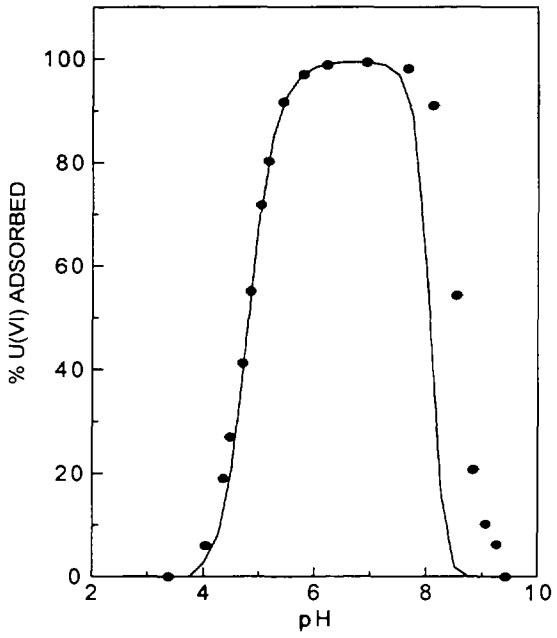

FIGURE 6.8 Experimental data obtained for the adsorption of 10^{-6}M U(VI) to 100 g/L quartz over the pH range 3-10. The solid line represents a surface complexation model with one surface site type, and a surface complex of the form $TOUO_2OH$ with (log) formation constant -5.42 (±0.02).

6.3.2 Modelling the effects of fluoride and phosphate

Uranyl fluoride complexes, UO_2F^+, $UO_2F_2^\circ$, $UO_2F_3^-$ and $UO_2F_4^{2-}$, with log (formation constants) of 5.09, 8.62, 10.90 and 11.70, may be formed in the presence of fluoride. Inclusion of these complexes in the thermodynamic data-base indicated that a significant proportion of the U would be present as the monofluoride complex under the experimental conditions. The fluoride anion will thus compete with surface sites for U(VI), and it would be expected that a lower proportion of U(VI) will be adsorbed when fluoride is present.

The results of surface complexation modelling with fluoride present (Figure 6.9) simulate the experimental data extremely closely, confirming that solution phase fluoride complexation of U(VI) satisfactorily accounts for the role played by this anion.

As previously indicated (Figure 5.15), addition of 2 μM phosphate had a negligible effect on the uptake of U(VI) on quartz. It should be noted however that this low concentration of phosphate would not be expected to have a great effect on uranyl adsorption, even if a ternary complex of the type proposed on ferrihydrite were to be formed.

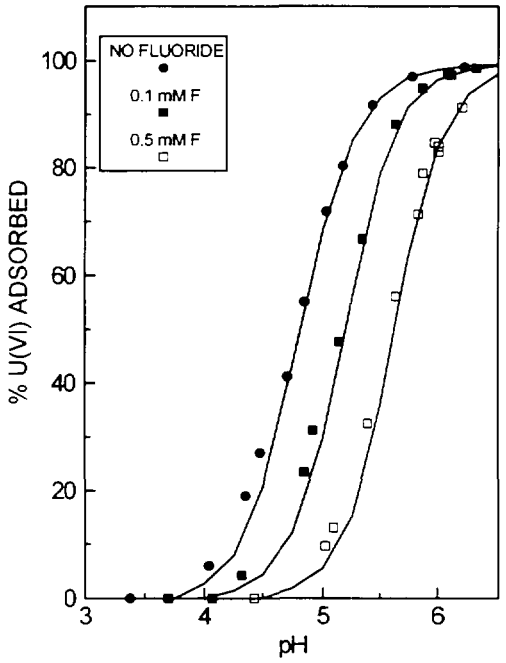

FIGURE 6.9 Results of adding solution phase uranyl fluoride complexes, UO_2F^+, $UO_2F_2^\circ$, $UO_2F_3^-$ and $UO_2F_4^{2-}$ to the optimal single site surface complexation model for adsorption of 10^{-6} M U (VI) to 100 g / L quartz. [TOH] = 1.229 x 10^{-4} M and $TOUO_2OH^0$ assumed to form with log (formation constant) of -5.42.

6.4 Results of Surface Complexation Modelling to Kaolinite

6.4.1 Discussion of kaolinite site types

U(VI) adsorption behaviour to KGa-1 and Nichika kaolinites shows a number of major differences when compared to U uptake on ferrihydrite and quartz. These features provide insights into the factors controlling uptake of U(VI) on these clay substrates.

Ionic strength effects

While U(VI) uptake on ferrihydrite exhibited no ionic strength effects within the studied range of experimental conditions, a small ionic strength effect may be discerned in the data for KGa-1 kaolinite (Figure 5.21). Slightly higher U(VI) adsorption to KGa-1 is evident at pH values less than around 5 at low (0.004M $NaNO_3$) compared to the higher (0.1M and 1.0M $NaNO_3$) ionic strengths. However, relatively few data-points for sorption in 0.004 M $NaNO_3$ were obtained, and (as pointed out in Section 4.3.1) the experimental techniques are far from optimal for quantifying small differences in U sorption under conditions when U uptake is small.

If there is a real effect of ionic strength on U sorption by the KGa-1 sample, this indicates that uptake of U(VI) occurs on ion exchange sites at low ionic strengths. At higher ionic strengths, U(VI) can no longer compete for these sites against the excess major cation (Na^+) present. Such an effect has been described for the interaction of Cd^{2+} with clays (Cowan et al., 1991). The macroscopic exchange between solution phase UO_2^{2+} (the principal uranyl species at low pH) and Na^+ on fixed-charge sites, X^-, may then be represented by the following reactions:

$$2NaX + UO_2^{2+} \leftrightarrow UO_2X_2 + 2Na^+ \quad (6.14)$$

$$NaX + UO_2^{2+} + H_2O \leftrightarrow UO_2OHX + Na^+ + H^+ \quad (6.15)$$

At *high ionic strengths, formation of strongly binding inner-sphere complexes at* edge hydroxyl sites of either aluminol (AlOH) or silanol (SiOH) groups may account for the observed pH dependency. The complexation reactions to these edge sites may be formulated as:

$$SOH + UO_2^{2+} \leftrightarrow SOUO_2^+ + H^+ \quad (6.16)$$

$$SOH + UO_2^{2+} + H_2O \leftrightarrow SOUO_2OH + 2H^+ \quad (6.17)$$

Some difficulty is expected in determining which (if any) of these specific binding reactions are important for uranyl uptake on kaolinite. Simplistically, the first order dependency of U(VI) uptake on pH exhibited by Equation 6.16 would appear closer to the slope of the low pH edges obtained for KGa-1. Further attention is given to this issue below.

Effect of CDB leaching

As indicated in Section 5.3.2, CDB leaching had little effect on U(VI) uptake by KGa-1 kaolinite but appeared to slightly increase uranyl adsorption to the more iron-contaminated Nichika kaolinite. The impact of CDB leaching is particularly marked for pH < 5.

Cowan et al. (1991) observed similar behaviour in studies of the impact of CDB treatment on cadmium interaction with clays and natural substrates. These workers concluded that the crystalline iron oxides in the substrates affected Cd sorption primarily through a particle association that limited access of Cd to ion exchange sites. A possible reaction involves the electrostatic association between crystalline Fe oxides ($FeOH^\circ$), that carry positive charge at pH's below their first acidity constant, and negatively charged sites on the clay, represented by:

$$FeOH^\circ + X^- + H_2O \leftrightarrow XFeOH_2 + OH^- \quad (6.18)$$

The pH edge prior to CDB leaching is relatively steep and typical of specific U(VI) binding to hydroxyl sites. Such sites may be associated with AlOH or SiOH edge groups, or may even be located on the iron oxides removed by the CDB reagent.

U(VI) concentration dependence

As discussed earlier, the availability of sorption data over a range of uranium concentrations enables the requirement for multiple site types in the adsorption model to be determined. The adsorption isotherm for U(VI) uptake on the Nichika kaolinite at pH 6.5 (Figure 5.20) exhibits Freundlich behaviour, with the log transformed plot having a slope of approximately 0.9. Deviation from Langmuirian behaviour thus does not appear severe, and a single site type would appear sufficient for modelling sorption under these conditions.

However, inspection of pH edges previously presented for adsorption of 10^{-4}, 10^{-6} and 10^{-8}M U(VI) to Nichika kaolinite (Figure 5.19) suggests that the situation at pH's more acidic than 6.5 may be considerably more complex (particularly for the Nichika kaolinite with its additional complement of iron oxides). Indeed, plotting the data at pH 4.5 in isotherm form (Figure 6.10) indicates a slope of only 0.74 - a slope indicative of multiple sites of different energies.

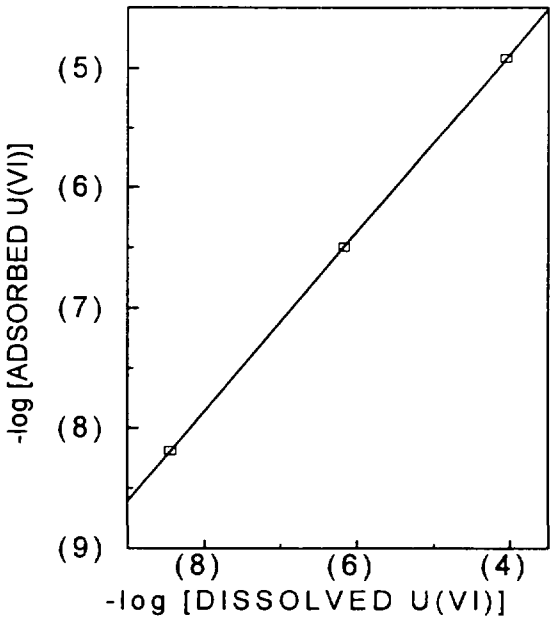

FIGURE 6.10 Adsorption isotherm for U(VI) interaction with Nichika kaolinite at pH 4.5. (0.1 M $NaNO_3$).

6.4.2 Quantitative analysis of U(VI) interaction with kaolinites

KGa-1

Although the data suggesting an ionic strength dependence are not conclusive, the experimental results (taken at face value) suggest slight adsorption of U(VI) (approx. 11%) at pH 3 in 0.004 M $NaNO_3$, but almost complete negation of uptake at this pH on increasing the ionic strength to 0.1 M $NaNO_3$. This may indicate that an interaction via ion exchange of the form shown in Equation 6.14 is operative. Assuming that essentially all exchange sites are present as NaX (a reasonable

assumption since $[U_{TOTAL}] << [X_{TOTAL}]$), a conditional equilibrium constant can be computed for this exchange reaction; i.e.

$$K = \frac{[UO_2X_2][Na^+]^2}{[NaX]^2[UO_2^{2+}]} \qquad (6.19)$$

After estimating the concentration of exchange sites from the cation exchange capacity (giving [NaX] = 8.0 x 10^{-5}M), we derived an intrinsic constant for this reaction of log K = 2.49. From Equation 6.19, an increase of ionic strength to 0.1 M $NaNO_3$ would be expected to reduce the amount of bound uranium to the low levels observed.

The increase of U(VI) adsorption with increasing pH may be accounted for either by formation of the hydroxylated exchange complex UO_2OHX (Equation 6.15), or by formation of specifically bound complexes $TOUO_2^+$ or $TOUO_2OH$ (Equations 6.16 or 6.17). As indicated above, the charged species $TOUO_2^+$ would seem most appropriate given the first power dependency on pH. A further FITEQL analysis, assuming formation of both the ion exchange and specifically bound complexes, resulted in an excellent fit to the I = 0.004 M data (Figure 6.11) using log K for UO_2OHX and $TOUO_2^+$ of -3.10 and 1.52 (and assuming the presence of UO_2X_2). Acidity constants typical of AlOH groups (Goldberg and Sposito, 1984) and site density based on 2.31 sites /nm^2 (Davis and Kent, 1990) were used in this analysis.

As shown in Figure 6.11, increasing the ionic strength to 0.1 M $NaNO_3$ resulted in an apparent decrease in uranyl sorption. Some under-prediction in uptake at low pH is now observed (right hand curve in Figure 6.11). FITEQL analysis indicated that a log K value for the UO_2OHX exchange complex on the order of -2.1 (with a small decrease in log K for $TOUO_2^+$ to 1.40) would satisfactorily describe the data (middle curve in Figure 6.11). A number of reasons could be hypothesized to account for the inconsistencies in model with change in ionic strength including i) poor choice of hypothesized surface complexes, ii) small deviation in ionic strength from that presumed (considered likely at the low ionic strength in question due to possible release of ions from the solid at low pH), and (iii) accumulated experimental uncertainties.

It is instructive to examine the distribution of surface complexes as a function of pH in the above cases. Distributions of uranyl surface species are shown in Figure 6.12 ((a) and (b)) for the experiments in 0.004M $NaNO_3$ and 0.1 M $NaNO_3$, respectively.

Nichika kaolinite

As discussed in qualitative terms above, the presence of excess iron on the Nichika kaolinite complicates the adsorption process by possibly blocking exchange sites. In addition, the iron oxides may create additional sites for specific uptake of uranyl species. We may thus hypothesize that the following three major surface interactions involving U(VI) are operative (in 0.1M $NaNO_3$):

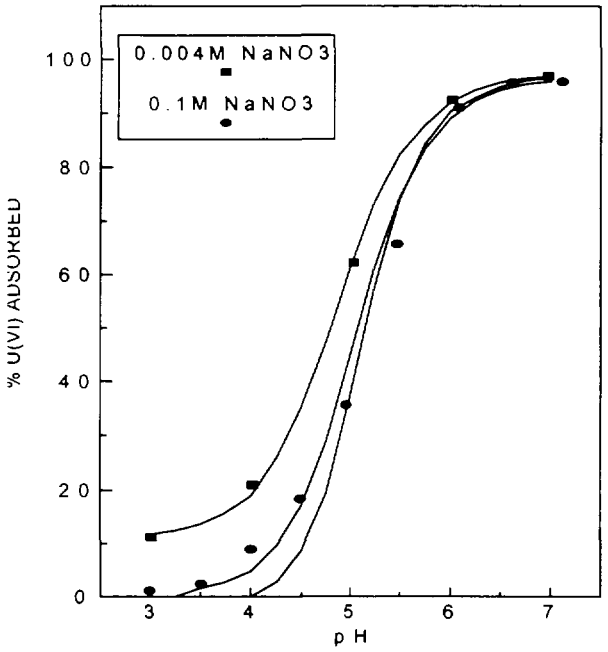

FIGURE 6.11 Comparison of data for U(VI) adsorption to KGa-1 kaolinite with a model having both ion exchange and specific sorption sites. The outer curves relate to I=0.004 (left) and I=0.1 (right) whereas the middle curve (for I=0.1) was obtained after adjustment of log K values for the sorption reactions (see text).

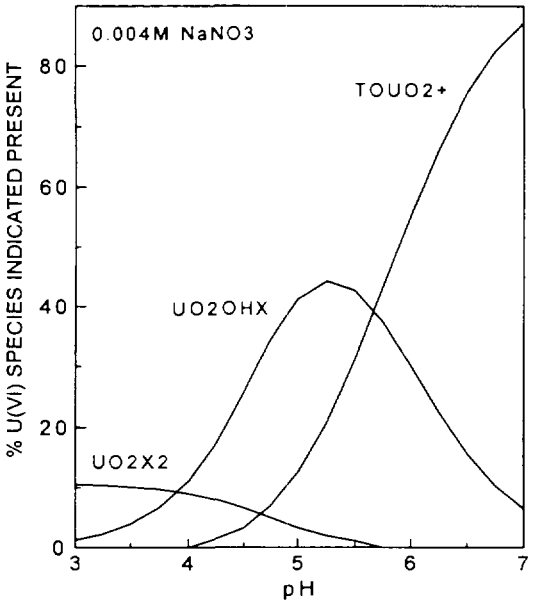

FIGURE 6.12 (a) Distribution of uranyl surface species from "best-fit" model to KGa-1 experimental data in 0.004M $NaNO_3$

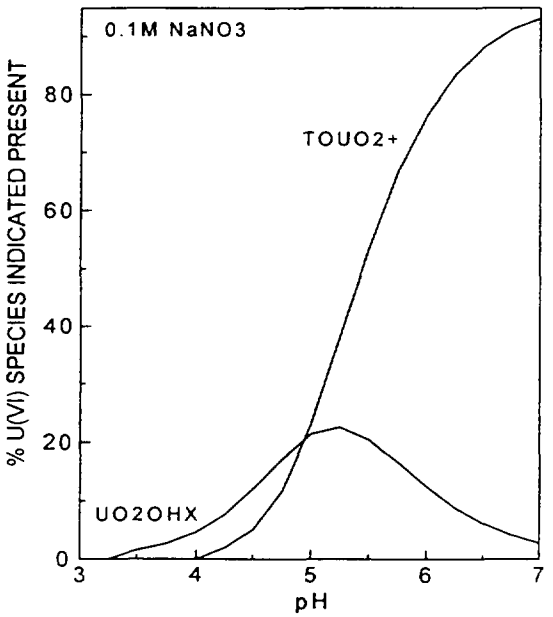

FIGURE 6.12 (b) Distribution of uranyl surface species from "best-fit" models to KGa-1 experimental data in 0.1M $NaNO_3$.

a) Formation of the hydroxylated exchange complex at cation exchange sites,

$$NaX + UO_2^{2+} + H_2O \leftrightarrow UO_2OHX + H^+ + Na^+ \quad (6.20)$$

b) Formation of specific U(VI) surface complexes at hydroxylated kaolinite edge sites

$$TOH + UO_2^{2+} \leftrightarrow TOUO_2^+ + H^+ \quad (6.21)$$

c) Formation of specific U(VI) complexes at iron oxide surface sites,

$$SOH + UO_2^{2+} + H_2O \leftrightarrow SOUO_2OH + 2H^+ \quad (6.22)$$

A squared dependency of uranyl uptake on pH, consistent with earlier results on the interaction of U(VI) with iron oxides, is assumed in Equation 6.22. As previously discussed, the uptake of U(VI) on iron oxide could be divided into strong and weak interactions, however, insufficient information is available for this level of analysis.

As derived above, site densities for NaX and TOH were estimated from the cation exchange capacity and surface area respectively, to yield $[NaX]_{TOTAL}$= 1.56 x 10^{-4}M and $[TOH]_{TOTAL}$= 4.05 x 10^{-4}M. Interestingly, the molar ratio of cation exchange sites to hydroxyl surface sites is significantly lower for Nichika (0.38) compared to KGa-1 kaolinite (0.60), and possibly reflects the blocking of exchange sites by iron oxides in the Nichika case.

Using the "best-fit" constants derived for formation of UO_2OHX and $TOUO_2^+$ on KGa-1 (in 0.1M $NaNO_3$ and for 10^{-6}M U(VI)) results in a surprisingly close correspondence between the model and the Nichika kaolinite experimental data (Figure 6.13). A small number of strong sites - possibly on iron oxides - can be added to give a reasonable description of the 10^{-8}M U(VI) data.

Unfortunately, the integrity of this analysis is weakened by a very poor correspondence between the model prediction and experimental data for $[U_{TOTAL}]$ = 10^{-4}M. Investigation of a range of alternative obvious options (site types and concentrations) led to no obvious solution which simulated the available data.

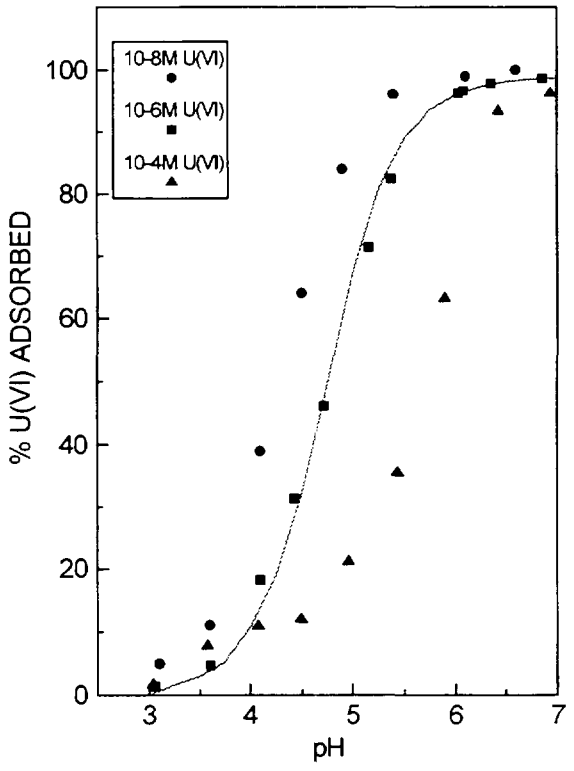

FIGURE 6.13 Comparison of experimental data obtained for uptake of 10^{-6}M U(VI) on 4 g/L Nichika kaolinite with model prediction assuming the formation of both a hydrolysed exchange complex UO_2OHX and a specifically bound surface complex $TOUO_2^+$. Constants (log K values) for these complexes have been derived from the KGa-1 data and are -2.09 and 1.40 respectively.

7 EFFECTS OF SUBSTRATE TRANSFORMATION ON U(VI) PARTITIONING

7.1 Introduction

Amorphous iron oxide (ferrihydrite) has a very high surface area (about 600 m^2/g), and thus a large capacity for adsorption of solution phase species such as uranyl ions. However, the more crystalline products to which it ages in the natural environment have much lower surface areas (typically at least an order of magnitude lower), and thus may be expected to have much less tendency to take up U(VI) species from solution. Furthermore, it has not been shown whether adsorbed species (such as U(VI)) are lost to solution on aging of these oxides, or are incorporated in some way into the crystal lattice of the aged substrate.

In this Section, isotope exchange techniques are used to examine:

i) the change in tendency of iron oxides to adsorb U(VI) from solution after aging, and

ii) the fate of adsorbed U(VI) when the oxide transforms to more crystalline forms.

7.2 Ferrihydrite Transformation on Aging

As succinctly described by Schwertmann and Cornell (1991), ferrihydrite is the initial product resulting from rapid hydrolysis of a ferric salt solution. It is thermodynamically unstable and, with time, transforms into goethite, hematite or a mixture of the two. These compounds form by different pathways. Hematite formation involves an internal dehydration/rearrangement process within the particles of ferrihydrite, whereas goethite formation proceeds via dissolution of ferrihydrite followed by nucleation and growth of the crystalline phase (Feitknecht and Michaelis, 1962; Schwertmann and Fischer, 1966; Johnston and Lewis, 1983).

Both processes take place only in the presence of water (Schwertmann and Cornell, 1991). Hematite formation is promoted by factors that induce aggregation of ferrihydrite particles (pH near the pzc of ferrihydrite, i.e. pH 7-8), or dehydration (i.e. increased temperature) (Cornell et al., 1989). The transformation to goethite is a dissolution/reprecipitation process in which the reaction rate is governed by the rate of dissolution of ferrihydrite or of nucleation/crystal growth of goethite (Schwertmann and Cornell, 1991). Formation of goethite is favoured by raising or lowering the pH away from the pzc, because this promotes dissolution of ferrihydrite (Schwertmann and Murad, 1983). A plot of the extent of transformation of ferrihydrite into goethite or hematite versus time displays an initial induction period corresponding to nucleation of the product followed by a faster stage which is first order with respect to the amount of precursor remaining in the system (Schwertmann and Fischer, 1966).

7.3 Previous Studies of the Impact of Mineral Aging on Trace Element Partitioning

Investigation of the impact of aging of hydrous oxides on the partitioning of trace elements between solid and solution phases has not been extensive. Shuman (1977) equilibrated zinc solutions with both fresh and aged Fe and Al oxyhydroxides and examined the resulting loss of cation from solution. The adsorption capacities for the fresh (amorphous) oxides were about ten times those of the aged oxides, which corresponded to a substantial difference between their respective CEC's and surface areas. Thus, for the iron oxide, CEC and surface area values were 354 meq/100 g and 303 m^2/g before aging and 8 meq/100 g and 29 m^2/g after aging. Corresponding amounts of zinc adsorbed were 10.3 mg Zn/g solid before aging and 0.9 mg Zn/g solid after aging. In another study it was shown that aging of hydrous ferric oxide at room temperature had little effect on Pb sorption (Gadde and Laitinen, 1974).

7.4 Experimental Study of Ferrihydrite Aging and its Effect on U(VI) Sorption

7.4.1 General experimental approach and particular considerations

The following general sequence was used in these iron oxide transformation and U(VI) uptake investigations:

(a) precipitate ferrihydrite,

(b) add ^{238}U to ferrihydrite,

(c) age the U(VI)/ferrihydrite mixture,

(d) take the solid substrate after aging and perform ^{236}U adsorption experiments over a wide pH range and, concomitantly, monitor ^{238}U desorption, and

(e) measure the distribution of both ^{236}U and ^{238}U after 2 days equilibration. The concentration of ^{236}U in solution indicates the amount adsorbed from solution, while the amount of ^{238}U in solution indicates the extent of release of ^{238}U from the transformed solid.

Before detailing the procedures used, it is of value to present particular issues considered in experimental design:

(a) All substrates used in these transformation/sorption studies should be formed by transformation from the same standard starting material.

(b) Parallel studies with fresh ferrihydrite (formed as described in Section 4.1.1, without aging) should be performed as a control.

(c) Experiments should be free of foreign ions such as oxalate, which may dramatically affect subsequent sorption experiments. This requirement negates the use of many published methods for inducing the transformation of iron oxides.

(d) The transformation should be achieved in such a way that the subsequent sorption experiments are carried out under conditions as close as possible to those used in sorption studies reported previously (Section 4).

(e) ^{238}U should be added to the experiment immediately after the initial formation of ferrihydrite but prior to the transformation step.

(f) The likely transformation products should be considered. As discussed earlier, goethite is the principal product formed after aging ferrihydrite at around 70°C and at pH values near 12. A slower transformation is achieved at near-neutral pH, with formation of greater amounts of hematite (particularly at higher temperatures).

7.4.2 Detailed procedure

Given the constraints outlined above, three types of experimental substrates were prepared:

Substrate A
Fresh ferrihydrite,

Substrate B
Ferrihydrite (plus U(VI)) aged at 70°C and pH 7 for one week, and

Substrate C
Ferrihydrite (plus U(VI)) aged at 70°C and pH 12 for one week.

These substrates were then used for U(VI) adsorption/desorption studies. Experimental conditions for the sorption investigations were selected to be similar to previous procedures, but suitable for ^{236}U and ^{238}U determination by α-spectrometry, i.e. 0.1M $NaNO_3$ containing 10^{-7}M ^{236}U, 10^{-5}M ^{238}U and 10^{-3}M Fe.

Detailed procedures for the three types of transformations were as follows:

Substrate A (Fresh ferrihydrite)

(a) place $Fe(NO_3)_3$ in a 25 mL teflon tube

(b) dissolve in 10 mL milli-Q water

(c) neutralise to pH 7 by dropwise addition of NaOH (5M then 0.5M and finally 0.05M); the precipitate forms immediately

(d) add sufficient ^{238}U to give 10^{-5}M in subsequent sorption experiments, allowing for later dilutions of the stock slurry

(e) dilute to exactly 20 mL with milli-Q water

(f) **transformation of the iron oxide**. There was no transformation step in this control experiment

(g) remove 0.5 g aliquots and place in centrifuge tube for sorption investigation

(h) add milli-Q water and $NaNO_3$

(i) immediately prior to commencement of the sorption experiment add ^{236}U and adjust the pH to the desired value (between 2 and 7)

(j) allow to equilibrate for two days while monitoring pH as in the standard sorption experiment procedure (Section 4), and

(k) separate a sample of the clear supernate and determine the concentrations of both ^{236}U and ^{238}U in solution by α-spectrometry.

Substrate B (aged at pH 7)

As above, except for the transformation step:

(f) **transformation of the iron oxide:** Age at 70°C for one week in the teflon tube maintaining pH close to 7.

Substrate C (aged at pH 12)

As above, except for the transformation step:

(f) **transformation of the iron oxide:** Raise the pH to 12 by addition of NaOH. Age at 70°C for one week.

Note that before commencing sorption experiments, the samples were returned to room temperature.

7.5 Results and Discussion

7.5.1 Fresh ferrihydrite (Substrate A)

XRD analysis of the freshly prepared iron oxide confirmed a lack of crystallinity (Figure 7.1).

Results of sorption studies on the fresh ferrihydrite (Figure 7.2) represent a typical U(VI) pH adsorption edge. Not surprisingly, the data for ^{238}U and ^{236}U are superimposed (within experimental error) since the ^{236}U was added to the system shortly after the ^{238}U and there was no intermediate aging step. Thus, the isotope exchange relationship in Figure 7.3 is linear and passes through 100%. In other words, 100% of the ^{238}U exchanges with the added ^{236}U during the course of the sorption experiment. There is no preference of either isotope for the surface.

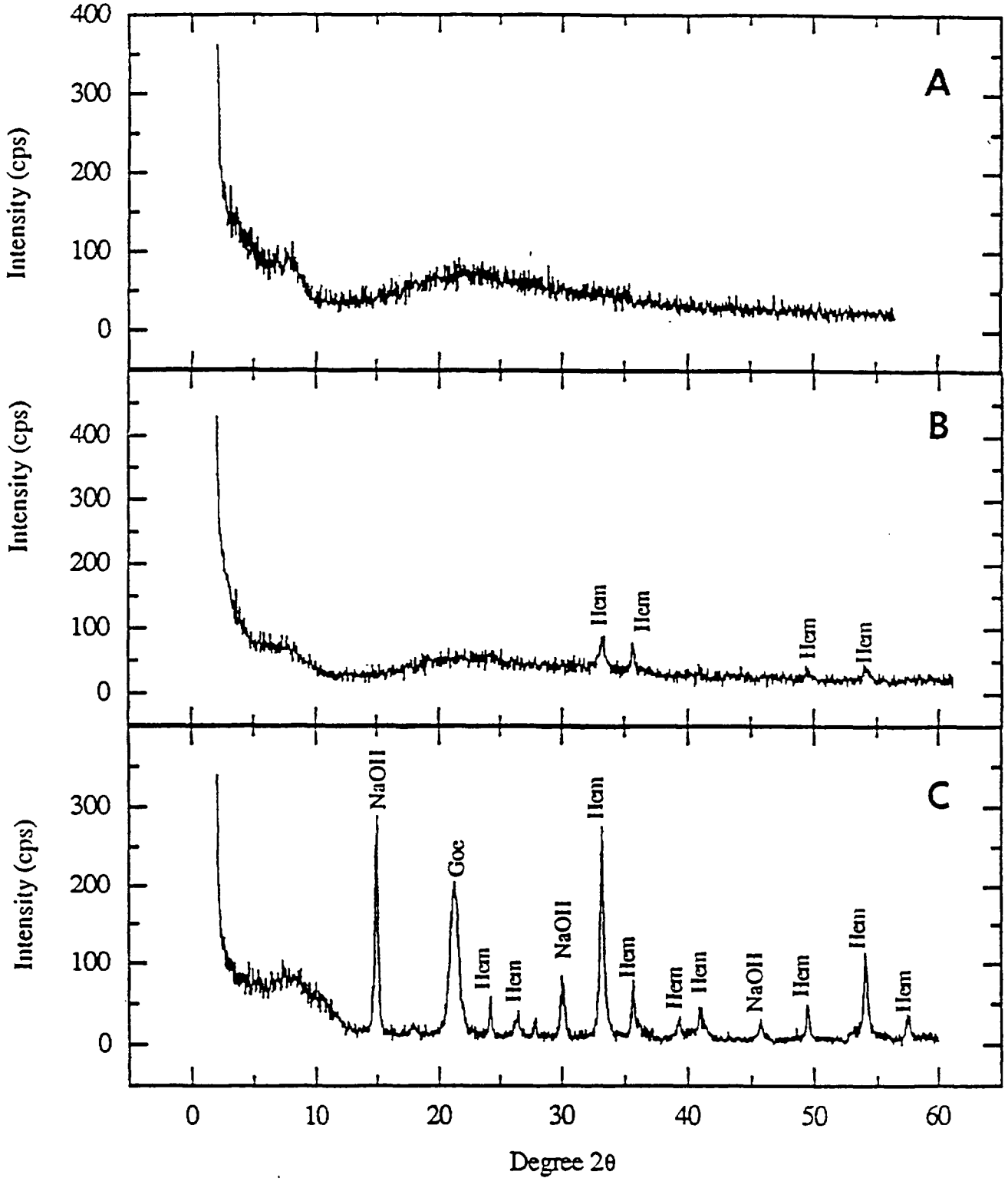

FIGURE 7.1 XRD spectra for fresh ferrihydrite (A) and for ferrihydrite aged for one week at pH 7 (B) and pH 12 (C).

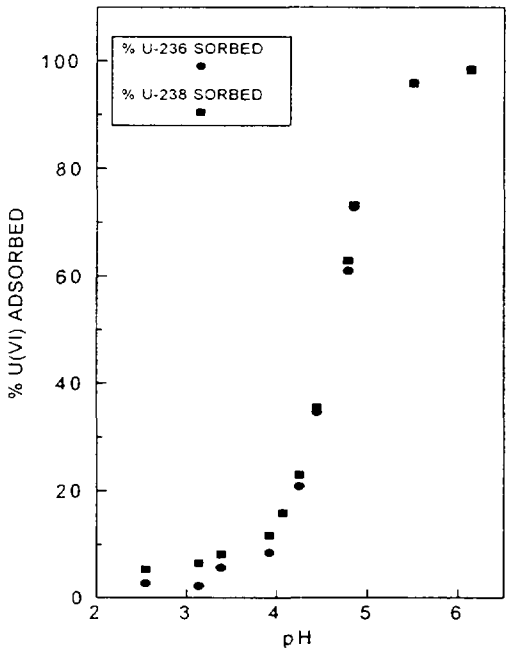

FIGURE 7.2 pH edges for ^{236}U and ^{238}U sorption to fresh ferrihydrite (sample A)

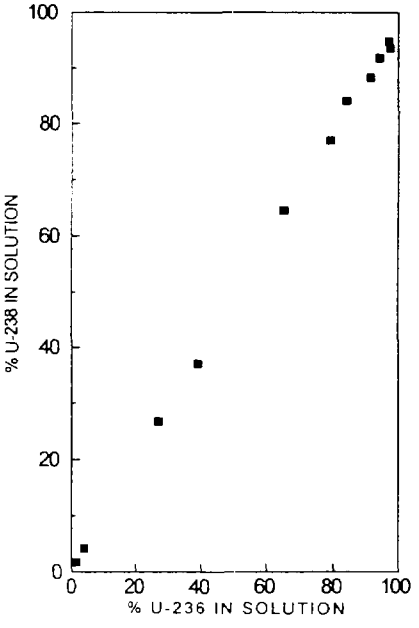

FIGURE 7.3 Relationship between the percentages of ^{236}U and ^{238}U in the aqueous phase at equilibrium with the fresh ferrihydrite (sample A).

A comparison of the above data with previous experimental results for the sorption of 10^{-5}M U(VI) to "standard" ferrihydrite (Figure 7.4) indicates a close similarity in uptake, despite the fact that the previous work was performed using ^{238}U only and was analysed by KPA. If anything, the new data curve is slightly displaced to the left. In the light of the results of subsequent experiments with substrates B and C (to be described), the slight displacement is attributed to this "control" experiment being performed with totally fresh ferrihydrite, rather than a sample aged for 65 hours at room temperature as previously used. A similar small shift was observed previously in results from the experiment in which U(VI) uptake on ferrihydrite (prepared in the "standard" fashion reported previously) was compared with uptake on co-precipitated oxide.

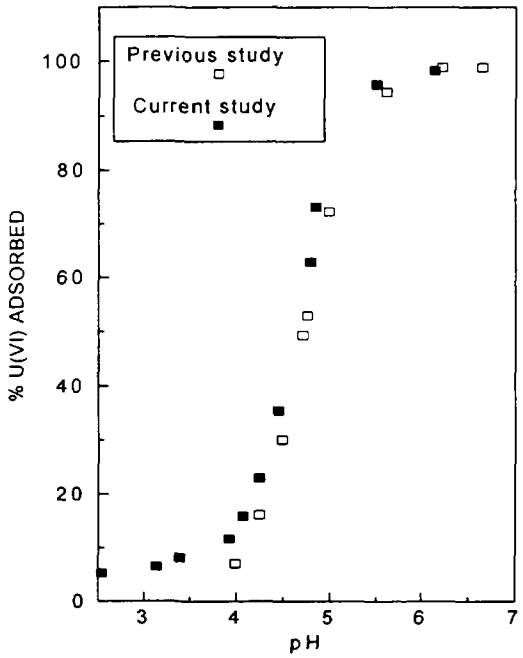

FIGURE 7.4 Comparison of uptake of 10^{-5}M ^{238}U on fresh ferrihydrite with results obtained for a similar substrate previously.

Tamms acid oxalate extraction of the ferrihydrite (Substrate A) at the conclusion of the experiment resulted in complete dissolution of the iron oxide, and total release of associated ^{238}U, indicating a complete absence of crystalline forms.

7.5.2 Aged ferrihydrite (pH 7, Substrate B)

Visually, the material aged at pH 7 appeared to be similar to the fresh ferrihydrite, but the XRD spectrum contained a weak hematite signal (Figure 7.1) indicating that some degree of transformation to a more crystalline form had occurred.

As can be seen in Figure 7.5, the proportions of ^{236}U and ^{238}U in solution are now distinctly different, particularly at low pH where some of the ^{238}U appears to be strongly retained by the solid thus preventing complete desorption.

The isotope exchange curve (Figure 7.6) is relatively linear up to a point where approximately 90% of ^{236}U is in solution. This corresponds to a pH of approximately 3.5. Above this pH, added ^{236}U is apparently exchangeable with a fixed proportion of the total ^{238}U present. At pH values more acidic than 3.5, an increase in the relative proportion of ^{238}U in solution is observed and this presumably occurs as the iron oxide undergoes acid dissolution with a concomitant release of bound ^{238}U.

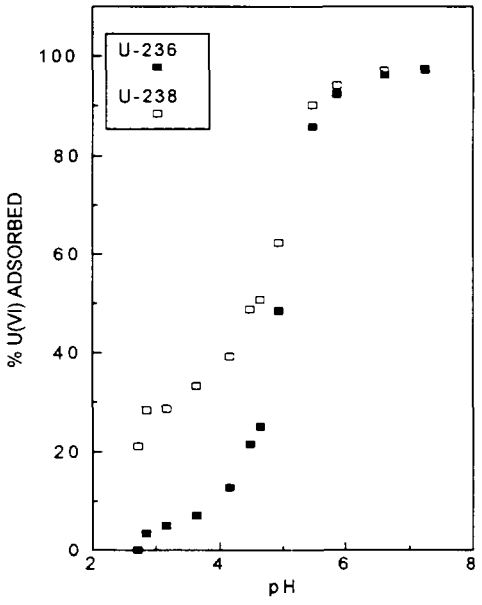

FIGURE 7.5 Comparison of percentage of ^{236}U and ^{238}U bound to Sample B (ferrihydrite aged at pH 7 for one week).

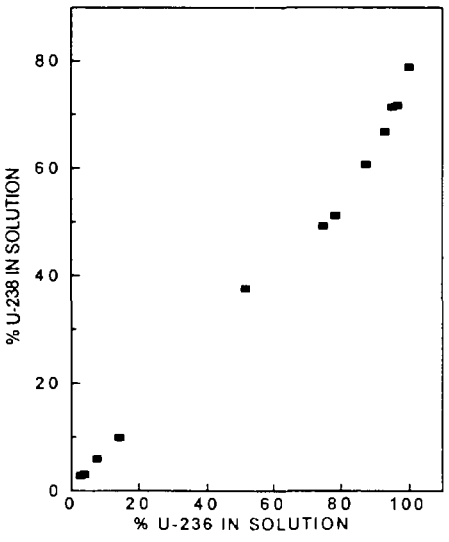

FIGURE 7.6 Relationship between percentages of ^{236}U and ^{238}U in the aqueous phase at equilibrium with samples prepared by method B.

TAO treatment of the oxide B at the conclusion of experiments resulted in only partial dissolution of the oxide. The phase removed by the TAO extraction was found to contain 78.4 ± 1.8% of the initial uranium content (Table 7.1), and 50.7%

of the Fe. This indicated that during the transformation process, about half of the Fe transformed to crystalline forms, and approximately 21.6% of the adsorbed ^{238}U was incorporated into the transformed Fe-oxide in such a way that it was resistant to leaching. A similar conclusion can be deduced from Figure 7.5, in that even at pH < 3, about 20% of ^{238}U remained bound by the solid, although no adsorption of ^{236}U occurred at such a low pH.

TABLE 7.1

PERCENTAGE OF URANIUM INCORPORATED INTO THE TRANSFORMED IRON MINERAL PHASE (DETERMINED BY TAO EXTRACTION)

Transformation experiment	% U(VI) incorporated in crystalline iron oxide[1]
A. Fresh ferrihydrite	Nil (fully soluble in TAO)
B. pH7, 1 week	21.6 ± 1.8
C. pH 12, 1week	30.1 ± 1.9

[1] Both TAO and residual fractions analysed for U
% Residual = $U_{residual}/(U_{accessible} + U_{residual})$

7.5.3 Aged ferrihydrite (pH 12, Substrate C)

Retention of ^{238}U within the solid matrix was even more distinct with this substrate than for Substrate B. In the pH range 2-5, there was significant association of the ^{238}U with the solid, whilst there was minimal adsorption of ^{236}U in this pH range.

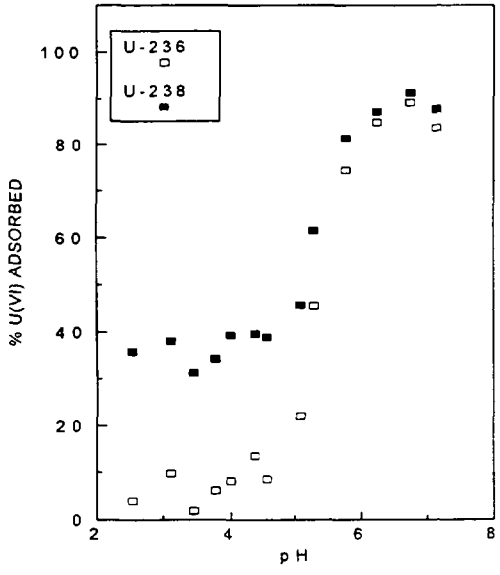

FIGURE 7.7 Comparison of percentage of ^{236}U and ^{238}U adsorbed to ferrihydrite aged at pH 12 for one week (Substrate C).

In this case the isotope exchange curve (Figure 7.8) is linear, but indicates that only a maximum of about 70% of the ^{238}U came into solution under the conditions of the sorption experiments, even when 100% of ^{236}U was in solution. The TAO extraction (Table 6.1) dissolved about 70% of the contained ^{238}U, also indicating that about 30% had been incorporated into the transformed Fe-oxide phase in a resistant form. Indeed, it was necessary to use a 6M HCl acid leach to dissolve this crystalline substrate and release the remaining bound ^{238}U to solution.

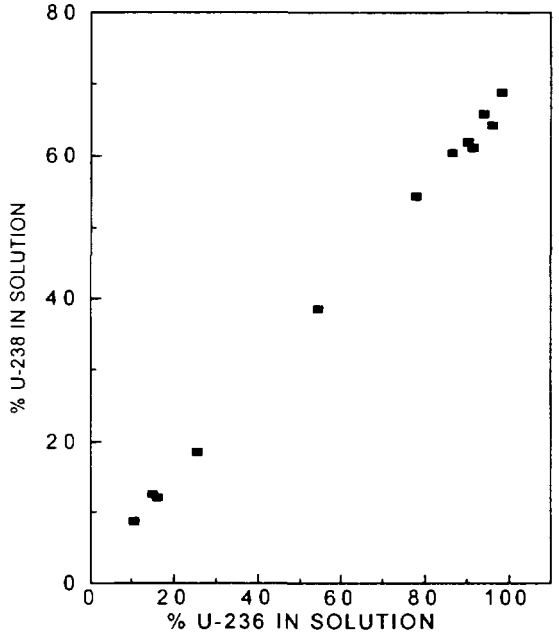

FIGURE 7.8 Relationship between percentages of ^{236}U and ^{238}U in the aqueous phase in equilibrium with substrate C (pH 12 aged ferrihydrite).

XRD analysis indicated that this sample was highly crystalline with significant quantities of both goethite and hematite (Figure 7.1). Visually the material was made up of compact pink particles, and appeared completely different to the fluffy red particles of Substrates A and B.

7.6 Conclusion

As has been previously suggested, the transformation of iron-oxides may be a significant process affecting the mobility of radionuclides in the environment. In this study we have demonstrated the potential influence of these transformations on U mobility. The first important effect of transformation is to produce a more stable substrate which has a greatly reduced tendency to adsorb U, relative to fresh ferrihydrite. The adsorption results for added ^{236}U on fresh and aged ferrihydrite (Substrates A, B and C) are brought together in Figure 7.9. The pH edges are observed to move to higher pH on aging, clearly demonstrating the decreasing affinity of the substrate for U(VI) as more crystalline phases are formed.

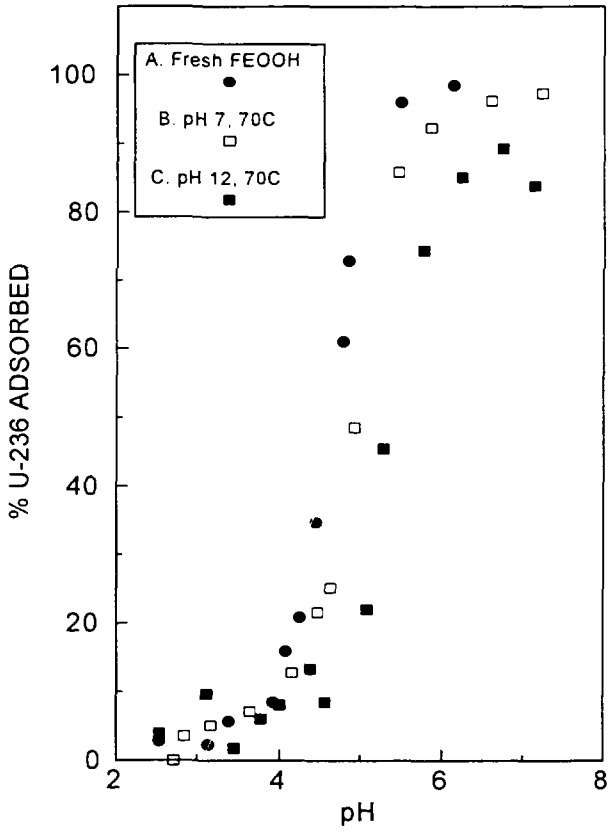

FIGURE 7.9 Comparison of pH edges for uptake of U on Fe-oxide substrates A, B and C. As can be seen, there is a decrease in sorption in the order A>B>C. Uranium uptake *decreases* with *increasing* crystallinity of the Fe-oxide.

As well as the reduced tendency of the transformed substrate to adsorb U, a second major conclusion can be drawn from this work. That is, there is some incorporation of adsorbed U during the transformation of iron-oxides, which makes it more resistant to leaching.

Thus, Fe-oxide transformations have a complex effect on U mobility. Whilst transformations provide a mechanism for U immobilisation by incorporation in the solid, the transformed solid has less ability to adsorb U directly from solution.

8 RESULTS OF EXPERIMENTAL AND COMPUTATIONAL STUDIES ON NATURAL SUBSTRATES

8.1 Introduction

As indicated above, particular attention was given in this study to natural substrates from Koongarra boreholes W1 and W2. Most of the adsorption work described in this Section was carried out using fine fractions obtained from these substrates. The separation and detailed characterisation of these materials was described in Section 4.

A similar range of experiments to that reported for the single substrates was undertaken, and these experiments are reported here. Thus, details of dependence of U(VI) sorption to these substrates as a function of pH, ionic strength, CO_2 partial pressure, CDB leaching and uranium concentration are given. Additionally, the relationship between ^{236}U in solution and ^{238}U leached was determined in these experiments, and this provides insight into the amount of "accessible" uranium present.

The motivation for these studies was to develop a predictive model of U(VI) partitioning between solution and the natural substrates. Based on the understanding of U(VI) sorption developed for single substrates, preliminary attempts at developing a surface complexation model of the natural substrate sorption data are described in the latter part of this Section.

8.2 Results of U(VI) Sorption Studies on W1 and W2 Fine Fractions

8.2.1 pH dependence and effect of carbonate

Results of experimental studies of the uptake of U(VI) on W1 and W2 fine fractions are given in Figure 8.1. These experiments were undertaken under air equilibration (0.03% CO_2) and also at elevated partial pressure of CO_2 (1% CO_2), over the pH range 2.5 - 10. As observed for the single phases, U(VI) is sorbed strongly to the natural substrate in the mid pH region (approx. 5 - 8) but increasingly exhibits a preference for the solution state as the pH falls below 5 (presumably because of the competition for surface sites with protons) and as the pH rises above 8 (attributed to the strength of uranyl carbonate complexes). This effect at high pH is enhanced at elevated partial pressures of CO_2.

The results shown in Figure 8.1 are quite similar for the two substrates. However, it should be noted that experimental conditions are not identical. A higher mass loading was used for the experiments with W1 substrate (20 g /L rather than 4 g /L as used for W2). As a result, the amount of sorption (expressed as % sorbed at a given pH) would be expected to be greater in the W1 case. In addition, whilst the *added* U is the same for both sets of experiments, the *total* U differs, on account of the higher accessible U content of the W2 sample.

In these studies, the total U(VI) concentration present is determined by the amount of accessible ^{238}U, which is different for each sample. Under the conditions of these

experiments, up to approximately 45 μg of ^{238}U may be leached per gram of W1, and up to approximately 250 μg of ^{238}U may be leached per gram of W2 (see Figure 8.2).

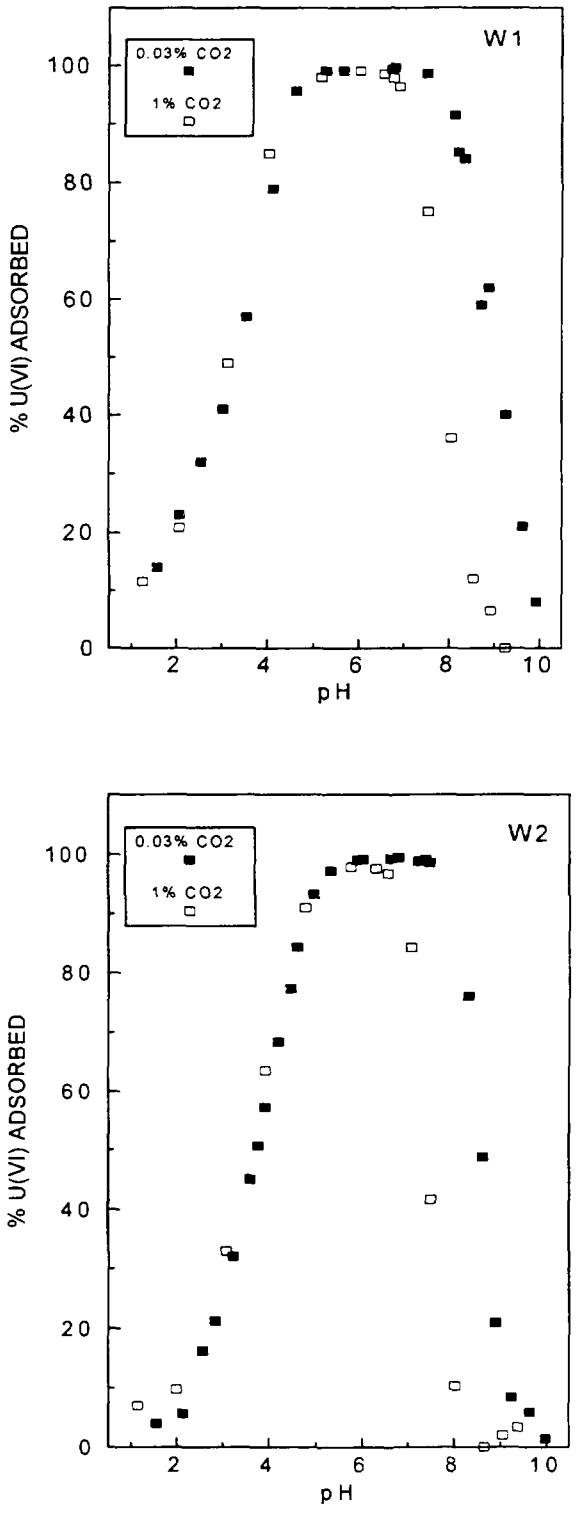

FIGURE 8.1 U(VI) adsorption to fine fractions of W1 (20 g /L) and W2 (4 g / L) core materials as a function of pH and at 0.03% and 1% CO_2. $[U]_{TOTAL}$ determined by concentration of accessible ^{238}U (see Figure 8.2).

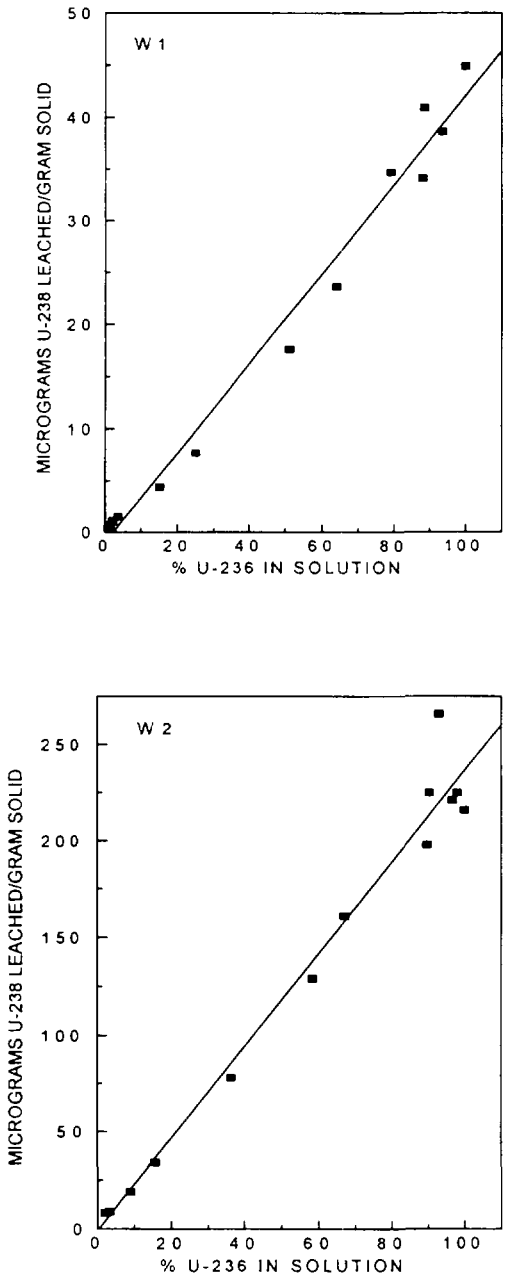

FIGURE 8.2 Relationship between the % of ^{236}U remaining in solution and the amount of ^{238}U leached from the solid over the range of pH depicted in Figure 8.1.

These amounts correspond to the Y value when the line of best fit in Figure 8.2 is extended to the point where 100% of the ^{236}U is in solution (this occurs at very high and very low pH where the affinity of the solid for U(VI) uptake is minimal). The amount of accessible U(VI) determined by this method in each case closely mirrors that observed in non-aggressive leaches by Morgans and TAO reagents (42.6 and 225 µg U extracted / g of W1 and W2 respectively, see Table 4.8). This observation

suggests that isotope exchange (as presented in Figure 8.2) is a convenient means of determining the amount of U(VI) that is accessible under the experimental conditions.

It should be pointed out that a linear relationship between ^{236}U and ^{238}U in solution can only be expected when the solution conditions are mild; i.e. the amount of accessible uranium is constant. Under extreme leaching conditions, the amount of ^{238}U available to the solution phase would be increased by the dissolution of stable mineral phases and the release of the uranium contained within these phases.

The results shown in Figure 8.1 demonstrate the effect of increased partial pressure of CO_2 on U(VI) adsorption to the solid phase. As previously shown for ferrihydrite, an increase in partial pressure of CO_2 results in an increased competition for U(VI) by carbonate anions, with a resultant decrease in the amount of U(VI) sorption by the solid phase.

8.2.2 Ionic strength dependence

As can be seen from the results in Figure 8.3, ionic strength does not appear to have a dramatic effect on U(VI) uptake to the natural Koongarra substrate in the low pH region.

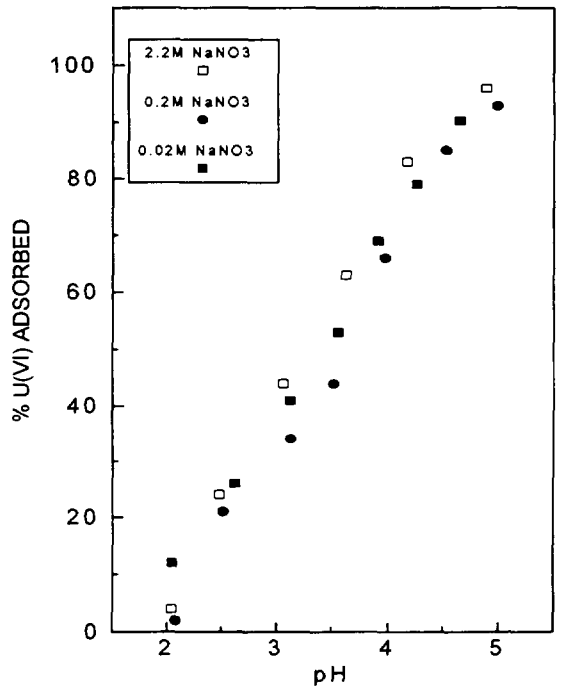

FIGURE 8.3 U(VI) uptake on W2 for solutions containing widely differing concentrations of $NaNO_3$ (0.02, 0.2 and 2.2 M $NaNO_3$).

This result suggests that ion exchange processes are not central to the association of U(VI) with the solid phase. The result could also be seen as confirmation that the uranyl surface complexes in the low pH region are not highly charged (highly charged surface species would be expected to exhibit some ionic strength dependency).

8.2.3 Uranium concentration dependence

As in the case of the single substrates, the low-pH sorption edge moved to a lower pH region with a decrease in the total amount of U in the system (Figure 8.4). Thus, on decreasing the concentration of U(VI) present from 100 to 3.8 μM in the presence of 4 g/L W2, the proportion of U(VI) adsorbed at pH 4 increased from approximately 15% to 60%.

In interpreting the results, it should be remembered that in the case of total U of 3.8 μM, a spike of ^{236}U (0.1 μM) was added, and most of the U in the system was derived from the W2 sample. (With an accessible U content of about 225 μg/g, a loading of 4 g/L yields about 900 μg/L or 3.8 μM total U). However, in the 100 μM case the majority of the U in the system was made up of U added to the aqueous phase. It should *not* be concluded that the curves in Figure 8.4 differ because one is desorption and the other is adsorption (although it is often experimentally found that desorption and adsorption curves are not super-imposed). In fact, both curves monitor the uptake (adsorption) of a spike. The difference in curve positions is attributed to a non-linear adsorption isotherm.

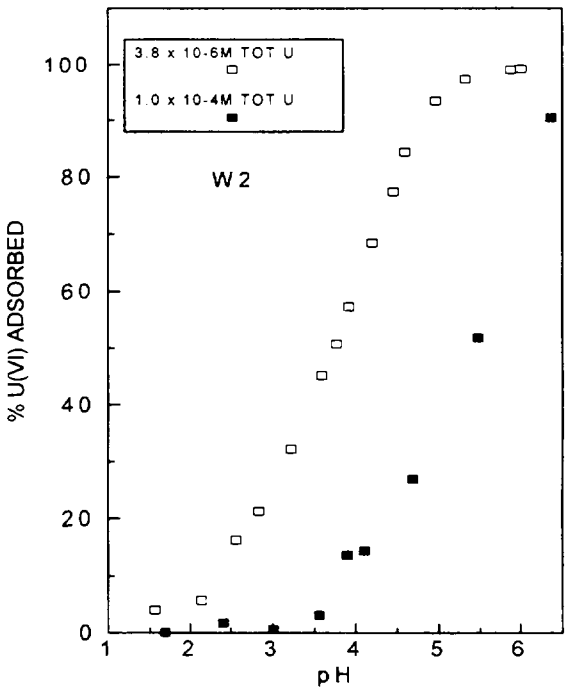

FIGURE 8.4 Uptake of UVI) on fine fractions of naturally occurring Koongarra W2 substrate.

Sorption is again not proportional to dissolved uranyl concentration, suggesting the presence of multiple site types (see earlier discussion) of differing concentrations and affinity for U(VI). The displacement between the two pH edges in Figure 8.4 is very large, and the U concentration dependence observed for this natural substrate is therefore much greater than that observed with 10^{-3} M ferrihydrite. This may indicate that site saturation is being approached in the sorption experiments on the W2 sample with total U of 10^{-4} M.

8.2.4 Effect of CDB leaching

The effect of CDB extraction was to move the pH of the sorption edge upwards. The reduced sorption on the CDB-treated Koongarra samples may be attributed to the removal of amorphous phases (such as SiO_2 and FeOOH), which make up a significant proportion of the surface area. Iron oxide removal does not always result in a decreased sorption of heavy metals (Section 5.3.2). However, in the case of the W2 sample it is clear that the phases removed by this reagent play a significant role in the uptake of U from solution.

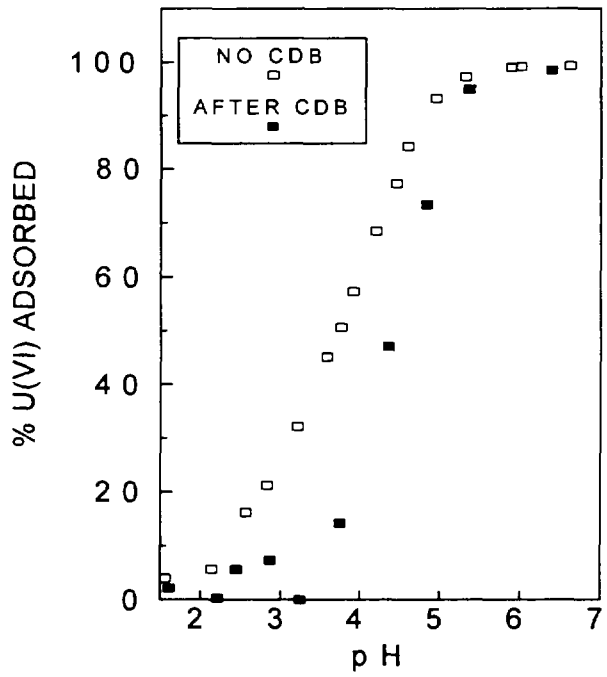

FIGURE 8.5 Effect of removal of amorphous and crystalline oxide phases (using the CDB reagent) on U(VI) adsorption to Koongarra natural substrate W2.

8.3 Modelling Uranyl Adsorption to Koongarra Substrates

Attention during the ARAP project focussed on modelling U(VI) adsorption by the fine particle fraction of the W2 sample, for which considerable characterisation data and experimental U sorption data is available. (At the time of writing, additional work on modelling uranyl adsorption to the W1 sample and other natural substrates is in progress).

Three different assumptions were used in modelling the uptake of U(VI) by the W2 substrate:

- Assumption that all U(VI) adsorbed to W2 is associated with the amorphous iron oxide phase,
- Assumption that a uniform site density over the complete surface accounts best for U(VI) uptake, or

- Assumption that strongly acidic sites in combination with more typical oxyhydroxide sites account for U(VI) uptake.

These options are considered below.

8.3.1 Adsorbed U(VI) associated with amorphous iron oxide phase only

In this modelling approach it is assumed that the residue after the TAO extraction consists of crystalline phases, which have a lower affinity for the adsorption of U(VI) from solution. In contrast, the TAO extraction is considered to remove coating phases and amorphous phases with a high surface area, and a correspondingly greater influence on adsorption. In addition to ignoring the contribution of TAO-residual phases, this approach (as applied here) also assumed that amorphous Fe phases dominate the sorption contribution of the phases removed by the TAO extraction.

It can be seen from Table 4.8 that the Morgans and TAO extractions (taken together) yield 1.69 mg Fe per gram of the W2 sample. Since mass loadings of 100 mg of W2 solids per 25 mL were used, this is equivalent to 6.8 mg Fe/L or 0.12 mM Fe. Using the strong and weak site densities found previously to be appropriate for U(VI) uptake on ferrihydrite (0.2 mol weak site/mol Fe and 0.0007 mol strong sites/mol Fe), we estimate that [TOH] = 2.4×10^{-5} M and [SOH] = 8.4×10^{-8} M.

In addition, based on a surface area for ferrihydrite of 600 m^2/g, this loading of ferrihydrite (equivalent to 0.12 mM as Fe) yields a surface area of 6.4 m^2/L.

For this part of the modelling, calculations were made with the equilibrium speciation computer code, HYDRAQL (Papelis et al., 1988). The HYDRAQL input data set for this case is given in Appendix 1, and the results are illustrated in Figure 8.6.

8.3.2 Uniform site density over complete surface

It is clear that the assumption that U(VI) uptake by the W2 sample can be accounted for by adsorption to amorphous iron oxide alone results in a major underprediction in extent of U(VI) uptake. In this section, it is instead assumed that sites distributed across the surface with a uniform density of 3.84 $\mu moles/m^2$ account for U(VI) uptake.

The surface area of W2 is 53.3 m^2/g. Since we have used 4 g of the W2 sample per L of solution, this is equivalent to 213.2 m^2/L or 8.19×10^{-4} M of sites. If we assume these sites are equivalent to the "weak" sites used to previously describe U(VI) uptake on ferrihydrite, then a log K = -5.21 and a surface complex stoichiometry of $TOUO_2OH$ may be considered appropriate. In this case (Figure 8.6, line marked TOH), the model accounts for a little more of the measured uptake, but still significantly underpredicts the extent of adsorption. The data set used in this instance is given in Appendix 2.

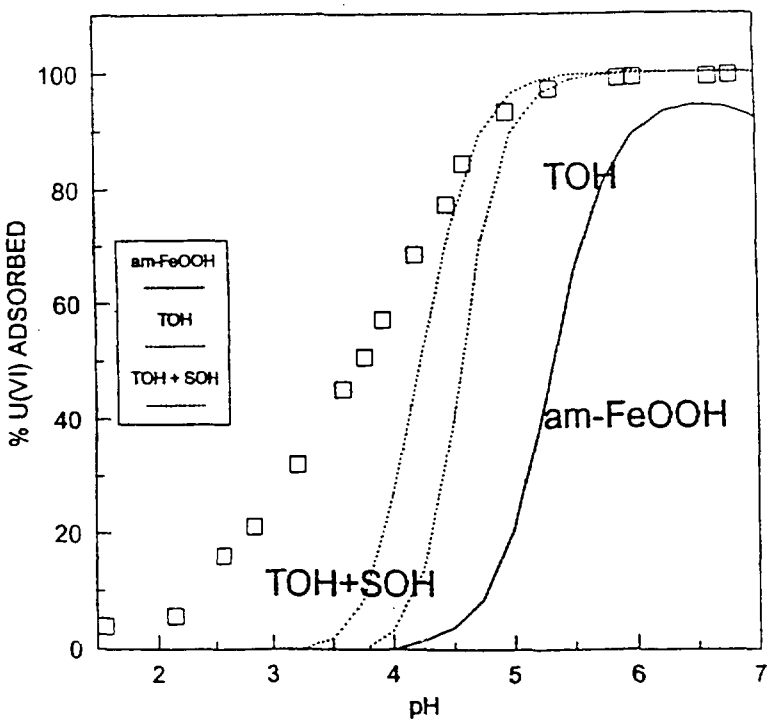

FIGURE 8.6 Results of diffuse double layer surface complexation model for U(VI) uptake on W2 assuming that a) only amorphous iron oxide accounts for the uptake (am-FeOOH), b) uniform density of "weak" sites (TOH) and c) uniform density of "strong" and "weak" sites (SOH + TOH).

The presence of strong U(VI) sorbing sites, as well as the weak sites (used above) might be expected to increase the predicted U uptake. Using the same proportion of strong and weak sites found most appropriate for ferrihydrite gives:

$[SOH] = 2.88 \times 10^{-6}$ M

$[TOH] = 8.19 \times 10^{-4}$ M

As can be seen from Figure 8.6 (the line marked TOH + SOH), the addition of the strong sites leads to some increase in predicted uptake, but this is insufficient to adequately describe the experimental data. The input data set corresponding to this case is given in Appendix 3.

8.3.3 Strongly acidic sites in combination with typical oxyhydroxide sites

A reasonable fit to the experimental data can be obtained using a model with the following features:

- Large concentration of strongly acidic, strongly binding sites; i.e.

$[SOH] = 10^{-4}$ M, $pK_{a1} = 1.75$, $pK_{a2} = 6.25$, $\log K = -1.80$

- Even larger concentration of weakly binding sites with acidic properties similar to ferrihydrite; i.e.

$[TOH] = 7.2 \times 10^{-4}$ M, $pK_{a1} = 7.29$, $pK_{a2} = 8.93$, log K = -5.00

The input data set corresponding to this model is given in Appendix 4, and the results of this modelling approach are shown in Figure 8.7.

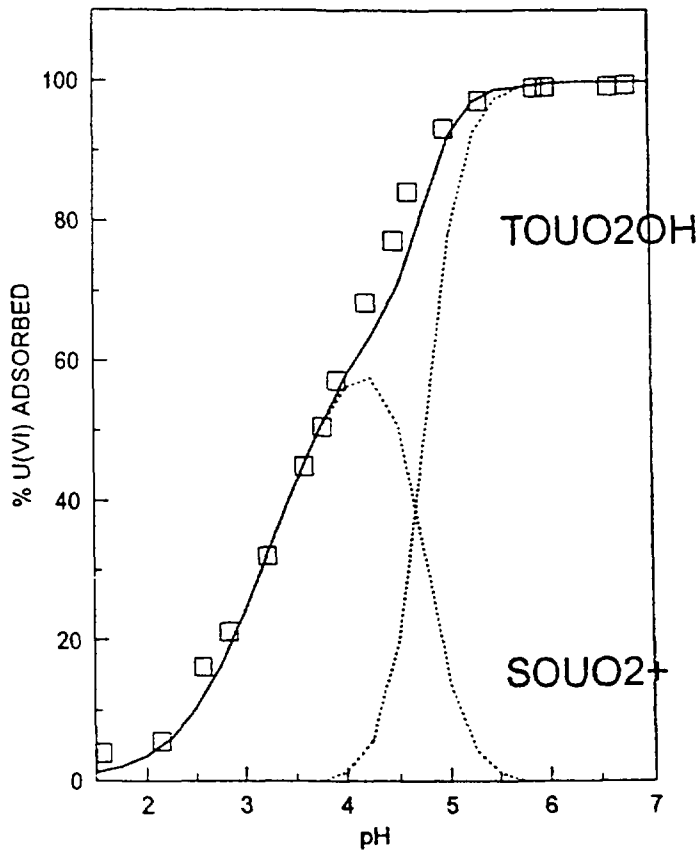

FIGURE 8.7 Comparison of experimental data and a model which contains both highly acidic strongly binding sites (forming $SOUO_2^+$) and sites more typical of iron oxyhydroxide (forming $TOUO_2OH$).

While this result demonstrates that a model can be derived that describes the experimental data satisfactorily, the parameters have been chosen by methods little better than trial and error. It is our view that considerably more insight into the nature of surface binding groups is required before undertaking more detailed modelling work.

Comprehensive experimental and modelling activities using the Koongarra substrates are continuing with additional support provided by the United States Nuclear Regulatory Commission. This research involves the Water Resources Division of the United States Geological Survey (Menlo Park), the University of New South Wales (Sydney) and the Australian Nuclear Science and Technology Organisation (Menai). Full reports of this research should be available through the USNRC after completion of this work.

9 SUMMARY AND CONCLUSIONS

9.1 Overview

Numerous studies of the partitioning of uranium between solid and solution phases have been reported, however, most of the available data is only of relevance to a particular solid substrate under a specific set of solution conditions. The distribution coefficients ("K_d values") obtained from such studies are of limited use in predicting the migration of uranium through porous media of variable composition, and under solution conditions that exhibit major spatial and temporal variability. There have been some attempts over the last ten years to develop more general models of the adsorption of U(VI) to solid substrates, but studies have only been conducted on a few simple (single mineral phase) substrates and little agreement exists either between the data obtained or in the optimal modelling approach.

In this study, uranium sorption to both single, well-defined mineral phases, and to selected natural substrates from Koongarra was experimentally studied. The surface properties of the experimental substrates were rigorously defined, and experiments were carried out over a wide range of solution conditions. Variables studied included pH, ionic strength, carbonate content, adsorbent and adsorbate concentrations and the presence of uranium complexants and (potentially) competing adsorbates (such as phosphate and fluoride).

9.2 Surface Complexation Modelling of Uranyl Sorption to Single Minerals

The adsorption of U to ferrihydrite was modelled using the surface complexation approach with a diffuse double layer description of the electrical double layer. While a single site type was used in our early studies, most success has been achieved by assuming the presence of two site types - one site type corresponding to a small set of high affinity cation binding sites and the other type corresponding to the total reactive sites available for sorption of protons, cations and anions. We have found that mononuclear uranyl surface species provide an adequate description of the adsorption results.

A combination of adsorption to "strong" sites >SOH (yielding uranyl surface complexes of the form $>SOUO_2^+$) and "weak" sites TOH (yielding $>TOUO_2OH$), i.e.

$$SOH + UO_2^{2+} \leftrightarrow SOUO_2^+ + H^+$$

$$TOH + UO_2^{2+} + H_2O \leftrightarrow TOUO_2OH + 2H^+$$

gave the most satisfactory agreement between model and experiment, with best-fit constants being derived using the non-linear optimisation program, FITEQL. Adsorption under basic conditions, where uranyl carbonate species dominate the solution speciation of U(VI), was also satisfactorily described without recourse to specific adsorption of uranyl carbonate complexes, even under elevated partial pressures of carbon dioxide typical of Koongarra groundwaters.

The presence of phosphate was found to increase the adsorption of U(VI) by ferrihydrite in the acidic pH region. The formation of ternary uranyl phosphate surface complexes appears to be the most likely reason for this enhanced U(VI) uptake. Incorporation of a ternary complex of the form $TPO_4UO_2^0$ in a surface complexation model of U(VI) sorption to ferrihydrite, with a formation constant determined using FITEQL provided close agreement between model and experiment.

Application of a surface complexation model involving only uptake on "weak" sites (to form $TOUO_2OH$) provided a good description of U(VI) sorption to quartz. This simple model adequately described the competing effect of solution complexation of U(VI) by fluoride.

The results of modelling uranyl adsorption to kaolinite were less satisfactory. Reasonable correspondence between experiment and model results was obtained at low U(VI) concentrations with a model incorporating both ion exchange and specific adsorption to strong and weak sites; i.e.

$$NaX + UO_2^{2+} + H_2O \leftrightarrow UO_2OHX + H^+ + Na^+$$

$$SOH + UO_2^{2+} \leftrightarrow SOUO_2^+ + H^+$$

$$TOH + UO_2^{2+} + H_2O \leftrightarrow TOUO_2OH + 2H^+$$

but this model did not adequately describe the experimental data obtained at high U(VI) concentrations. In addition, the ion exchange processes appeared to be most important under low pH conditions, where the sorption of U was relatively small and experimental errors comparatively large. These conditions are rarely found in the natural environment, and the experimental limitations raise questions about the applicability of the proposed model. Further insight into the factors controlling uranyl uptake on the kaolinitic clays examined here is obviously needed.

A range of ancillary studies have assisted in the definition of important sorbing surfaces, and in the elucidation of the effect of chemical processes on uranium partitioning between the solid and solution phases. In particular, U(VI) uptake on pre-formed and co-precipitated iron oxides indicated very little difference in partitioning, and suggested that short term aging of amorphous iron oxide phases does not dramatically influence the sorbing capacity.

The results of longer term aging studies (accelerated in these studies by heating) are also reported. Ferrihydrite aging (transformation to the more crystalline forms of goethite and hematite) decreases the surface area, with a concomitant reduction in capacity for adsorption of U(VI). Uranium present during the transformation process was partially incorporated into the re-crystallised mineral phases. The aging of amorphous iron oxides is therefore predicted to have a complex effect on U mobility. Whilst some U adsorbed to the solid will be immobilised during the transformation, the ability of the transformed solid to adsorb U from solution is lower than that of fresh ferrihydrite.

9.3 Studies on Koongarra Substrates

Fine fractions (nominally < 10 μm) of selected natural substrates from Koongarra were prepared, and uranyl partitioning between solution and solid phases was examined under a variety of conditions. These studies were typically undertaken using a trace of ^{236}U, enabling studies of isotopic exchange between ^{236}U and intrinsic ^{238}U to be undertaken. The amount of ^{238}U leached into the solution phase comprised "accessible" uranium, and generally exhibited a direct proportionality with the concentration of ^{236}U in solution. An estimate of the total accessible U(VI) present in natural substrates by this method was found to be in good agreement with the Tamms acid oxalate (TAO) extractable uranium in these samples.

Preliminary modelling studies, in which it was assumed that all U(VI) adsorption to the natural substrates could be accounted for by uptake on amorphous (TAO extractable) iron oxides were reasonably successful. However, more detailed analysis indicated significant difficulties with this approach. Consideration in this report was given to modelling the results using a "uniform site density", based on the BET surface area, but this also led to serious underprediction of U adsorption (when reasonable site densities were used).

A reasonable fit to the experimental data was achieved using a model with the following features:

- Large concentration of strongly acidic, strongly binding sites
- Even larger concentration of weakly binding sites with acidic properties similar to ferrihydrite.

While the agreement obtained between experiment and model demonstrates that a model can be derived that describes the experimental data satisfactorily, the parameters were chosen by methods little better than trial and error.

For the natural substrates (as well as the model minerals), the nature of surface complexes (and surface complexation reactions) remain poorly understood, and have not been directly established. Nonetheless, the amount of data obtained in this study, with a number of experimental parameters being varied over a wide range, has enabled more confidence to be placed in the modelling results. The derived model for ferrihydrite adequately accounts for the effect on U sorption of a number of parameters, most notably pH, pCO_2 and total U present. Few (if any) of the models previously proposed are adequate in this respect.

While the modelling of the data for the natural substrates is not as advanced, the U sorption data on the natural substrates show similar features to the U sorption on the model substrates. This suggests that the insights obtained in the modelling of the data for ferrihydrite will be valuable in deriving a model for the more complex natural substrates. However, it is our view that considerably more insight into the nature of surface binding groups on the natural Koongarra substrate is required before undertaking more detailed modelling work.

10 REFERENCES

Ames, L.L., McGarrah, J.E., Walker, B.A. and Salter, P.F. (1982) Sorption of uranium and cesium by Hanford basalts and associated secondary smectite. Chem. Geol. 35, 205-225.

Ames, L.L., McGarrah, J.E. and Walker, B.A. (1983a) Sorption of uranium and radium by biotite, muscovite and phlogopite. Clays and Clay Minerals 31, 343-351.

Ames, L.L., McGarrah, J.E. and Walker, B.A. (1983b) Sorption of trace constituents from aqueous solutions onto secondary minerals. I. Uranium. Clays and Clay Minerals 31, 321-334.

Balistrieri, L.S. and Chao, T.T. (1987) Selenium adsorption by goethite. Soil Sci. Soc. Am. J. 51, 1145-1151.

Balistrieri, L.S. and Murray, J.W. (1984) Marine scavenging: trace metal adsorption by interfacial sediment from MANOP site H. Geochim. Cosmochim. Acta 48, 921-929.

Belzile, N. and Tessier, A. (1990) Interactions between arsenic and iron oxyhydroxides in lacustrine sediments. Geochim. Cosmochim. Acta 54, 103-110.

Benson, L.V. and Teague, L.S. (1982) Diagenesis of basalts from the Pasco Basin, Washington. I. Distribution and composition of the secondary mineral phases. J. Sed. Petrol. 52, 595-613.

Borovec, Z. (1981) The adsorption of uranyl species by fine clay. Chem. Geol. 32, 45-58.

Cornell, R.M., Giovanolli, R. and Schneider, P.W. (1989). Review of the hydrolysis of iron(III) and the crystallization of amorphous iron (III) hydrate. J. Chem. Technol. Biotechnol. 46, 115-134.

Cowan, C.E., Zachara, J.M. and Resch, C.T. (1990) Cadmium adsorption on iron oxides in the presence of alkaline earth elements. Environ. Sci. Technol.

Cowan, C.E., Zachara, J.M., Smith, S.C. and Resch, C.T. (1991) Cadmium sorption to soil separates containing layer silicates and iron and aluminium oxides. Soil Sci. Soc. Am. J. (in press).

Davis, J.A. and Kent, D.B. (1990) Surface complexation modelling in aqueous geochemistry. In Hochella M.F. and A.F. White (eds.) Mineral-water interface geochemistry. Reviews in Mineralogy, Vol 23. Mineralogical Society of America, Washington, DC.

Davis, J.A., Fuller, C.C. and Cook, D.A. (1987) Mechanisms of trace metal adsorption by calcite: adsorption of Cd^{2+} and subsequent solid-solution formation. Geochim. Cosmochim. Acta 51, 1477-1490.

Davis, J.A., James, R.O. and Leckie, J.O. (1978a) Surface ionization and complexation at the oxide/water interface. I. Computation of electrical double layer properties in simple electrolytes. J. Colloid Interface Sci. 63, 480-499.

Davis, J.A., James, R.O. and Leckie, J.O. (1978b) Surface ionization and complexation at the oxide/water interface. II. Surface properties of amorphous iron oxyhydroxide and adsorption of metal ions. J. Colloid Interface Sci. 67, 90-107.

Davis, J.A., Kent, D.B., Rea, B.R., Maest, A.S. and Garabedian, S.P. (1990) Influence of redox environment and aqueous speciation on metal transport in groundwater: preliminary results of tracer injection studies. In H. Allen, D. Brown and E.M. Perdue (eds.). Metals in groundwater, Lewis Publishers, Chelsea, MI.

Dubinin, M.M. and Radushkevich, L.V. (1947) Equation of the characteristic curve of activated charcoal. Proc. Acad. Sci. U.S.S.R., Phys. Chem. Sect., 55: 331-333.

Duerden, P. et al (1987) Radionuclide migration around uranium ore bodies - analogue of radioactive waste repositories. United States Nuclear Regulatory Commission Contract NRC-04-81-172. Annual Report, August, 1986-87. Australian Atomic Energy Commission Report No. AAEC/C72.

Dzombak, D.A. and Morel, F.M.M. (1987) Adsorption of inorganic pollutants in aquatic systems. J. Hydraul. Eng. 113, 430-475.

Dzombak, D.A. and Morel, F.M.M. (1990) Surface complexation modelling: hydrous ferric oxide, John Wiley and Sons, New York.

Elliott, H.A., Liberati, M.R. and Huang, C.P. (1986) Effect of iron oxide removal on heavy metal sorption by acid subsoils. Water, Air and Soil Pollution 27, 379-389.

Feitknecht, W. and Michaelis, W. (1962) Uber die Hydrolyse von Eisen (III)-perchlorat-Losungen. Helv. Chim. Acta 45, 212-224.

Fritz, S.J. and Mohr, D.W. (1984) Chemical alteration in the micro-weathering environment within a spheroidally-weathered anorthosite boulder. Geochim. Cosmochim. Acta 48, 2527-2535.

Gadde, R.R. and Laitinen, H.A. (1974) Studies of Heavy Metal Adsorption by Hydrous Iron and Manganese Oxides, Anal. Chem. 46, 2022-2026.

Gee, G.W. and Bauder, J.W. (1986) Particle size analysis. In Methods of Soil Analysis, Part 1. Physical and Mineralogical Methods, 2nd Edition. A. Klute (Ed.). American Society of Agronomy/Soil Science Society of America.

Goldberg, S. and Sposito, G. (1984) A Chemical Model of Phosphate Adsorption by Soils. I. Reference Oxide Minerals. Soil Sci. Soc. Am. J. 48, 772-778.

Goldsztaub, S. and Wey, R. (1955) Absorption des ions uranyles par les argiles. Bull. Soc. Franc. Miner. Crist. 78, 242-248.

Gruebel, K.A., Davis, J.A. and Leckie, J.O. (1988) The feasibility of using sequential extraction techniques for arsenic and selenium in soils and sediments. Soil Sci. Soc. Am. J. 52, 390-397.

Gupta, A.R. and Venkataramani, B. (1988) Sorption of Uranyl Ions on Hydrous Oxides. A New Surface Hydrolysis Model. Bull. Chem. Soc. Jpn. 61, 1357-1362.

Guthrie, V.A. and Kleeman, J.D. (1986) Changing uranium distributions during weathering of granite. Chem. Geol. 54, 113-126.

Higgo, J.J. and Rees, L.V.C. (1986) Adsorption of actinides by marine sediments: effect of the sediment/seawater ratio on the measured distribution ratio. Environ. Sci. Technol. 20, 483-490.

Ho, C.H. and Doern, D.C. (1985) The sorption of uranyl species on a hematite sol. Can. J. Chem. 63, 1100-1104.

Ho, C.H. and Miller, N.H. (1986) Adsorption of uranyl species from bicarbonate solution onto hematite particles. J. Colloid Interface Sci. 110, 165-171.

Honeyman, B.D. and Santschi, P.H. (1988) Metals in aquatic systems. Environ. Sci. Technol. 22, 862-871.

Hsi, C.D. and Langmuir, D. (1985) Adsorption of uranyl onto ferric oxyhydroxides: Application of the surface complexation site-binding model. Geochim. Cosmochim. Acta 49, 1931-1941.

Huang, C.P. and Stumm, W. (1973) Specific adsorption of cations on hydrous α-Al_2O_3. J. Colloid Interface Sci. 22, 231-259.

Ivanovich, M., Longworth, G., Wilkins, M.A., Hasler, S.E. and Lloyd, M.J. (1988) Measurement of effective K_d factors for the long-lived uranium and thorium isotopes in sample of London Clay (Bradwell) and mudrock (Fulbeck). Nirex (UK) report NSS-R117. Nirex, London.

James, R.O and Parks, G.A. (1982). Characterisation of aqueous colloids by their electrical double layer and intrinsic surface chemical properties. Surface and Colloid Science, 12, 119-216.

Johnston, J.H. and Lewis, D.G. (1983). A detailed study of the transformation of ferrihydrite to hematite in an aqueous medium at 92°C. Geochim. Cosmochim. Acta 47, 1823-1831.

Kent, D.B., Tripathi, V.J., Ball, N.B. and Leckie, J.O. (1986) Surface-complexation modeling of radionuclide adsorption in sub-surface environments. Stanford University Department of Civil Engineering Technical Report No. 294.

Kinniburgh, D.G. (1986) General purpose adsorption isotherm. Environ. Sci. Technol. 20, 895-904.

Kohler, M., Honeyman, B.D. and Leckie, J.O. (1992) U(VI) sorption on goethite: effects of ionic strength and C_T. Geochim. Cosmochim. Acts (in press).

Krishnaswami, S., Graustein, W.C., Turekian, K.K. and Dowel, J.F. (1982) Radium, thorium and lead isotopes in groundwaters: aplication to the *in situ* determination of adsorption-desorption rate constants and retardation factors. Water Resour. Res. 18, 1663-1675.

Landstroem, O. and Tullborg, E-L. (1989) The influence of fracture mineral groundwater interaction on the mobility of U, Th, REE and other trace elements in different redox environments. In Miles, D.L. (ed.) Proceedings of International Symposium on Water Rock Interaction, Rotterdam, The Netherlands.

Langmuir, D. (1978) Uranium solution-mineral equilibria at low temperatures with applications to sedimentary ore deposits. Geochim. Cosmochim. Acta 42, 547-569.

Lauerer, B., Pusch, A., Stadler, K.H. and Boehm, H.P. (1992) Adsorption of tetrammine-carbonato and tetrammine-cis-diaqua and triethylene tetramine-carbonato and triethylenetetramine-cic-diaqua complexes of cobalt (III) on titanium dioxide as models for the binding of uranyl ions from the tricarbonatouranyl complex ion. Zeitschrift fur Naturforschung Section B - A Journal of Chemical Sciences 47(5), 625-634.

Laul, J.C. and Smith, M.R. (1988) Disequilibrium study of natural radionuclides of uranium and thorium series in cores and briney groundwaters from the Palo Duro Basin, Texas. Rad. Waste Manag. Nucl. Fuel Cycle 11, 169-225.

Laul, J.C., Smith, M.R. and Hubbard, N. (1985) Behaviour of natural uranium, thorium and radium isotopes in the Wolfcamp brine aquifers, Palo Duro Basin, Texas. Sci. Basis Nucl. Waste Manag. IX, 673-680.

Leckie, J.O. and Tripathi, V.J. (1985) Effect of geochemical parameters on the distribution coefficient K_d. Proceedings of the 5th International Conference on Heavy Metals in the Environment, Athens, Greece, Volume 2.

Luoma, S.N. and Davis, J.A. (1983). Requirements for modelling trace metal partitioning in oxidised estuarine sediments. Marine Chem. 12, 159-181.

Maya, L. (1982). Sorbed uranium (VI) species on hydrous titania, zirconia and silica gel. Radiochim. Acta 31, 147-151.

McKinley, I.G. and Alexander, W.R. (1992a). Constraints on the applicability of "in situ distribution coefficient" values. J. Environ. Radioactivity 15, 19-34.

McKinley, I.G. and Alexander, W.R. (1992b) Assessment of radionuclide retardation: realistic application of natural analog studies. Radiochim. Acta (in press).

Means, J.L., Crerar, D.A. and Duguid, J.O. (1978) Migration of radioactive wastes: radionuclide mobilisation by complexing agents. Science 200, 1479-1481.

Megumi, K. and Mamuro, T. (1977) Concentration of uranium series nuclides in soil particles in relation to their size. J. Geophys. Res. 82, 353-356.

Megumi, K., Oka, T., Yaskawa, K. and Sakanoue, M. (1982) Contents of natural radioactive nuclides in soils in relation to their surface area. J. Geophys. Res. 87, 10857-10860.

Morel, F.M.M. (1983) Principles of aquatic chemistry. Wiley, New York.

Nesbitt, H.W. (1979) Mobility and fractionation of rare earth elements during weathering of granodiorite. Nature 279, 206-210.

Nuss, L. and Wey, R. (1956). Sur l'adsorption des cations uranyles par la montmorillonite. Bull. Gr. Franc. Argiles 7, 15-19.

Page, A.L., Miller, R.H. and Keeney, D.R. (1982) Methods of Soil Analysis, Part 2, Chemical and Biological Properties. American Society of Agronomy, Madison, Wisconsin.

Papelis, C., Hayes, K.F. and Leckie, J.O. (1988) HYDRAQL: A Program for the Computation of Aqueous Batch Systems Including Surface Complexation Modeling of Ion Adsorption at the Oxide / Solution Interface. Tech. Rep. 306. Dept. of Civil Engineering, Stanford University.

Payne, T.E. and Waite, T.D. (1991) Surface complexation modelling of uranium sorption data obtained by isotope exchange techniques. Radiochim. Acta 52/53, 487-493.

Ryden, J.C., McLaughlin, J.R. and Syers, J.K. (1977). Mechanisms of phosphate sorption by soils and hydrous ferric oxide gel. J. Soil Sci. 28, 72-92.

Sagert, N.H., Ho, C.H. and Miller, N.H. (1989) The adsorption of uranium(VI) onto a magnetite sol. J. Colloid Interface Sci. 130, 283-287.

Santschi, P.H., Bajo, C., Mantovani, M., Orciuolo, D., Cranston, R.E., and Bruno, J. (1988) Uranium in pore waters from North Atlantic (GME and Southern Nares Abyssal Plain) sediments. Nature 331, 155-157.

Schindler, P.W. and Gamsjager, H. (1972) Acid-base reactions of the TiO_2 (anatase)-water interface and the point of zero charge of TiO_2 suspensions. Kolloid Z. u. Z. Polymere 250, 759-763.

Schindler, P.W. and Kamber, H.R. (1968) Die aciditat von silanolgruppen. Helv. Chim. Acta 51, 1781-1786.

Schwertmann, U. and Cornell, R.M. (1991). Iron oxides in the laboratory: Preparation and characterisation. VCH Publishers, New York.

Schwertmann, U. and Fischer, W.R. (1966). Zur Bildung von α-FeOOH and α-Fe_2O_3 aus amorphem Eisen(III)-hydroxid. III. Z. Anorg. Allg. Chem. 346, 137-142.

Schwertmann, U. and Murad, E. (1983). Effect of pH on the formation of goethite and hematite from ferrihydrite. Clays Clay Min. 31, 277-284.

Shuman, L.M. (1977). Adsorption of Zn by Fe and Al hydrous oxides as influenced by aging and pH. Soil Sci. Soc. Am. J. 41, 703-706.

Sibley, T.H. and Myttenaere, C. (1986) Application of distribution coefficients to radiological assessment models. Elsevier, The Netherlands.

Sokolowska, Z. and Szczypa, J. (1980) Adsorption isotherms for weak acid anions in soils. Geoderma 24, 349-361.

Sposito, G. (1984). The Surface Chemistry of Soils. Oxford University Press, New York.

Sposito, G.(1986) On distinguishing adsorption from surface precipitation. In J.A. Davis and K.F. Hayes (eds.) Geochemical processes at mineral surfaces. ACS Symp. Ser. 323, Am. Chem. Soc., Washington, D.C.

Starik, I.E., Starik, F.E. and Appolonova, A.N. (1958) Adsorption of microquantities of uranium by iron hydroxides and its desorption by the carbonate method. J. Inorg. Chem. USSR 3, 181-193.

Stumm, W., Huang, C.P. and Jenkins, S.R. (1970) Specific chemical interactions affecting the stability of dispersed systems. Croat. Chem. Acta 42, 223-244.

Tessier, A., Campbell, P.G.C. and Bisson, M. (1979) Sequential extraction procedure for the speciation of particulate trace metals, Anal. Chem. 51, 844-851.

Tessier, A., Carignan, R., Dubreuil, B. and Rapin, F. (1989) Partitioning of zinc between the water column and the oxic sediments in lakes. Geochim. Cosmochim. Acta 53, 1511-1522.

Tripathi, V.S. (1983) Uranium transport modelling: geochemical data and sub-models. PhD Dissertation, Stanford University, Stanford, CA.

Tsunashima, A., Brindley, G.W. and Bastovanov, M. (1981) Adsorption of uranium from solutions by montmorillonite: compositions and properties of uranyl montmorillonites. Clays and Clay Minerals 29, 10-16.

Van der Weijden, C.H., van Leeuwen, M. and Peters, A.F. (1985) The adsorption of U(VI) onto precipitating amorphous ferric hydroxide. Uranium 2, 53-58.

Van Olphen, H. and Fripiat, J.J. (1979) Data handbook for clay materials and other non-metallic minerals. Pergamon, Oxford.

Veith, J.A. and Sposito, G. (1977) On the use of the Langmuir equation in the interpretation of "adsorption" phenomena. Soil Sci. Soc. Am. J. 41, 697-702.

Venkataramani, B. and Gupta, A.R. (1991) Effect of anions on the sorption of uranyl ions on hydrous oxides: Application of the surface hydrolysis model. Colloids and Surfaces 53, 1-19.

Warnecke, E., Hollman, A. and Stier-Friedland, G. (1984) Migration of radionuclides. Experiments within the site investigation program at Gorleben. Mater. Res. Soc. Symp. Proc. 26, 41-48.

Westall, J (1982) FITEQL: A program for the determination of chemical equilibrium constants from experimental data. Chemistry Department, Oregon State University, Corvallis, Oregon.

Yanase, N., Nightingale, T., Payne T. and Duerden, P. (1991) Uranium distribution in mineral phases of rock by sequential extraction procedure. Radiochim. Acta 52/53, 387-393.

APPENDICES

Appendices 1-4 contain the HYDRAQL input data sets used for modelling U-sorption to the W2 substrate (section 8.3).

APPENDIX 1

HYDRAQL INPUT DATA SET ASSUMING THAT ALL U(VI) ADSORBED TO W2 IS ASSOCIATED WITH THE AMORPHOUS IRON OXIDE PHASE

```
 Modeling of U(VI) adsorption on Fe(OH)3 in W2 as a f(pH, conc U), DDL model
 0.100 M NaNO3  0.12 mM Fe; 600 m2/gm
0.1000 0 0.0000 25.00 1.000E-05 1 100 /XMU KEYMU ACTCOR TEMP EPS NCASES ITMAX
1     1      0       1       1      1       /IHYDRA IINPUT ICHARG IPDIST IPCENT IALL
1     1      2       1       80000          /KEY IADS MODEL IDIFOP LIMADS
0     0    0  6.4     0  0   0  0         /C11 C21 C31 AREA1 C12 C22 C32 AREA2
32    86520    86530      0      0         0      0      0      0
0       0 0 0 0 0 0 0 0 0 0 /
3.00   10.00 0.25                         /LINE FOR PH STEPPING
  5    -1.000    1.000E-1                 /DATA FOR COMPONENTS  Na+
157    -1.000    1.000E-1                 /                     NO3-
 50    -2.890    0.000E-0                 /                     H+
101   -16.000    0.000E-0                 /                     CO3
 32    -6.000    3.800E-6                 /                     U(VI)
184    -8.000    8.400E-8                 /                     SOH
185    -5.000    2.400E-5                 /                     TOH
183    -1.000    0.000                    /                     PSID
  0     0.000    0.000                    /
2                                         /
86105   -8.93  184 1  50 -1  183  -1     0  0      0  0    0    0 /
86110    7.29  184 1  50  1  183   1     0  0      0  0    0    0 /
86115   -8.93  185 1  50 -1  183  -1     0  0      0  0    0    0 /
86120    7.29  185 1  50  1  183   1     0  0      0  0    0    0 /
86520   -1.60  184 1  50 -2   32   1     0  0      0  0    0    0 /
86530   -5.21  185 1  50 -2   32   1     0  0      0  0    0    0 /
12130    9.70  101 1  32  1    0   0     0  0      0  0    0    0 /
12135   17.00  101 2  32  1    0   0     0  0      0  0    0    0 /
12140   21.63  101 3  32  1    0   0     0  0      0  0    0    0 /
12141   -1.18  101 1  32  2   50  -3     0  0      0  0    0    0 /
12100   -5.20   32 1  50 -1    0   0     0  0      0  0    0    0 /
12112  -12.00   32 1  50 -2    0   0     0  0      0  0    0    0 /
12114  -20.00   32 1  50 -3    0   0     0  0      0  0    0    0 /
12116  -33.00   32 1  50 -4    0   0     0  0      0  0    0    0 /
12118   -2.80   32 2  50 -1    0   0     0  0      0  0    0    0 /
12120   -5.63   32 2  50 -2    0   0     0  0      0  0    0    0 /
12123   -11.9   32 3  50 -4    0   0     0  0      0  0    0    0 /
12125  -15.56   32 3  50 -5    0   0     0  0      0  0    0    0 /
12127   -21.9   32 4  50 -7    0   0     0  0      0  0    0    0 /
12128   -31.0   32 3  50 -7    0   0     0  0      0  0    0    0 /
 0     0.0    0 0   0  0    0   0    0  0      0  0   0    0 /
3                                                                 /
50      3.00  0 0 0 0 0 0 0 0 0 0 0 0 0 0 0 0 0 0 0 0 0 0 0 0 0 0 0 0 0 0 0 0 0 /
25000  21.64  0 0 0 0 0 0 0 0 0 0 0 0 0 0 0 0 0 0 0 0 0 0 0 0 0 0 0 0 0 0 0 0 0 /
0       0.00  0 0 0 0 0 0 0 0 0 0 0 0 0 0 0 0 0 0 0 0 0 0 0 0 0 0 0 0 0 0 0 0 0 /
6                                                                                 /
183     0.00  0 0 0 0 0 0 0 0 0 0 0 0 0 0 0 0 0 0 0 0 0 0 0 0 0 0 0 0 0 0 0 0 0 /
 0 0 0 0 0 0 0 0 0 0 0 0 0 0 0 0 0 0 0 0 0 0 0 0 0 0 0 0 0 0 0 0 0 0 0 0 0 0 0 /
 0 0 0 0 0 0 0 0 0 0 0 0 0 0 0 0 0 0 0 0 0 0 0 0 0 0 0 0 0 0 0 0 0 0 0 0 0 0 0 /
```

APPENDIX 2

HYDRAQL INPUT DATA SET ASSUMING THAT A UNIFORM SITE DENSITY OVER THE COMPLETE SURFACE ACCOUNTS BEST FOR U(VI) UPTAKE (WEAK SITE ONLY)

```
 Modeling of U(VI) adsorption on Fe(OH)3 in W2 as a f(pH, conc U), DDL model
 0.100 M NaNO3  0.12 mM Fe; 600 m2/gm
0.1000 0 0.0000 25.00 1.000E-05 1 100 /XMU KEYMU ACTCOR TEMP EPS NCASES ITMAX
1     1      0       1       1      1       /IHYDRA IINPUT ICHARG IPDIST IPCENT IALL
1     1      2       1       80000          /KEY IADS MODEL IDIFOP LIMADS
0     0    0   213.2     0   0   0   0       /C11 C21 C31 AREA1 C12 C22 C32 AREA2
32     86530  0    0      0       0      0      0      0
0      0 0 0 0 0 0 0 0 0 0 /
3.00   10.00 0.25                           /LINE FOR PH STEPPING
  5    -1.000    1.000E-1                  /DATA FOR COMPONENTS  Na+
157    -1.000    1.000E-1                  /                     NO3-
 50    -2.890    0.000E-0                  /                     H+
101   -16.000    0.000E-0                  /                     CO3
 32    -6.000    3.800E-6                  /                     U(VI)
184    -4.000    8.190E-4                  /                     TOH
183    -1.000    0.000                     /                     PSID
  0     0.000    0.000                     /
2                                          /
86115   -8.93   184 1   50 -1   183   -1     0   0      0   0    0    0 /
86120    7.29   184 1   50  1   183    1     0   0      0   0    0    0 /
86530   -5.21   184 1   50 -2    32    1     0   0      0   0    0    0 /
12130    9.70   101 1   32  1     0    0     0   0      0   0    0    0 /
12135   17.00   101 2   32  1     0    0     0   0      0   0    0    0 /
12140   21.63   101 3   32  1     0    0     0   0      0   0    0    0 /
12141   -1.18   101 1   32  2    50   -3     0   0      0   0    0    0 /
12100   -5.20    32 1   50 -1     0    0     0   0      0   0    0    0 /
12112  -12.00    32 1   50 -2     0    0     0   0      0   0    0    0 /
12114  -20.00    32 1   50 -3     0    0     0   0      0   0    0    0 /
12116  -33.00    32 1   50 -4     0    0     0   0      0   0    0    0 /
12118   -2.80    32 2   50 -1     0    0     0   0      0   0    0    0 /
12120   -5.63    32 2   50 -2     0    0     0   0      0   0    0    0 /
12123   -11.9    32 3   50 -4     0    0     0   0      0   0    0    0 /
12125  -15.56    32 3   50 -5     0    0     0   0      0   0    0    0 /
12127   -21.9    32 4   50 -7     0    0     0   0      0   0    0    0 /
12128   -31.0    32 3   50 -7     0    0     0   0      0   0    0    0 /
 0     0.0     0 0    0  0     0    0     0  0      0  0    0    0 /
3                                                                      /
50      3.00  0 0 0 0 0 0 0 0 0 0 0 0 0 0 0 0 0 0 0 0 0 0 0 0 0 0 0 0 0 0 0 0 /
25000 21.64   0 0 0 0 0 0 0 0 0 0 0 0 0 0 0 0 0 0 0 0 0 0 0 0 0 0 0 0 0 0 0 0 /
0       0.00  0 0 0 0 0 0 0 0 0 0 0 0 0 0 0 0 0 0 0 0 0 0 0 0 0 0 0 0 0 0 0 0 /
6                                                                              /
183     0.00  0 0 0 0 0 0 0 0 0 0 0 0 0 0 0 0 0 0 0 0 0 0 0 0 0 0 0 0 0 0 0 0 /
 0 0 0 0 0 0 0 0 0 0 0 0 0 0 0 0 0 0 0 0 0 0 0 0 0 0 0 0 0 0 0 0 0 0 0 0 0 0 /
 0 0 0 0 0 0 0 0 0 0 0 0 0 0 0 0 0 0 0 0 0 0 0 0 0 0 0 0 0 0 0 0 0 0 0 0 0 0 /
```

APPENDIX 3

HYDRAQL INPUT DATA SET ASSUMING THAT A UNIFORM SITE DENSITY OVER THE COMPLETE SURFACE ACCOUNTS BEST FOR U(VI) UPTAKE (STRONG AND WEAK SITES PRESENT)

```
 Modeling of U(VI) adsorption on Fe(OH)3 in W2 as a f(pH, conc U), DDL model
  0.100 M NaNO3  0.12 mM Fe; 600 m2/gm
0.1000 0 0.0000 25.00 1.000E-05 1 100 /XMU KEYMU ACTCOR TEMP EPS NCASES ITMAX
1     1      0       1       1      1       /IHYDRA IINPUT ICHARG IPDIST IPCENT IALL
1     1      2       1       80000          /KEY IADS MODEL IDIFOP LIMADS
0     0    0  213.2     0  0  0  0          /C11 C21 C31 AREA1 C12 C22 C32 AREA2
32    86520    86530       0      0       0      0      0      0
0      0 0 0 0 0 0 0 0 0 0 0 /
3.00   10.00 0.25                          /LINE FOR PH STEPPING
  5    -1.000    1.000E-1                  /DATA FOR COMPONENTS  Na+
157    -1.000    1.000E-1                  /                     NO3-
 50    -2.890    0.000E-0                  /                     H+
101   -16.000    0.000E-0                  /                     CO3
 32    -6.000    3.800E-6                  /                     U(VI)
184    -6.000    2.880E-6                  /                     SOH
185    -4.000    8.190E-4                  /                     TOH
183    -1.000    0.000                     /                     PSID
  0     0.000    0.000                     /
2                                          /
86105   -8.93   184 1   50 -1   183   -1     0  0      0  0    0    0 /
86110    7.29   184 1   50  1   183    1     0  0      0  0    0    0 /
86115   -8.93   185 1   50 -1   183   -1     0  0      0  0    0    0 /
86120    7.29   185 1   50  1   183    1     0  0      0  0    0    0 /
86520   -1.60   184 1   50 -2    32    1     0  0      0  0    0    0 /
86530   -5.21   185 1   50 -2    32    1     0  0      0  0    0    0 /
12130    9.70   101 1   32  1     0    0     0  0      0  0    0    0 /
12135   17.00   101 2   32  1     0    0     0  0      0  0    0    0 /
12140   21.63   101 3   32  1     0    0     0  0      0  0    0    0 /
12141   -1.18   101 1   32  2    50   -3     0  0      0  0    0    0 /
12100   -5.20    32 1   50 -1     0    0     0  0      0  0    0    0 /
12112  -12.00    32 1   50 -2     0    0     0  0      0  0    0    0 /
12114  -20.00    32 1   50 -3     0    0     0  0      0  0    0    0 /
12116  -33.00    32 1   50 -4     0    0     0  0      0  0    0    0 /
12118   -2.80    32 2   50 -1     0    0     0  0      0  0    0    0 /
12120   -5.63    32 2   50 -2     0    0     0  0      0  0    0    0 /
12123   -11.9    32 3   50 -4     0    0     0  0      0  0    0    0 /
12125  -15.56    32 3   50 -5     0    0     0  0      0  0    0    0 /
12127   -21.9    32 4   50 -7     0    0     0  0      0  0    0    0 /
12128   -31.0    32 3   50 -7     0    0     0  0      0  0    0    0 /
 0     0.0     0 0   0  0    0   0     0  0      0  0    0    0 /
3                                                                    /
50      3.00  0 0 0 0 0 0 0 0 0 0 0 0 0 0 0 0 0 0 0 0 0 0 0 0 0 0 0 0 0 0 0 0 0 /
25000  21.64  0 0 0 0 0 0 0 0 0 0 0 0 0 0 0 0 0 0 0 0 0 0 0 0 0 0 0 0 0 0 0 0 0 /
0       0.00  0 0 0 0 0 0 0 0 0 0 0 0 0 0 0 0 0 0 0 0 0 0 0 0 0 0 0 0 0 0 0 0 0 /
6                                                                                /
183     0.00  0 0 0 0 0 0 0 0 0 0 0 0 0 0 0 0 0 0 0 0 0 0 0 0 0 0 0 0 0 0 0 0 0 /
 0 0 0 0 0 0 0 0 0 0 0 0 0 0 0 0 0 0 0 0 0 0 0 0 0 0 0 0 0 0 0 0 0 0 0 0 0 0 0 /
 0 0 0 0 0 0 0 0 0 0 0 0 0 0 0 0 0 0 0 0 0 0 0 0 0 0 0 0 0 0 0 0 0 0 0 0 0 0 0 /
```

APPENDIX 4

HYDRAQL INPUT ASSUMING THAT STRONGLY ACIDIC SITES IN COMBINATION WITH MORE TYPICAL OXYHYDROXIDE SITES ACCOUNT FOR U(VI) UPTAKE

```
 Modeling of U(VI) adsorption on Fe(OH)3 in W2 as a f(pH, conc U), DDL model
 0.100 M NaNO3  0.12 mM Fe; 600 m2/gm
0.1000 0 0.0000 25.00 1.000E-05 1 100 /XMU KEYMU ACTCOR TEMP EPS NCASES ITMAX
1     1      0       1       1      1       /IHYDRA IINPUT ICHARG IPDIST IPCENT IALL
1     1      2       1       80000          /KEY IADS MODEL IDIFOP LIMADS
0     0    0   213.2     0   0   0   0       /C11 C21 C31 AREA1 C12 C22 C32 AREA2
32    86520    86530       0      0       0      0      0      0
0       0 0 0 0 0 0 0 0 0 0 /
1.50   10.00 0.25                           /LINE FOR PH STEPPING
  5    -1.000    1.000E-1                  /DATA FOR COMPONENTS  Na+
157    -1.000    1.000E-1                  /                     NO3-
 50    -2.890    0.000E-0                  /                     H+
101   -16.000    0.000E-0                  /                     CO3
 32    -6.000    3.800E-6                  /                     U(VI)
184    -4.000    1.000E-4                  /                     SOH
185    -4.000    7.200E-4                  /                     TOH
183    -1.000    0.000                     /                     PSID
  0     0.000    0.000                     /
2                                          /
86105   -6.25   184 1   50 -1   183   -1     0  0      0  0    0    0 /
86110    1.75   184 1   50  1   183    1     0  0      0  0    0    0 /
86115   -8.93   185 1   50 -1   183   -1     0  0      0  0    0    0 /
86120    7.29   185 1   50  1   183    1     0  0      0  0    0    0 /
86520   -1.80   184 1   50 -1    32    1   183 -1      0  0    0    0 /
86530   -5.00   185 1   50 -2    32    1     0  0      0  0    0    0 /
12130    9.70   101 1   32  1     0    0     0  0      0  0    0    0 /
12135   17.00   101 2   32  1     0    0     0  0      0  0    0    0 /
12140   21.63   101 3   32  1     0    0     0  0      0  0    0    0 /
12141   -1.18   101 1   32  2    50   -3     0  0      0  0    0    0 /
12100   -5.20    32 1   50 -1     0    0     0  0      0  0    0    0 /
12112  -12.00    32 1   50 -2     0    0     0  0      0  0    0    0 /
12114  -20.00    32 1   50 -3     0    0     0  0      0  0    0    0 /
12116  -33.00    32 1   50 -4     0    0     0  0      0  0    0    0 /
12118   -2.80    32 2   50 -1     0    0     0  0      0  0    0    0 /
12120   -5.63    32 2   50 -2     0    0     0  0      0  0    0    0 /
12123   -11.9    32 3   50 -4     0    0     0  0      0  0    0    0 /
12125  -15.56    32 3   50 -5     0    0     0  0      0  0    0    0 /
12127   -21.9    32 4   50 -7     0    0     0  0      0  0    0    0 /
12128   -31.0    32 3   50 -7     0    0     0  0      0  0    0    0 /
 0     0.0     0 0   0  0     0   0     0  0      0  0   0    0 /
3                                                                    /
50      3.00  0 0 0 0 0 0 0 0 0 0 0 0 0 0 0 0 0 0 0 0 0 0 0 0 0 0 0 0 0 0 0 0 /
25000  21.64  0 0 0 0 0 0 0 0 0 0 0 0 0 0 0 0 0 0 0 0 0 0 0 0 0 0 0 0 0 0 0 0 /
0       0.00  0 0 0 0 0 0 0 0 0 0 0 0 0 0 0 0 0 0 0 0 0 0 0 0 0 0 0 0 0 0 0 0 /
6                                                                              /
183     0.00  0 0 0 0 0 0 0 0 0 0 0 0 0 0 0 0 0 0 0 0 0 0 0 0 0 0 0 0 0 0 0 0 /
 0 0 0 0 0 0 0 0 0 0 0 0 0 0 0 0 0 0 0 0 0 0 0 0 0 0 0 0 0 0 0 0 0 0 0 0 0 0 /
 0 0 0 0 0 0 0 0 0 0 0 0 0 0 0 0 0 0 0 0 0 0 0 0 0 0 0 0 0 0 0 0 0 0 0 0 0 0 /
```